ABSTRACT

DEOL, PUKHRAJ. Developing Methodology to Characterize Soil-limited Evaporation. (Under the direction of Prof. Josh Heitman and Prof. Aziz Amoozegar).

Evaporation from bare soil has classically been considered to occur in three stages, consisting of a relatively high and constant rate stage when the soil surface is wet, followed by a falling rate or soil-limited stage, and eventually shifting to a low and relatively constant evaporation rate stage. After drying of surface soil, evaporation occurs in the subsurface, but there is no clear evidence for when this shift to the subsurface occurs with respect to the stages of evaporation. Consequently, the role of steep, near-surface temperature gradients on evaporation is often ignored in land surface modeling schemes, which results in significant error. We used a newly developed sensible heat balance (SHB) measurement approach with heat-pulse sensors in a series of laboratory and field experiments to elucidate heat transfer during the soil-limited evaporation stage. Our primary objectives were to: 1) quantify sub-surface, non-isothermal evaporation profiles and examine the development of a dry surface layer (DSL) during falling rate evaporation; 2) determine timing of the onset of subsurface evaporation with respect to the stages of evaporative drying; and 3) investigate the effect of radiative versus non-radiative boundary conditions on evaporation front dynamics. Laboratory and field results show that the SHB method effectively measures total subsurface evaporation rates, and heat-pulse measurement-based estimates of the DSL thickness are consistent with destructively measured DSL thickness. For the first time, this SHB approach also quantifies mm-scale non-isothermal subsurface evaporation profile dynamics over a drying event. In addition, our laboratory study demonstrates that Fickian diffusion could account for evaporation rates once the DSL is formed, with rates dependent on DSL thickness. Results from the field study indicate that shift of the evaporation front to the

subsurface coincides with the drop in evaporation rates below the potential evaporation rate predicted from atmospheric conditions. Measured soil surface albedo may provide means to detect the transition from surface to subsurface evaporation. Results based on the laboratory experiments comparing radiative and non-radiative conditions (with the same potential evaporation rate) indicate differences in dynamics of the evaporation front between these conditions, which results in a higher sustained (soil-limited) evaporation rates under radiative conditions. These results highlight shortcomings in common approaches using an isothermal modeling scheme to predict soil-limited evaporation.

Developing Methodology to Characterize Soil-limited Evaporation

by
Pukhraj Deol

A dissertation submitted to the Graduate Faculty of
North Carolina State University
in partial fulfillment of the
requirements for the degree of
Doctor of Philosophy

Soil Science

Raleigh, North Carolina

2012

APPROVED BY:

Assoc. Prof. Josh Heitman Committee Chair	Prof. Aziz Amoozegar Committee Co-Chair
Prof. Edwin Fiscus	Assoc. Prof. Sukanta Basu

DEDICATION

To My Family

BIOGRAPHY

Pukhraj Deol was born to Mrs. Darshan Kaur and Mr. Kanwaljeet Singh in Ludhiana, Punjab, India. After completing her schooling, she went to Punjab Agricultural University at Ludhiana where she earned her Bachelor of Science degree in Agriculture and Masters of Science in Agronomy (2005). After graduation, she worked as a Research Fellow at Punjab Agricultural University. She joined NC State University's Department of Soil Science in the Fall of 2009 for her doctoral research, which involved methodology development to characterize soil-limited evaporation, under the guidance of Assoc. Prof. Josh Heitman and Prof. Aziz Amoozegar. She is married to Alok who is also an NC State University alumnus with a Ph. D in Materials Science and Engineering.

ACKNOWLEDGMENTS

First and foremost, I would like to express my sincerest thanks to my major advisor Dr. Josh Heitman for his constant encouragement, enthusiasm, patient guidance and above all his unfailing belief in me throughout this work. His expertise in the field, innovative ideas and critical feedback played a very important role in completion of my work and my development as a researcher. I would also like to express my deepest appreciation to my co-advisor Dr. Aziz Amoozegar for his motivation, steadfast encouragement and expert advice for successful completion of this work. I could not have imagined having better advisors and mentors for my Ph. D. Their immense knowledge, commitment towards research and passion for science has left a lasting impression on me.

I am highly indebted to our research collaborators Dr. Robert Horton of Iowa State University and Dr. Tusheng Ren of China Agricultural University for their important role in this research project and for developing the instrumentation used in my research work. I am also thankful to my committee members Dr. Sukanta Basu and Dr. Edwin Fiscus for their contributions of time and suggestions to improve the quality of my dissertation.

I am very thankful to our lab's research technician Adam Howard and my lab mates Amanda Liesch and Steven Holland for their pleasant company and offering a helping hand whenever needed. A special word of appreciation and thanks goes to our graduate coordinator Dr. Jot Smyth, graduate secretary Dee Ann Cooper and Martha Leary for their prompt help with the administrative work. Heartfelt thanks to all my friends at NC State for making my graduate

school life an enjoyable experience. A special thanks to Sushila Chaudhari and Lucky Mehra for their friendship, support and pleasant company during my dissertation writing.

My deepest gratitude goes to my parents for their hard work, sacrifices, unconditional love and support. I am also grateful to my in-laws and all other family members for their unbridled encouragement. Most importantly, I have to thank my dear husband Alok Gupta for his love, support and encouragement. He has been a constant source of strength and inspiration throughout this dissertation research and writing work.

Finally, I would like to acknowledge National Science Foundation and US-Israel Bi-Nation Agricultural Research and Development Fund for supporting this research work.

TABLE OF CONTENTS

LIST OF TABLES

LIST OF FIGURES

1. Introduction

Understanding soil water evaporation and associated energy exchange between land and atmosphere in the form of latent heat of evaporation (LE) is very important for hydrologic and environmental studies, as well as for crop management and soil water conservation. Evaporation from bare soil is an important component of water and energy budgets not only in arid regions, but also in semi-arid and humid regions, as large agricultural lands remain bare during field preparation, planting and crop establishment phases. Soil water evaporation constitutes a considerable proportion of evapotranspiration (ET), therefore it is a major component in soil water balance in field crops with incomplete crop cover [Qui and Ben-Asher, 2009; Ritchie et al., 2009]. In systems with wide rows and open canopy (e.g., vineyards), bare surface evaporation is important throughout the growing season. Parameterization of evaporation from a bare land surface is also very important in the hierarchy strategy of modeling land surface processes [Mihailovic et al., 1995; Mihailovic and Ruml, 1996].

Soil water evaporation has frequently been considered a three-stage process [Lemon, 1956; Feddes, 1971; Idso et al., 1974] starting with a relatively high and constant evaporation rate (stage 1) followed by a falling rate (stage 2) and eventually shifting to a very low and relatively constant rate (stage 3). During stage 1, water is available at the soil surface and evaporation is limited by atmospheric evaporative demand [Lemon, 1956]. At this stage, a large portion of surface net radiation is readily dissipated as latent heat of vaporization. As

the soil moisture at the surface is depleted, stage 2 evaporation begins, during which time evaporation drops below the potential rate and decreases with time. This shift in the evaporation regime has also been referred to as the falling rate or transition stage [Shokri and Or, 2011]. Eventually, a very low and relatively constant evaporation rate is observed during stage-3 evaporation.

When a moist soil exposed to sun dries, it comes in equilibrium with the overlying air and becomes approximately air-dry [Hillel, 1980]. This results in formation of a dry surface layer (DSL), also referred to as "soil mulch" [Kimball, 1973], which acts as a barrier to liquid water flow from moist sub-surface soil to the dry soil surface [Jalota and Parihar, 1998]. This process also has a significant effect on heat and mass transfer within the soil [Liu et al., 2005]. Hillel [1971] and Campbell [1985] reported that vaporization of water occurs at the bottom boundary of the DSL. This was confirmed by laboratory [Yamanaka et al., 1997] and numerical experiments [Yamanaka et al., 1998]. Formation of DSL and the shift of the evaporation front from surface to subsurface also involve a significant change in the surface energy balance as the location of latent heat sink moves from surface to subsurface. Heitman et al. [2010] demonstrated presence of a subsurface latent heat sink and emphasized the need to account for it for estimating an accurate surface energy budget.

Radiant energy fluxes at a dry soil surface in a field environment result in steep temperature gradients, making the surface soil heat flux a large fraction of the surface energy budget [de Vries and Philip, 1986; Mayocchi and Bristow, 1995; Heitman et al., 2010]. Partitioning of

this surface heat flux between latent and sensible heat within soil depends on tightly linked thermal and hydraulic processes. Soil thermal properties control the energy available for subsurface evaporation by influencing conduction heat flow and sensible heating, while soil hydraulic properties control the rate of liquid water supply from the moist subsurface to the evaporation zone, as well as the rate of vapor loss from the soil surface. The depth of soil drying or location of the evaporation front depends on the balance between transfer rates of heat, liquid, and vapor [Bitelli et al., 2008]. Previous studies by Idso et al. [1974] recognized a connection between changes in surface albedo (indicating surface drying) and the onset of falling-rate evaporation, suggesting a loss of liquid water connectivity to the surface at the beginning of stage-2 evaporation. Idso et al. [1975] further connected falling rate evaporation to the soil energy budget, making use of increasing soil surface temperatures to mark the transition to falling-rate evaporation.

Several recent studies have attempted to better elucidate soil hydraulic controls on evaporation through experiment, focusing on differences between early and late stage evaporation. By measuring evaporation from an initially saturated porous media under isothermal conditions, Shokri and Or [2011] reported “jumps” in the evaporation front from the surface to the subsurface at the end of stage 1. They reported that the jump length is affected primarily by porous media properties. Shokri and Salvucci [2011] related the low rate of evaporation during late stage evaporation to the water table depth at which the liquid water connection to the surface is lost for several sand materials under isothermal conditions. Shokri and Or [2011] emphasized the need for further investigation to accurately characterize

the abruptness and dynamics of the important transition from high rate to low rate stage evaporation (i.e., stage 1 to stage 3). Most soil water evaporation in arid regions occurs during stage 2 [Brutsaert and Chen, 1995; Snyder et al., 2000; Ventura et al., 2001] under non-isothermal, transient conditions; which further emphasizes the need to thoroughly investigate this important transition in evaporation regimes, as well as related implications for the surface energy budget.

1.1 Problem statement

Many research studies have been conducted to understand evaporation, but challenges still exist in accurate estimation of soil water evaporation. Decreasing trends in pan evaporation are widely observed across the world and have been attributed to changes in temperature, precipitation, incoming radiation and wind speed. Nevertheless, we only partially understand how these trends are linked to actual evaporation [Brutsaert and Parlange, 1998]. Recent studies show that in order to estimate possible effects of climate change on evaporative demand, and eventually on actual evaporation, it is very important to consider spatially and temporally dynamic data describing all drivers of evaporative demand [for example see Donohue et al., 2010; van Heerwaarden et al., 2010]. Due to knowledge limitations as well as difficulty in measuring near-surface temperature, many land surface models employ an isothermal scheme, which results in their poor performance under arid and semi-arid regions [Li and Sun, 2008]. Recent studies have emphasized the need for physics-based models and consideration of thermal boundary effects and dry surface layer (DSL) formation to

accurately estimate energy balance components for better understanding of large scale hydrologic and climatic patterns [Heitman et al., 2010; Novak, 2010; Zeng et al., 2011].

There is a need to better understand the physics of evaporation, especially the role of near-surface temperature gradients, on evaporation front dynamics and onset of the subsurface evaporation stage with respect to three stages of evaporative drying of soil. A main reason for knowledge gaps in soil-limited evaporation research is the difficulty in studying the evaporation front dynamics in the highly dynamic near-surface zone. For example, the shallowest measurements by Yamanaka et al. [1999] were taken for 0-1 cm depth layer which might have limited their ability to study the subsurface evaporation process from its inception. Numerical simulation studies by Novak [2010] have shown the diurnal and inter-diurnal dynamics of the subsurface evaporation profile in the near-surface zone and have emphasized the need for measurement-based studies to evaluate the existing theories based on modeling exercises. Measurements necessary to capture the dynamics in the near-surface zone, however, are very challenging which is presumably a main reason for related knowledge gaps in the soil water evaporation literature on transitions between early- and late-stage evaporation.

A sensible heat balance (SHB) approach based on fine-scale temperature and thermal property measurements in the near-surface zone has been proposed to estimate sub-surface, non-isothermal evaporation under transient conditions [Heitman et al., 2008a, b]. The SHB approach estimates latent heat flux for a soil layer as the residual to a balance between the

divergence in sensible heat flux across the layer and the change in sensible heat storage for the soil layer. Field experiments [Heitman et al., 2008a, b; Xiao et al., 2011] and model evaluations [Sakai et al., 2011] indicate that the SHB approach is accurate for measuring *in situ*, subsurface soil-controlled evaporation. The main limitation of the SHB approach in these studies was the inability of instrumentation to quantify evaporation during the initial shift between surface and subsurface evaporation, when evaporation occurs at depths shallower than approximately 3 mm [Sakai et al., 2011]. Specifically, depth resolution was constrained by the 6-mm needle spacing of the three-needle probe design used in the original SHB studies to measure near-surface temperature gradients. Recent adaptations to the probe design, with closer needle spacing near the surface, have narrowed this "undetectable" zone to as shallow as 0.5 mm soil depth (i.e., the mid-point between the shallowest temperature sensing needles at 0 and 1 mm depths) [Zhang et al., 2012]. Full realization of the potential of the SHB approach, using improved instrumentation, requires further testing and evaluation.

1.2 Research objectives and thesis organization

Considering the uncertainty related to soil-limited evaporation processes, especially the evaporation front dynamics and thermal effects on evaporation, and the potential utility of the heat-pulse measurement-based SHB approach to study the highly dynamic near-surface layer, we conducted experiments with the following objectives: 1) evaluate SHB-estimated evaporation under controlled laboratory non-isothermal conditions by comparing it with mass-balance evaporation estimates; 2) quantify sub-surface, non-isothermal evaporation

profiles and examine the development of the DSL during falling rate evaporation; 3) determine the timing of the onset of subsurface evaporation with respect to the three stages of evaporative drying; and 4) investigate the effect of thermal boundary conditions on a) evaporation front dynamics and b) actual to pan evaporation ratios under steady-state, soil-limited conditions.

Soil column studies were conducted under controlled laboratory conditions to address objectives 1 and 2. Eleven-needle heat pulse probes were used to continuously measure near-surface soil temperature and thermal property distributions at the millimeter scale under steady-state and transient conditions. These measurements were used to quantify non-isothermal sub-surface evaporation profiles. Depth-integrated SHB evaporation rates were compared with mass-balance evaporation estimates under controlled laboratory conditions (Chapter 2).

Bare field evaporation studies were conducted to further investigate the timing of the onset of subsurface evaporation with respect to the three stages of evaporative drying (objective 3). Micro-lysimeter (ML) and SHB approaches were used to estimate total and subsurface evaporation over several natural drying events under field conditions in a bare loamy-sand soil (Chapter 3). Soil surface albedo was also measured during the drying periods for its potential use as an indicator of formation of a DSL and onset of subsurface evaporation stage.

Meanwhile the laboratory column studies were continued to address objective 4 a and b (Chapter 4). Heat-pulse measurements were used to study evaporation front dynamics under changing thermal boundary conditions simulating change from non-isothermal daytime to isothermal nighttime conditions. To specifically compare the effect of non-isothermal vs. isothermal boundary conditions on soil-limited evaporation and DSL thickness, we also conducted two separate steady-state evaporation experiments. For these experiments the potential evaporative demand was the same, but one case involved isothermal boundary conditions generated using a fan to adjust wind speed, while the other case employed a radiation heat emitter to generate non-isothermal surface boundary conditions. A general summary and conclusions from all of the above studies along with recommendations for future research are discussed in Chapter 5.

1.3 References

Bittelli, M., F. Ventura, G.S. Campbell, R.L. Snyder, F. Gallegati, and P.R. Pisa (2008), Coupling of heat, water vapor, and liquid water fluxes to compute evaporation in bare soils, *J. Hydrol*., 362, 191-205, doi:10.1016/j.jhydrol.2008.08.014.

Brutsaert, W., and D. Chen (1995), Desorption and the two stages of drying of natural tallgrass prairie, *Water Resour. Res*., 31, 1305-1313.

Brutsaert, W., and M. B. Parlange (1998), Hydrologic cycle explains the evaporation paradox, *Nature*, 396, 30.

Campbell, G.S. (1985), *Soil Physics with Basic Transport Models for Soil-Plant System*. Elsevier, New York.

Donohue, R. J., T. R. McVicar, and M. L. Roderick (2010) Assessing the ability of potential evaporation formulations to capture the dynamics of evaporative demand with a changing climate. J. Hydrol., 386, 186-197.

Feddes, R.A. (1971), Water, heat and crop growth, PhD thesis, Comm. Agric. Univ., Institute of Land and Water Management Research, Wageningen, 184pp.

Heitman, J.L., R. Horton, T.J. Sauer, and T.M. DeSutter (2008a), Sensible heat observations reveal soil-water evaporation dynamics, *J. Hydromet*., 9, 165-171.

Heitman, J.L., R. Horton, T.J. Sauer, T.S. Ren, and X. Xiao (2010), Latent heat in soil heat flux measurements, *Ag. Forest. Met.*, 150, 1147-1153.

Heitman, J.L., X. Xiao, R. Horton, and T.J. Sauer (2008b), Sensible heat measurements indicating depth and magnitude of subsurface soil water evaporation, *Water Resour. Res.*, 44, W00D05.

Hillel, D. (1971), *Soil and Water: Physical Principles and Processes*. Academic Press, New York.

Idso, S.B., R.D. Jackson, and R.J. Reginato (1975), Estimating evaporation: A technique adaptable to remote sensing, *Science*, 189, 991-992.

Idso, S.B., R.J. Reginato, R.D. Jackson, B.A. Kimball, and F.S. Nakayama (1974), The three stages of drying of a field soil, *Soil Sci. Soc. Am. Proc.*, 38, 831-837.

Jalota, S.K. and S.S. Prihar (1998), *Reducing soil-water evaporation with tillage and straw mulching*. Iowa State University Press, Ames (ISBN 0-8138-2857-0), p. 142.

Kimball, B.A. (1973), Water vapor movement through mulches under field conditions, *Soil Sci. Soc. Am. Proc.*, 37, 813−818.

Lemon, E. R. (1956), The potentialities for decreasing soil moisture evaporation loss, *Soil Sci. Soc. Am. Proc*., 20, 120-125.

Li, Q., and S. F. Sun (2008), Development of universal and simplified soil model coupling heat and water transport. *Science in China Series (D)*, 51, 88–102.

Liu, B.C., W. Liu, and S.W. Peng. (2005), Study of heat and moisture transfer in soil with a dry surface layer, *International Journal of Heat and Mass Transfer*, 48 (21–22), 4579-4589.

Mayocchi, C.L., and K.L. Bristow (1995), Soil surface heat flux: some general questions and comments on measurements, *Ag. Forest Meteor*. 75, 43-50.

Mihailovic, D.T., B. Rajkovic, L. Dekic, R. A. Pielke, T. J. Lee, and Z. Ye (1995), The validation of various schemes for parameterizing evaporation from bare soil for use in meteorological models: a numerical study using in situ data. *Boundary-Layer Meteorol*. 76, 259–289.

Mihailovic, D.T., and M. Ruml (1996). Design of land-air parameterization scheme (LAPS) for modeling boundary layer surface processes. *Meteorol. Atmos. Phys*. 58, 65–81.

Novak, M.D. (2010), Dynamics of the near-surface evaporation zone and corresponding effects on the surface energy balance of a drying bare soil, *Ag. Forest Meteor*., 150, 1358-1365.

Qiu, G. Y., and J. Ben-Asher (2009). "Experimental Determination of Soil Evaporation Stages with Soil Surface Temperature." *Soil Sci. Soc. Am. J.* 74(1): 13-22.

Ritchie, J. T. and C. H. Porter, (2009). Extension of an Existing Model for Soil Water Evaporation and Redistribution under High Water Content Conditions. *Soil Sci. Soc. Am. J.* 73(3): 792-801.

Sakai, M., S.B. Jones, and M. Tuller (2011), Numerical evaluation of subsurface soil water evaporation derived from sensible heat balance. *Water Resour. Res*., 47, W02547.

Shokri, N., and D. Or. (2011), What determines drying rates at the onset of diffusion controlled stage-2 evaporation from porous media? *Water Resour. Res*., 47, W09513.

Shokri, N., and G.D. Salvucci (2011), Evaporation from porous media in the presence of a water table. , *Vadose Zone J*., 10, 1-10.

Snyder, R.L., K. Bali, F. Ventura, and H. Gomez-Macpherson, (2000), Estimating evaporation from bare or nearly bare soil, *J. Irrig. Drain. Eng*., 126 (6), 399–403.

van Heerwaarden, C. C., J. Vilà-Guerau de Arellano, and A. J. Teuling (2010), Land-atmosphere coupling explains the link between pan evaporation and actual evapotranspiration trends in a changing climate, *Geophys. Res. Lett.*, 37, L21401, doi:10.1029/2010GL045374.

Ventura, F., B. Faber, K. Bali, R.L. Snyder, D. Spano, P. Duce, and K.F. Schulbach, (2001), A model for estimating evaporation and transpiration from row crops, *J. Irrig. Drain. Eng*., 127 (6), 339-345.

Xiao, X., R. Horton, T. Sauer, J.L. Heitman, and T. Ren (2011), Cumulative soil water evaporation as a function of depth and time, *Vadose Zone J*., 10, 1016-1022.

Yamanaka, T., and T. Yonetani (1999), Dynamics of the evaporation zone in dry sandy soils, *J. of Hydrol.*, 217(1–2), 135-148.

Yamanaka, T., A. Takeda, and J. Shimada (1998), Evaporation beneath the soil surface: Some observational evidence and numerical experiments. , *Hydrol. Process.*, 12, 2193-2203.

Yamanaka, T., and J. Shimada, (1997), Simple but reliable method to extract soil water for stable isotope analysis, *Journal of Japan Society of Hydrology and Water Resources*, 10, 181-184 in Japanese with English abstract.

Zeng, Y., Z. Su, L. Wan, and J. Wen (2011), Numerical analysis of air-water-heat flow in unsaturated soil: Is it necessary to consider airflow in land surface models?, *J. Geophys. Res.*, 116, D20107, doi:10.1029/2011JD015835.

Zhang X., J.L. Heitman, R. Horton, and T. Ren (2012), Measuring subsurface soil-water evaporation with an improved heat-pulse probe. *Soil Sci. Soc. Am. J.*, 76, 876-879.

2. Quantifying Non-isothermal Sub-surface Soil Water Evaporation

A manuscript accepted for publication in Water Resources Research

Pukhraj Deol[1], Josh Heitman[1], Aziz Amoozegar[1], Tusheng Ren[2], and Robert Horton[3]

(1) NC State University, Raleigh, North Carolina 27695-7619

(2) China Agricultural University, Beijing

(3) Iowa State University, Ames, IA 50011-1010

Abstract

Accurate quantification of energy and mass transfer during soil water evaporation is critical for improving understanding of the hydrologic cycle and for many environmental, agricultural, and engineering applications. Drying of soil under radiation boundary conditions results in formation of a dry surface layer (DSL), which is accompanied by a shift in the position of the latent heat sink from the surface to the sub-surface. Detailed investigation of evaporative dynamics within this active near-surface zone has mostly been limited to modeling, with few measurements available to test models. Soil column studies were conducted to quantify non-isothermal sub-surface evaporation profiles using a sensible heat balance (SHB) approach. Eleven-needle heat pulse probes were used to measure soil temperature and thermal property distributions at the millimeter scale in the near-surface soil. Depth-integrated SHB evaporation rates were compared with mass-balance evaporation estimates under controlled laboratory conditions. The results show that the SHB method effectively measured total subsurface evaporation rates with only 0.01-0.03 mm/h difference from mass balance estimates. The SHB approach also quantified mm-scale non-isothermal

subsurface evaporation profiles over a drying event, which has not been previously possible. Thickness of the DSL was also examined using measured soil thermal conductivity distributions near the drying surface. Estimates of the DSL thickness were consistent with observed evaporation profile distributions from SHB. Estimated thickness of the DSL was further used to compute diffusive vapor flux. The diffusive vapor flux also closely matched both mass balance evaporation rates and subsurface evaporation rates estimated from SHB.

2.1 Introduction

Accurate quantification of energy and mass transfer during soil water evaporation is critical for improving our understanding of large scale hydrologic and climatic patterns as well as for many environmental, agricultural, and engineering applications. Soil water evaporation has frequently been considered a three stage process [Lemon, 1956; Feddes, 1971; Idso et al., 1974] starting with a relatively high and constant evaporation rate (stage 1) followed by a falling rate (stage 2) and eventually shifting to a very low and relatively constant rate (stage 3). During stage 1, water is available at the soil surface and evaporation is limited by atmospheric evaporative demand [Lemon, 1956]. At this stage, a large portion of the surface net radiation is readily dissipated as latent heat of vaporization. With progressive drying, the surface soil comes in equilibrium with the overlying air and it becomes approximately air-dry [Hillel, 1980]. This results in formation of a dry surface layer (DSL), also referred to as “soil mulch” [Kimball, 1973], which acts as a barrier to liquid water flow from moist sub-surface soil to the dry soil surface [Jalota and Parihar, 1998]. This process also has a significant effect on heat and mass transfer within the soil [Liu et al., 2005]. Hillel [1971] and Campbell

[1985] reported that vaporization of water occurs at the bottom boundary of the DSL. This was confirmed by laboratory [Yamanaka et al., 1997] and numerical experiments [Yamanaka et al., 1998], which concluded that in addition to the vaporization occurring at the bottom boundary of the DSL, transient vaporization or condensation also occurs within the DSL when there are notable changes in soil temperature [Yamanaka et al., 1999]. Recently, Novak [2010] studied dynamics of the near-surface evaporation zone numerically in a bare, drying silt-loam soil under clear sky conditions and observed a strong diurnal pattern superimposed on inter-diurnal changes associated with progressive drying. The Novak [2010] simulation indicated that the transition between surface and subsurface evaporation occurred daily early in the drying period, and it affected the surface energy balance and near-surface temperature and water content profiles.

Radiant energy fluxes at a dry soil surface in a field environment result in steep temperature gradients, making the surface soil heat flux a large fraction of the surface energy budget [de Vries and Philip, 1986; Mayocchi and Bristow, 1995; Heitman et al., 2010]. Partitioning of this surface heat flux between latent and sensible heat within soil depends on tightly linked thermal and hydraulic processes. Soil thermal properties control the energy available for subsurface evaporation by influencing conduction heat flow and sensible heating, while soil hydraulic properties control the rate of liquid water supply from the moist subsurface to the evaporation zone, as well as the rate of vapor loss from the soil surface. The depth of soil drying or location of the evaporation front depends on the balance between transfer rates of heat, liquid, and vapor [Bitelli et al., 2008]. Previous studies by Idso et al. [1974] recognized

a connection between changes in surface albedo (indicating surface drying) and the onset of falling-rate evaporation, suggesting a loss of liquid water connectivity to the surface at the beginning of stage-2 evaporation. Idso et al. [1975] further connected falling rate evaporation to the soil energy budget, making use of increasing soil surface temperatures to mark the transition to falling-rate evaporation.

Several recent studies have attempted to better elucidate soil hydraulic controls on evaporation through experiment, focusing on differences between early and late stage evaporation. By measuring evaporation from an initially saturated porous media under isothermal conditions, Shokri and Or [2011] reported "jumps" in the evaporation front from the surface to the subsurface at the end of stage 1. They reported that the jump length is affected primarily by porous media properties. Shokri and Salvucci [2011] related the low rate of evaporation during late stage evaporation to the water table depth at which the liquid water connection to the surface is lost for several sand materials under isothermal conditions. Shokri and Or [2011] emphasized the need for further investigation to accurately characterize the abruptness and dynamics of the important transition from high rate to low rate stage evaporation (i.e., stage 1 to stage 3). Most soil water evaporation in arid regions occurs during stage 2 [Brutsaert and Chen, 1995; Snyder et al., 2000; Ventura et al., 2001] and under non-isothermal, transient conditions, which further emphasizes the need to thoroughly investigate this important transition in evaporation regimes, as well as related implications for the surface energy budget.

To date few attempts have been made to quantify sub-surface evaporation profiles, especially under non-isothermal, transient conditions. This requires detailed fine-scale investigation of the highly dynamic near-surface zone. Measurements necessary to capture the dynamics in the near-surface zone, however, are very challenging which is presumably a main reason for related knowledge gaps in the soil water evaporation literature on transitions between early and late stage evaporation. A sensible heat balance (SHB) approach based on fine-scale temperature and thermal property measurements in the near-surface zone has been proposed to estimate sub-surface, non-isothermal evaporation under transient conditions [Heitman et al., 2008b, c]. The SHB approach estimates latent heat flux for a soil layer as the residual to a balance between the divergence in sensible heat flux across the layer and the change in sensible heat storage for the soil layer. Field experiments [Heitman et al., 2008b, c; Xiao et al., 2011] and model evaluations [Sakai et al., 2011] indicate that the SHB approach is accurate for measuring *in situ*, subsurface soil-controlled evaporation. The main limitation of the SHB approach in these studies was the inability of instrumentation to quantify evaporation during the initial shift between surface and subsurface evaporation, when evaporation occurs at depths shallower than approximately 3 mm [Sakai et al., 2011]. Specifically, depth resolution was constrained by the 6-mm needle spacing of the three-needle probe design used in the original SHB studies to measure near-surface temperature gradients. Recent adaptations to the probe design, with closer needle spacing near the surface, have narrowed this "undetectable" zone to as shallow as 0.5 mm soil depth (i.e., the mid-point between the shallowest temperature sensing needles at 0 and 1 mm depths) [Zhang

et al., 2012]. Full realization of the potential of the SHB approach, using improved instrumentation, requires further testing and evaluation.

Considering the knowledge gaps for evaporation, especially related to the transition between atmospherically controlled and late stage evaporation under non-isothermal conditions, and the potential utility of the measurement-based SHB approach to study the highly dynamic near-surface layer, we conducted experiments with three primary objectives: 1) evaluate SHB-estimated evaporation under controlled laboratory non-isothermal conditions by comparing it with mass-balance evaporation estimates; 2) quantify sub-surface, non-isothermal evaporation profiles during falling rate evaporation; and 3) examine the development of the DSL during falling rate evaporation.

2.2 Materials and Methods

2.2.1 General Experimental Set-up and Soil Properties

Studies were conducted under controlled laboratory conditions to allow data collection during a continuous drying event and to have an accurate mass evaporation estimate to validate the SHB-estimated evaporation. Non-isothermal conditions were chosen to simulate drying under radiation boundary conditions common in the field. A steady-state evaporation study was conducted first to test SHB approach under simple conditions. A transient evaporation study was also performed to quantify subsurface evaporation profiles over a drying event. A 34-cm long open top column, constructed of 6-inch (15.25 cm inside diameter) polyvinyl chloride (PVC), was packed with sand material, similar to that used by

Arya et al. [2008 and 2010], at a uniform bulk density of 1.65 g/cm^3. The bottom of the column was connected to a Marriott bottle to wet the soil from the bottom and also to control the saturated zone within the column (Figure 2.1A). The soil column and Marriott bottle were placed on separate weighing scales for measuring the mass losses of water. Mass losses of water from soil column and Marriott bottle were manually recorded at 0.1 g resolution using separate digital scales. A ceramic heat emitter was installed at 20 cm distance above the column to uniformly heat the soil surface.

The particle size distribution and saturated hydraulic conductivity of the sand material are given in Table 2.1 [adapted from Arya et al., 2008]. Wet end water retention at zero (saturation) to 100 cm tension (equivalent to -100 cm soil water pressure head) was determined destructively following Howard et al. [2010] (Figure 2.2; data shown for 0 to -30 cm range). Eleven-needle heat-pulse probes (Figure 2.1 B, details in the following section) were used for measurement of soil temperature and thermal properties. In addition to heat-pulse data collected during the experiments (described below), the soil thermal conductivity (λ)-volumetric water content (θ) relationship for the sand was determined independently by packing the soil in a separate column at a bulk density = 1.65 g/cm^3 and measuring λ at various θ using the KD2 Pro Thermal Property Sensor (Decagon Devices Inc., Pullman, WA). The observed λ-θ relationship for this soil closely matches the Chung and Horton [1987] model for λ for sandy soils (Figure 2.3).

2.2.2 Soil Heat Balance

The SHB approach was proposed by Heitman et al. [2008b, c] as a method for estimating sub-surface evaporation. Fine-scale temperature and thermal property measurements collected with heat-pulse probes (HPP) are used to compute the heat balance for a soil layer. For this study, heat-pulse measurements were taken using an 11-needle HPP [Zhang et al., 2012]. All 11 needles of the HPP contained 40-gauge type E (chromel-constantan) thermocouples for temperature measurement (Figure 2.1 B). The four longer needles also contained a resistance heater made of 38-gauge Nichrome 80 wire for producing a heat pulse. Further details on the HPP design are given in Zhang et al. [2012]. The HPP was installed in vertical orientation with its needles parallel to the soil surface and the top needle, barely covered with soil. The HPP was used for two functions: (i) collecting soil temperature data each hour to assess temperature gradients imposed between the surface and subsurface boundaries of the soil column; and (ii) making heat-pulse measurements from each heater needle every 2 h to determine soil thermal properties.

Measurements included soil temperatures at all 11 needle locations at 0, 1, 2, 6, 12, 18, 24, 30, 36, 42 and 48 mm depths followed by heat-pulse measurements via two heaters at a time. Heaters 1 and 3, located at 6 and 30 mm depth, respectively, were activated together after one ambient temperature measurement; and heaters 2 and 4, located at 18 and 42 mm depths, respectively, were activated together after the next ambient temperature measurement 1 h later. The heaters were activated for 8 s. Temperature traces of the needles adjacent to the

heaters were recorded at 0.5-s intervals for a total of 100 s during each heat pulse measurement. A 1-h recovery period was given after each heat-pulse cycle to allow local temperatures to return to ambient temperature before the next soil temperature measurement. A data logger (CR 3000, Campbell Scientific, Logan, UT) was used to collect temperature and heat-pulse data. Temperature responses of needles adjacent to heater needles were used to compute soil thermal diffusivity and volumetric heat capacity following Bristow et al. [1994] and Knight and Kluitenberg [2004], respectively, and thermal conductivity (λ) was determined as the product of thermal diffusivity and volumetric heat capacity.

Temperature and thermal property data were used as described in Zhang et al. [2012] to compute the sensible heat balance for different soil layers with layer boundaries corresponding to the middle of adjacent needles. Latent heat flux originating from these layers was estimated following the sensible heat balance for a soil layer [Gardner and Hanks, 1966]:

$$LE = (H_1 - H_2) - \Delta S \qquad [1]$$

where, LE is the latent heat flux, H_1 and H_2 are the conduction heat fluxes at upper and lower boundaries of the soil layer, respectively, and ΔS is the change in sensible heat storage for the layer.

Heat flux at the middle location of two adjacent needles was calculated from temperature gradient and heat pulse estimated λ. For calculating the temperature gradient, apparent

spacing between the needles was determined by calibrating the probe in agar-stabilized water before probe installation [Campbell et al., 1991]. Change in sensible heat storage, ΔS was calculated from volumetric heat capacity and the change in ambient temperature of the soil layer during a given time step [Ochsner, 2007]. Detailed conceptual background of this method is given by Heitman et al. [2008b, c].

2.2.3 Steady-state Evaporation

For the steady-state evaporation experiment, the soil was initially saturated and then drained to reach equilibrium with a constantly maintained water table at 29 cm below the soil surface. The upper boundary conditions were constant radiation maintained via the ceramic heat emitter (150 W), zero wind speed and constant relative humidity (30%) at constant air temperature (20^{o}C). An open pan evaporation rate of 0.7 mm/h was observed under these boundary conditions. The lower boundary conditions were constant temperature (20^{o}C) at equilibrium with the simulated water table positioned and maintained 29 cm below the soil surface using the Marriott bottle. The initial condition for water content was a drained profile at equilibrium with the water table (Figure 2.2). The column was left under the described boundary conditions until the soil column mass became constant and a steady change in mass with time was observed for the Marriott bottle, indicating steady-state evaporation conditions. Steady-state evaporation was observed (via mass measurements) after approximately 70 h. Thereafter, both SHB and mass balance measurements were recorded from 72 to 120 h.

2.2.4 Transient Evaporation

For the transient evaporation experiment, the same soil column set up as the steady-state evaporation study was used, except that there was no external water supply to the column during the study. The column was first saturated and drained such that the initial water content condition was a drained profile (Figure 2.2) with a water table at 29 cm depth. Water supply to the column was then disconnected at 0 h. At the same time, the heat emitter was turned on to maintain a constant radiation load at the soil surface. As before, an open pan evaporation of 0.7 mm/h was observed under the experimental conditions. Mass-loss evaporation, soil temperature, and heat-pulse data were collected for a period of 90 h.

2.3 Results and Discussion

2.3.1 Steady-state Evaporation

After attaining near steady-state evaporation at approximately 70 h, an average mass balance evaporation rate of 0.28 mm/h (ranging 0.26-0.32 mm/h) was observed from 72 to 120 h, when the experiment was terminated. This evaporation rate, approximately 40% of pan evaporation (0.7 mm/h) recorded under the same surface boundary conditions, indicates soil-limited evaporation. After 70 h of drying under these conditions, the soil surface was visibly dry, indicating formation of a DSL and shift in control of evaporation from atmosphere to soil.

Figure 2.4A shows the temperature profile near the surface of the column. The steepest temperature gradient was observed for the 0-1 mm soil layer. The inflection point in the

temperature profile was at approximately 1 mm, suggesting a heat sink and/or a sharp contrast in soil thermal properties [Heitman et al., 2008a]. Calculating heat flux requires a known temperature gradient and λ at the depth of interest. In this study, using the 11-needle HPP, we were able to measure near-surface temperature gradients for 0-1, 1-2 and 2-4 mm layers. Thermal properties of the 0-1 and 1-2 mm layers cannot be measured directly using the HPP because the first heater needle is located at 6 mm depth (6-mm radial distance from the needles at 1 and 2 mm depths) in accordance with geometric constraints imposed by the heat-pulse method [Zhang et al., 2012]. We were, however, able to detect differences in thermal properties of the 0-6, 1-6 and 2-6 mm depth layers based on temperature responses at 0, 1, and 2-mm depths to the heat input from the heater needle at 6 mm depth.

Thermal conductivities of 1.35, 1.45 and 1.51 W/(m^{o}C) were recorded for the 0-6, 1-6 and 2-6 mm layers, respectively. A comparison between λ of the 0-6 mm layer and that of the 2-6 mm layer shows that including the surface 0-2 mm depth increment resulted in significant decrease in bulk λ for the 0-6 mm depth layer. Alternately, λ for the 1-6 mm layer is relatively close to that of the 2-6 mm layer. This suggests that the 0-1 mm layer had much lower λ as compared to the wetter subsurface layer. Thermal resistance of a layer per unit area can be expressed as the ratio of thickness of the layer to the thermal conductivity of the layer. For heat flow perpendicular to soil layers, effective thermal resistance will be equal to the sum of thermal resistance values of constituent layers (analogous to resistance in series). Hence, the effective thermal resistance is equal to the depth-weighted harmonic mean of the thermal conductivities of constituent layers. By assuming λ for the 1-6 mm layer as a depth-

weighted harmonic mean of λ for the 1-2 and 2-6 mm layers, and treating λ for the 1-2 mm layer as the unknown, we estimated λ of the 1-2 mm layer to be 1.22 W/(m^{o}C). Similarly, by assuming λ for the 0-6 mm layer as a harmonic mean of λ for the 0-1, 1-2, and 2-4 mm layers with λ of the 0-1 mm layer unknown, we estimated λ for the 0-1 mm layer to be 0.83 W/(m^{o}C). Thus, a complete near-surface thermal property profile was obtained (Figure 2.4B).

Soil samples were collected destructively from the 0-1 and 1-2-mm soil layers of the experimental soil column under steady-state evaporation conditions. Water content of the collected samples was determined gravimetrically and converted to θ using the column bulk density. Thermal conductivity corresponding to measured θ of the 0-1 mm and 1-2 mm depth layers from the independently obtained λ-θ relationship (Figure 2.3) were 0.75 and 1.05 W/(m^{o}C), respectively. These values were similar to the estimated values of 0.83 and 1.22 W/(m^{o}C), respectively, indicating that the estimated values well represented thermal properties in the "undetectable" near-surface zone described by Sakai et al. [2011].

Evaporation rates estimated using the SHB (Eq. 1) were 0.26 and 0.03 mm/h for the 0.5-1.5 and 1.5-4 mm layers, respectively, with no measureable evaporation in deeper layers (Figure 2.4C). In the full evaporation zone of 0-4 mm, 90% of evaporation occurred in the 0.5-1.5 mm layer, which corresponds with the inflection point in the temperature profile (Figure 2.4A). This peak rate of evaporation within the 0-2 mm layer indicates that the downward

migration of the DSL was restricted by the constant water supply from the relatively shallow water table.

The depth-integrated evaporation rate (i.e., summation of evaporation rate for all depth increments) estimated by the SHB approach was 0.29 mm/h (ranging 0.25-0.35 mm/h) for the 0.5-4 mm layer during the 48 h observation period. This was close to the average evaporation rate of 0.28 mm/h (ranging 0.26-0.32 mm/h) determined by the mass balance approach, with a difference of only 0.01 mm/h. These results, which constitute the first test of the SHB approach under controlled laboratory conditions, support less precise tests under field conditions [Heitman et al., 2008 b, c; Xiao et al., 2011], as well as numerical studies for isothermal and non-isothermal conditions [Sakai et al., 2011], and demonstrate that the SHB approach is accurate for measuring the *in situ*, subsurface evaporation rate.

2.3.2 Transient Evaporation

As described before, for the transient experiment, the water supply was disconnected and the heat emitter was turned on at time 0. Immediately after turning on the heat emitter, a high mass-balance evaporation rate of 0.61 mm/h, comparable to pan evaporation rate of 0.7 mm/h, was recorded in the first hour. The mass-balance evaporation rate dropped to 0.38 mm/h by 5 h (Figure 2.5) and remained nearly constant until approximately 40 h. Experimental conditions essentially resulted in very short-lived stage-1 type conditions (< 2 h) followed by a period of near-constant stage-2 evaporation (2 to 40 h), buoyed by water storage in the bottom of the column. The initial condition of a drained profile with water

table at 29 cm left 5 cm of saturated soil at the bottom of the column. This provided a water supply for maintaining the evaporation front close to the surface, but the rate at which water was supplied was not enough to maintain evaporation at potential rate. This resulted in a near-constant, soil-limited evaporation from 2 to 40 h and prolonged the period before transient falling-rate evaporation was observed. The soil surface became visibly dry around 30 h into the drying period. A steep decrease in evaporation rate was observed from 40 h to 78 h with evaporation rates decreasing from 0.33 to 0.14 mm/h. A relatively low and constant evaporation rate (approximately 0.14 mm/h) was observed from 78 to 90 h (when measurements were discontinued), possibly indicating stage-3 evaporation.

Figure 2.6A shows soil temperature profiles for the 0-18 mm layer at different times during the transient evaporation experiment. The shape of the temperature profile remained almost constant from 1 to 10 h with approximately 3.5°C increase in ambient temperature. About 1°C increase in temperature was observed from 10 to 30 h. A comparison between 30 and 40 h shows that the temperature profile for 0-2 mm depth layer became steeper at 40 h. This change in soil temperature profile at 40 h coincides with the beginning of a steep decrease in mass-balance evaporation rates (Figure 2.5). The temperature profile for the 2-6 mm depth layer is steeper at 50 h as compared to that at 40 h. The temperature profile in the 6-12 mm depth zone became relatively steep at 70 h as compared to that at 50 h. The soil temperature profile remained almost the same from 80 to 90 h. This coincides with the low, constant mass-balance evaporation rate during this period (Figure 2.5).

For the steady-state evaporation experiment (previous section), the thermal property profile remained constant with time, which allowed precise λ estimates by repeated heat-pulse measurements under the same conditions. Similar efforts under transient conditions produced inconsistent results. So, for the transient experiment, heat-pulse estimated λ for the 0-6 and 1-6 mm layers were used directly for heat flux calculations at 0.5 mm and 1.5 mm depths following Zhang et al. [2012]. Near-surface λ profiles at different times during transient evaporation experiment are shown in Figure 2.6B. The data show a decreasing trend in near-surface λ with drying from 10 to 90 h. At 10 h, λ ranged from approximately 0.76 W/(m^{o}C) in the surface 2 mm to 1.4 W/(m^{o}C) for 4 mm and deeper. From 10 to 20 h, λ at 4 mm and deeper decreased by approximately 0.2 W/(m^{o}C), whereas the respective decrease in λ was only 0.08 W/(m^{o}C) for the upper 2 mm depth. A more pronounced decline in λ was observed from 20 to 30 h with about 0.3 W/(m^{o}C) decrease in λ in the 0-12 mm layer. Thereafter, λ continued to decrease, though more subtly, from 30 to 80 h. After 40 h, the λ for 0-2 mm was very low (0.45 W/(m^{o}C)), equivalent to a θ of approximately 0.01 m^3/m^3 (Figure 2.3), indicating an almost air-dry 0-2 mm layer from 40 h onwards. The λ profile remained almost constant from 80 to 90 h corresponding to the period of low and constant mass-balance evaporation.

Using temperature and λ profiles shown in Figure 2.6, total subsurface evaporation rates of 0.21 and 0.28 mm/h were observed at 28 and 32 h, respectively. These values were lower than the mass-balance evaporation rates of 0.35 and 0.34 mm/h at the same times,

respectively. These data indicate that at 28 and 32 h, some evaporation was still taking place at the surface or shallower than the 0.5 mm depth. An increasing proportion of evaporation originating from the subsurface with progressive drying (0.21 mm/h at 28 h and 0.28 mm/h at 32 h) suggests a transition from surface to subsurface (depth > 0.5 mm) evaporation.

Figure 2.7 shows SHB estimated subsurface evaporation rates in comparison to mass evaporation at 40 h and thereafter. Total subsurface evaporation rates estimated by the SHB approach were 0.36, 0.23, 0.17, and 0.14 mm/h at 40, 56, 66, and 78 h, respectively, which were close to the mass evaporation rates of 0.33, 0.21, 0.18, and 0.14 mm/h observed at the same times, respectively. This period corresponded to the falling rate evaporation stage indicated by a steep fall in mass-balance evaporation rates between 40 and 78 h. At 40 h, the SHB estimated evaporation rate (0.36 mm/h) originated from the 1.5-4 mm depth layer indicating a very narrow evaporation zone close to the surface (Figure 2.8). With further drying of the soil, the evaporation front moved deeper and widened from 40 to 66 h, eventually reaching a very low evaporation rate of 0.14 mm/h at 78 h with 77% of evaporation occurring in the 9-15 mm depth layer. Later at 84 h, the sub-surface evaporation rate stayed the same as that observed at 78 h (possibly indicating stage-3 evaporation) but the evaporation front narrowed, with all of the sub-surface evaporation occurring in the 9-15 mm layer.

Comparison of the SHB estimated evaporation with mass balance data shows that there was a transition from surface to sub-surface evaporation, with some evaporation occurring below

0.5 mm depth at 28 h and 38 h. After 40 h, the SHB estimated evaporation was close to the mass-balance evaporation, indicating that evaporation was taking place entirely within the subsurface (below 0.5 mm depth). This suggests that there was a loss of liquid water connectivity to the surface at about 40 h or possibly earlier. This agrees with suggestions by Idso et al. [1974] about the loss in liquid water connectivity to the surface at the beginning of falling rate evaporation (stage 2). After this time period, the SHB approach effectively estimated subsurface evaporation with only 0.01 to 0.03 mm/h difference between SHB and mass balance. The SHB approach also provided an estimate of the evaporation profile and showed the dynamics of the evaporation front at mm-scale over a drying event, which has not been demonstrated before, except with numerical modeling [e.g., Novak, 2010].

2.3.3 Estimation of the Thickness of the Dry Surface Layer

The undetectable zone close to soil surface remains a challenge in studying energy and mass transfer with the SHB approach in the highly dynamic near-surface zone [Sakai et al., 2011]. It may not be possible to directly measure thermal properties of this undetectable near-surface zone with sensor designs implemented to date. In the present experiment, we were able to detect the differences in λ of the 0-6 mm, 1-6 mm and 2-6 mm depth zones using an 11-needle HPP. For steady-state evaporation conditions, λ profiles remained constant with time, so we were able to further make repeated heat-pulse measurements for estimating λ of different layers. We were also able to test these estimates via destructive sampling. Under transient conditions, however, a similar exercise is cumbersome and probably not feasible.

To further evaluate the implications of heat-pulse estimated thermal properties under transient conditions, we consider an approximate structure for the DSL and underlying soil. After formation of a DSL, the near-surface soil layer is approximately comprised of two different zones of contrasting water content and thermal properties (Figure 2.9). We refer to this near-surface layer as a transition layer where the distributions of moisture and thermal properties are varying rapidly with drying, i.e., the thickness of the DSL changes rapidly under transient conditions. Estimated thickness of the DSL at a given time during a drying period can give important information about the dynamics of the subsurface evaporation front and possible mechanisms for heat transfer.

The near-surface soil layer (transition layer with thickness z_{trans}) can be divided into two zones, a DSL of thickness z_{dry} and a wet subsurface layer of thickness z_{wet}, so that $z_{trans} - z_{wet} = z_{dry}$ (Figure 2.9). Thermal conductivity of the near-surface transition layer (λ_{trans}) can be expressed as the depth weighted harmonic mean of λ of the constituent layers (as described in section 3.1):

$$\frac{z_{trans}}{\lambda_{trans}} = \frac{z_{dry}}{\lambda_{dry}} + \frac{z_{wet}}{\lambda_{wet}} \qquad [2]$$

where, subscripts dry and wet indicate properties for dry and wet layers, respectively.

We estimated λ_{trans} from the bulk heat-pulse measurements in the near-surface layer, i.e., 0-6 mm depth. Thermal conductivity for the wet subsurface layer was estimated from heat-pulse

measurements at the bottom boundary of the transition layer, i.e., 6-12 mm depth. Thermal conductivity of the DSL (λ_{dry}) was estimated from independent measurements of dry soil at the same bulk density. The thickness of the DSL (z_{dry}) could then be calculated from Eq. [2] and heat-pulse measurements collected throughout the evaporation experiments. Kluitenberg et al. [2010] suggested that λ measured by heat-pulse sensors may be more robust than heat capacity and thermal diffusivity measurements (i.e., less sensitive to needle spacing change). Thus we used measured λ for estimation of DSL thickness instead of considering other thermal properties. The estimation of thickness of DSL by Eq. [2] is independent of evaporation profiles determined from the SHB (described in previous sections) but both are related by using the same heat-pulse determined thermal properties in calculations.

The thickness of the DSL calculated for the steady-state evaporation experiment was about 1 mm, which indicates that the evaporation front remained close to the soil surface. The subsurface evaporation estimated by the SHB approach also indicates that about 90% of total evaporation occurred in the 0.5-1.5 mm depth layer. Figure 2.9 shows the estimated z_{dry} during transient evaporation measurements. The estimated z_{dry} at 18 h was close to zero indicating water connectivity to the soil surface. Estimated z_{dry} reached 1 mm at 28 h and about 2 mm at 40 h. This agrees with the subsurface evaporation of 0.36 mm/h occurring in the 1.5-4 mm layer as estimated by the SHB approach at 40 h (Figure 2.8). With progressive drying the evaporation front moved deeper and the estimated z_{dry} increased to 3.3 mm at 56 h, and eventually reached 5 mm at 84 h.

Sensible heat balance evaporation profiles show that evaporation was mainly occurring below the estimated depth of the DSL for our experimental conditions. This agrees with previous studies indicating that vaporization of water occurs at the bottom boundary of the DSL [Hillel, 1971; Campbell, 1985; Yamanaka et al. 1998] and liquid water connectivity to the surface is lost at the beginning of falling rate/stage-2 evaporation [Idso et al., 1974].

2.3.4 Diffusive Vapor Flux during Transient Stage-2 Evaporation

We estimated diffusive water vapor flux for stage-2 evaporation from 40 h onwards in the transient experiment, i.e., for the period when SHB subsurface evaporation profiles indicated that all the evaporation was occurring in the subsurface (Figure 2.8). The diffusive vapor flux (J) was calculated according to Fick's Law (Eq. 3) using DSL thickness estimated in the preceding section and the diffusion coefficient model for dry porous media given by Millington [1959]:

$$J = \varepsilon^{4/3} D \frac{e_{soil} - e_{air}}{z_{\mathrm{dry}}} \qquad [3]$$

where, ε is the soil air-filled porosity, D is the diffusion coefficient of vapor in free air (2.57×10^{-5} m^2/s), e_{soil}= 3.03 x 10^{-2} kg/m^3 is water vapor density at the drying front, and e_{air} = 5.2×10^{-3} kg/m^3 is water vapor density in the air above the column at ambient air temperature (20°C) and humidity (30%).

Figure 2.7 shows that calculated *J* closely matches evaporation determined by the SHB and mass balance approaches during transient stage-2 evaporation. This further supports results from the SHB indicating that liquid water connection to the surface is lost early in the falling rate stage of evaporation (stage 2). Studies under isothermal conditions also showed "jumps" in the evaporation plane from the surface to the subsurface at the end of stage 1, but liquid water connectivity to the surface was reported to be lost at the onset of low, constant rate evaporation [Shokri and Or, 2011]. These "jumps" were reported to be affected primarily by porous media properties. However, under non-isothermal conditions, we observed steep temperature gradients in the near surface as compared to the underlying subsurface layers, in agreement with previous studies [Heitman et al., 2010, Xiao et al., 2011, Zhang et al., 2012]. This sharp temperature gradient suggests the importance of energy transfer driven by the radiation boundary condition, which may drive the formation and downward migration of the DSL for non-isothermal conditions.

Together, our observations suggest that under non-isothermal conditions, the DSL forms early in the falling rate stage of evaporation. Evaporation then occurs in the subsurface. The zone of subsurface evaporation is narrow and close to the surface at the beginning (Figure 2.8). With progressive drying, the thickness of the DSL increases (Fig. 2.9) and the evaporation front moves deeper and widens, eventually becoming narrow again at the end of the falling rate stage (Figure 2.8). It is evident that under non-isothermal conditions, temperature gradients in addition to hydraulic properties of porous media play an important role in evaporation dynamics, resulting in relatively quick drying of the soil surface and

formation of a DSL early in falling rate evaporation. After formation of a DSL, evaporation occurs in the sub-surface and evaporated water is transferred to the atmosphere via vapor diffusion through the DSL. These results are consistent with a number of previous reports [e.g. Hillel, 1971; Idso et al., 1974; Hillel, 1980; Campbell, 1985, de Vries and Philip, 1986; Mayocchi and Bristow, 1995; Yamanaka et al., 1997; Yamanaka et al., 1998; Heitman et al., 2008b,c; Shokri et al., 2009, Heitman et al., 2010; and Novak, 2010], but differ from recent studies suggesting loss of hydraulic connection to the surface at the onset of stage 3 for isothermal conditions [e.g., Shokri and Or, 2011].

2.4 Summary and Conclusions

Non-isothermal evaporation is a complex process involving both mass and energy transfer. To date, understanding of the transition between atmospherically controlled and late stage evaporation remains limited. The results from our study show that the SHB approach effectively estimated the subsurface evaporation rate with only 0.01-0.03 mm/h difference from the mass balance evaporation rate under steady-state as well as transient stage-2 evaporation conditions. The SHB approach also provided measurement-based quantification of subsurface, non-isothermal evaporation profiles (i.e., the distribution of the evaporation zone) at mm-scale under transient conditions over a drying event. Subsurface evaporation matched mass balance in the early falling rate stage, indicating a loss in liquid water connectivity to the surface. Further studies under a wider range of textures and under natural radiation conditions can improve our knowledge of soil water evaporation, especially at the

onset and during falling rate evaporation when the evaporation front shifts from the surface to the subsurface.

It remains challenging to directly measure thermal properties of the "undetectable" zone near the soil surface. However, the observed ability of HPPs to detect differences in thermal properties of 0-6 mm, 1-6 mm and 2-6 mm depth zones in the present experiments opens the possibility of a measurement-based estimate of thermal property profiles for the highly dynamic near-surface zone. We used heat-pulse measurements along with independent measurements of λ for dry soil to continuously estimate the thickness of the DSL over a drying period. The estimated thickness of the DSL was used to compute diffusive vapor flux with Fick's Law, which closely matched the mass balance evaporation and subsurface evaporation estimated by the SHB approach.

Measurement-based estimates of near-surface thermal property profiles, DSL thickness, and the capability of the SHB approach to estimate mm-scale evaporation profiles provides an opportunity to test existing theories and can help in developing new models capable of precise estimates of near-surface energy and mass transfer occurring at the land surface. The improved knowledge about the soil water evaporation process and near-surface energy and mass transfer will influence research and understanding of various natural processes occurring at wide range of scales (e.g., microclimate for seeds and microbes in the near-surface to large scale hydrologic and climatic patterns), and has a wide range of applications, such as agricultural and forestry water management and conservation, evaporation from

landfill covers, industrial drying processes and vapor fluxes of various substances from the land surface.

2.5 References

Arya, L.M., D.C. Bowman, B.B. Thapa, and D.K. Cassel (2008), Scaling soil water characteristics of golf course and athletic field sands from particle size distribution, *Soil Sci. Soc. Am. J.*, 72, 25-32, doi: 10.2136/sssaj2006.0232.

Arya, L.M., J.L. Heitman, B.B. Thapa, and D.C. Bowman (2010), Predicting saturated hydraulic conductivity of golf course sands from particle-size distribution, *Soil Sci. Soc. Am. J.*, 74, 33-37, doi: 10.2136/sssaj2009.0022.

Bittelli, M., F. Ventura, G.S. Campbell, R.L. Snyder, F. Gallegati, and P.R. Pisa (2008), Coupling of heat, water vapor, and liquid water fluxes to compute evaporation in bare soils, *J. Hydrol*., 362, 191-205, doi:10.1016/j.jhydrol.2008.08.014.

Bristow, K. L., G. J. Kluitenberg and R. Horton (1994), Measurement of soil thermal properties with a dual-probe heat-pulse technique, *Soil Sci. Soc. Am. J*., 58, 1288-1294.

Brutsaert, W. and D. Chen (1995), Desorption and the two stages of drying of natural tallgrass praire, *Water Resour. Res*., 31, 1305-1313.

Campbell, G.S. (1985), *Soil Physics with Basic Transport Models for Soil-Plant System*. Elsevier, New York.

Campbell, G.S., C. Calissendorff, and J.H. Williams (1991), Probe for measuring soil specific heat 2 using a heat-pulse method, *Soil Sci. Soc. Am. J.*, 55, 291-293.

Chung, S. O., and R. Horton (1987), Soil heat and water flow with a partial surface mulch, *Water Resour. Res.*, 23, 2175-2186.

Feddes, R.A. (1971), Water, heat and crop growth, PhD thesis, Comm. Agric. Univ., Institute of Land and Water Management Research, Wageningen, 184pp.

Gardner, H. R. and R. J. Hanks (1966), Evaluation of the evaporation zone in soil by measurement of heat flux, *Soil Sci. Soc. Am. J.*, 30, 425-428.

Heitman, J., R. Horton, T. Ren, I. Nassar, and D. Davis (2008a), A test of coupled soil heat and water transfer prediction under transient boundary temperatures, *Soil Sci. Soc. Am. J.*, 72, 1197–1207.

Heitman, J.L., R. Horton, T.J. Sauer, and T.M. DeSutter (2008b), Sensible heat observations reveal soil-water evaporation dynamics, *J. Hydromet*., 9, 165-171.

Heitman, J.L., R. Horton, T.J. Sauer, T.S. Ren, and X. Xiao (2010), Latent heat in soil heat flux measurements, *Ag. Forest. Met.*, 150, 1147-1153.

Heitman, J.L., X. Xiao, R. Horton, and T.J. Sauer (2008c), Sensible heat measurements indicating depth and magnitude of subsurface soil water evaporation, *Water Resour. Res.*, 44, W00D05. doi:10.1029/2008WR006961.

Hillel, D. (1971), *Soil and Water: Physical Principles and Processes*. Academic Press, New York.

Howard, A., J.L. Heitman, D. Bowman (2010), A Simple Approach for Demonstrating Water Retention and Field Capacity, *J. Nat. Res. Life Sci. Ed.*, 39, 120-124.

Idso, S.B., R.D. Jackson, and R.J. Reginato (1975), Estimating evaporation: A technique adaptable to remote sensing, *Science*, 189, 991-992.

Idso, S.B., R.J. Reginato, R.D. Jackson, B.A. Kimball, and F.S. Nakayama (1974), The three stages of drying of a field soil, *Soil Sci. Soc. Am. Proc.*, 38, 831-837.

Jalota, S.K. and S.S. Prihar (1998), *Reducing soil-water evaporation with tillage and straw mulching*. Iowa State University Press, Ames (ISBN 0-8138-2857-0), p. 142.

Kimball, B.A. (1973), Water vapor movement through mulches under field conditions, *Soil Sci. Soc. Am. Proc.*, 37, 813−818.

Kluitenberg, G.J., T. Kamai, and J.A. Vrugt (2010), Effect of Probe Deflection on Dual-Probe Heat-Pulse Thermal Conductivity Measurements, *Soil Sci. Soc. Am. J.*,74(5), 1537-1540.

Knight, J.H. and G.J. Kluitenberg (2004), Simplified computational approach for the dual-probe heat-pulse method, *Soil Sci. Soc. Am. J.*, 68, 447-449.

Lemon, E. R. (1956), The potentialities for decreasing soil moisture evaporation loss, *Soil Sci. Soc. Am. Proc.*, 20, 120-125.

Liu, B.C., W. Liu, S.W. Peng. (2005), Study of heat and moisture transfer in soil with a dry surface layer, *International Journal of Heat and Mass Transfer*, 48 (21–22), 4579-4589.

Mayocchi, C.L., and K.L. Bristow (1995), Soil surface heat flux: some general questions and comments on measurements, *Ag. Forest Meteor*. 75, 43-50.

Millington, R.J. (1959), Gas diffusion in porous media,. *Science*, 130, 100–102.

Novak, M.D. (2010), Dynamics of the near-surface evaporation zone and corresponding effects on the surface energy balance of a drying bare soil, *Ag. Forest Meteor*., 150, 1358-1365.

Ochsner, T.E., T.J. Sauer, and R. Horton (2007), Soil heat storage measurements in energy balance studies, *Agron. J*., 99, 311-319.

Philip, J.R., and D.A. de Vries (1957), Moisture movement in porous materials under temperature gradients. Transactions, American Geophysical Union, 38(2), 222-232.

Sakai, M., S.B. Jones, and M. Tuller (2011), Numerical evaluation of subsurface soil water evaporation derived from sensible heat balance. *Water Resour. Res*., 47, W02547.

Shokri, N., and D. Or. (2011), What determines drying rates at the onset of diffusion controlled stage-2 evaporation from porous media? *Water Resour. Res*., 47, W09513.

Shokri, N., and G.D. Salvucci (2011), Evaporation from porous media in the presence of a water table. , *Vadose Zone J*., 10, 1-10.

Shokri, N., P. Lehmann, and D. Or (2009), Critical evaluation of enhancement factors for vapor transport through unsaturated porous media,. *Water Resour. Res*., 45, WR007769.

Snyder, R.L., K. Bali, K., F. Ventura, F., and H. Gomez-Macpherson, (2000), Estimating evaporation from bare or nearly bare soil., *J. Irrig. Drain. Eng*., 126 (6), 399–403.

Ventura, F., B. Faber, K. Bali, R.L. Snyder, D. Spano, P. Duce, and K.F. Schulbach, (2001), A model for estimating evaporation and transpiration from row crops, *J. Irrig. Drain. Eng*., 127 (6), 339-345.

Xiao, X., R. Horton, T. Sauer, J.L. Heitman, and T. Ren (2011), Cumulative soil water evaporation as a function of depth and time, *Vadose Zone J*., 10, 1016-1022.

Yamanaka, T., and J. Shimada, (1997), Simple but reliable method to extract soil water for stable isotope analysis, *Journal of Japan Society of Hydrology and Water Resources*, 10, 181-184 in Japanese with English abstract.

Yamanaka, T. and, T. Yonetani (1999), Dynamics of the evaporation zone in dry sandy soils, *J. of Hydrol.*, 217(1–2), 135-148.

Yamanaka, T., A. Takeda, and J. Shimada (1998), Evaporation beneath the soil surface: Some observational evidence and numerical experiments. , *Hydrol. Process.*, 12, 2193-2203.

Zhang X., J.L. Heitman, R. Horton, and T. Ren (2012), Measuring subsurface soil-water evaporation with an improved heat-pulse probe. *Soil Sci. Soc. Am. J.*, 76, 876-879.

Table 2.1 Particle size distribution, bulk density and saturated hydraulic conductivity of the soil used in the study. Size separate classifications are according to USDA-NRCS system. (After Arya et. al. [2008])

Particle diameter, mm									
0.002	0.002-0.053	0.053-0.106	0.106-0.180	0.180-0.250	0.250-0.355	0.355-0.500	0.500-0.710	0.710-1.000	1.000-2.000
Clay	Silt	Very Fine Sand	Fine Sand		Medium Sand		Coarse Sand		Very Coarse Sand
----------% particles by weight----------									
0	0	2.1	6.9	11.6	29.7	27.2	14.3	6.1	2.2

Bulk Density, g/cm	1.65
Saturated Hydraulic Conductivity , m/h	2.8

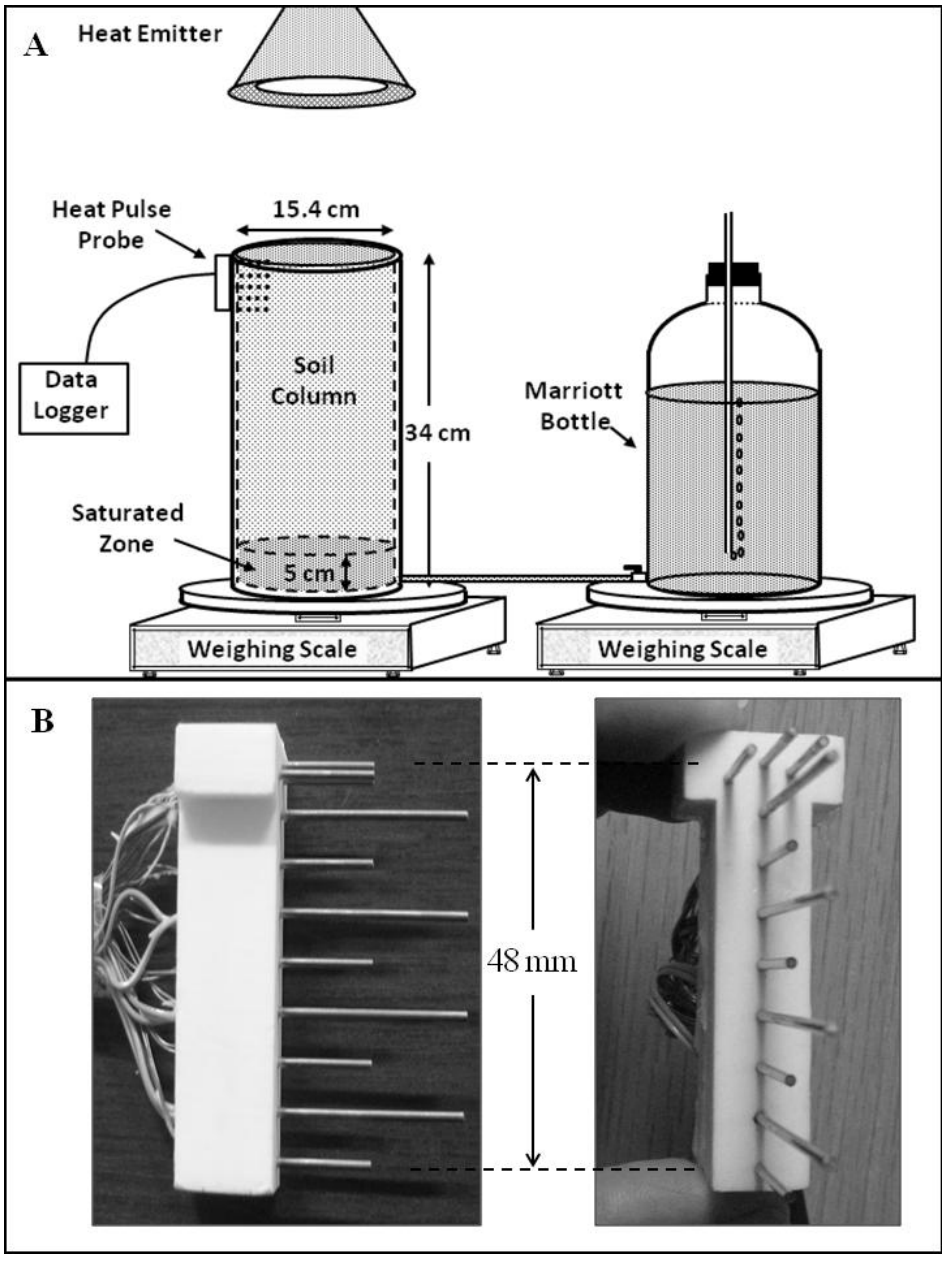

Figure 2.1 (A) Set-up for soil column experiments. The Marriott bottle was disconnected for transient experiments. (B) Multi-needle heat-pulse probe used in the experiments. All 11 needles contain thermocouples. The four long needles also contain a resistance heater. Spacing between adjacent needles is 6-mm for needles positioned along the vertical midline of the probe. The upper three needles are spaced at 1-mm increments vertically; each of the three uppermost needles is at 6 mm radial spacing from the uppermost heater needle.

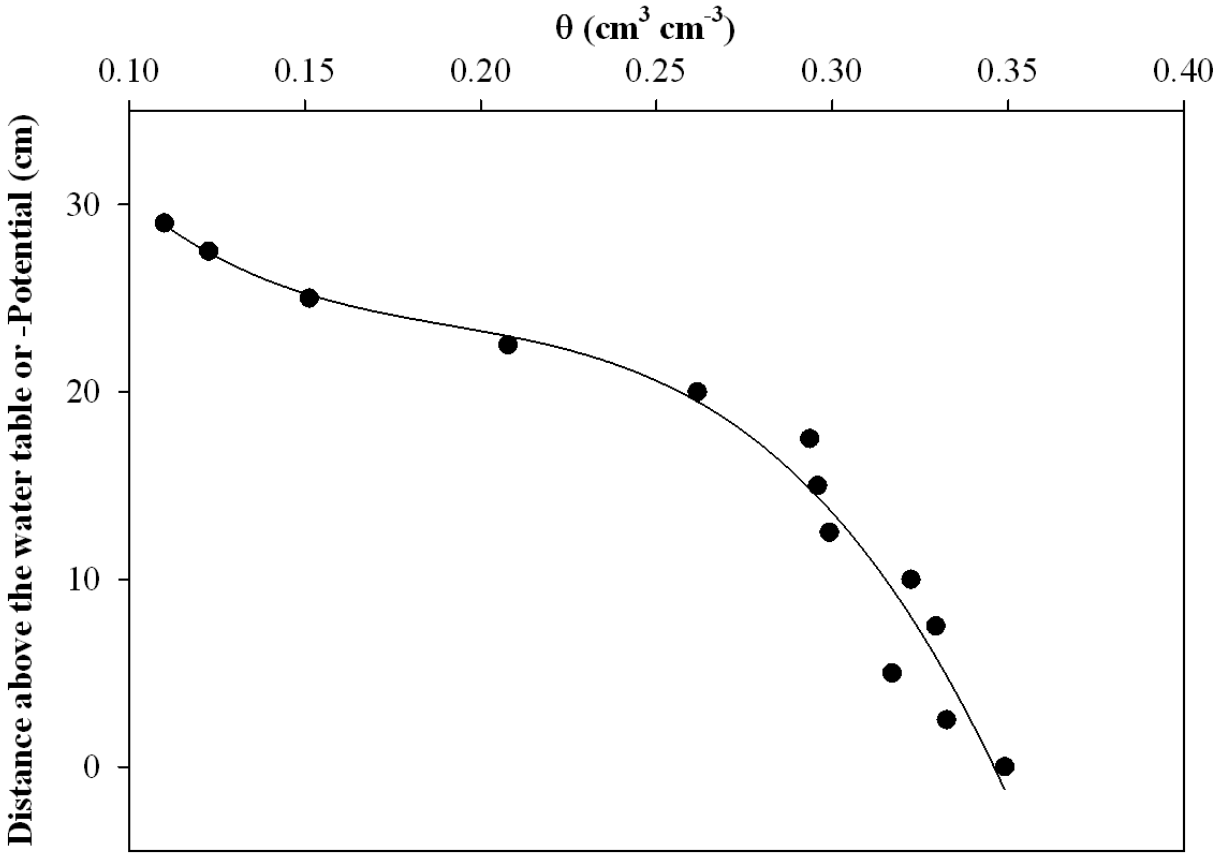

Figure 2.2 Initial volumetric water content (θ) at different depths in the drained column with water table at 29 cm depth. These data also correspond to water retention for the 0 to -30 cm potential range.

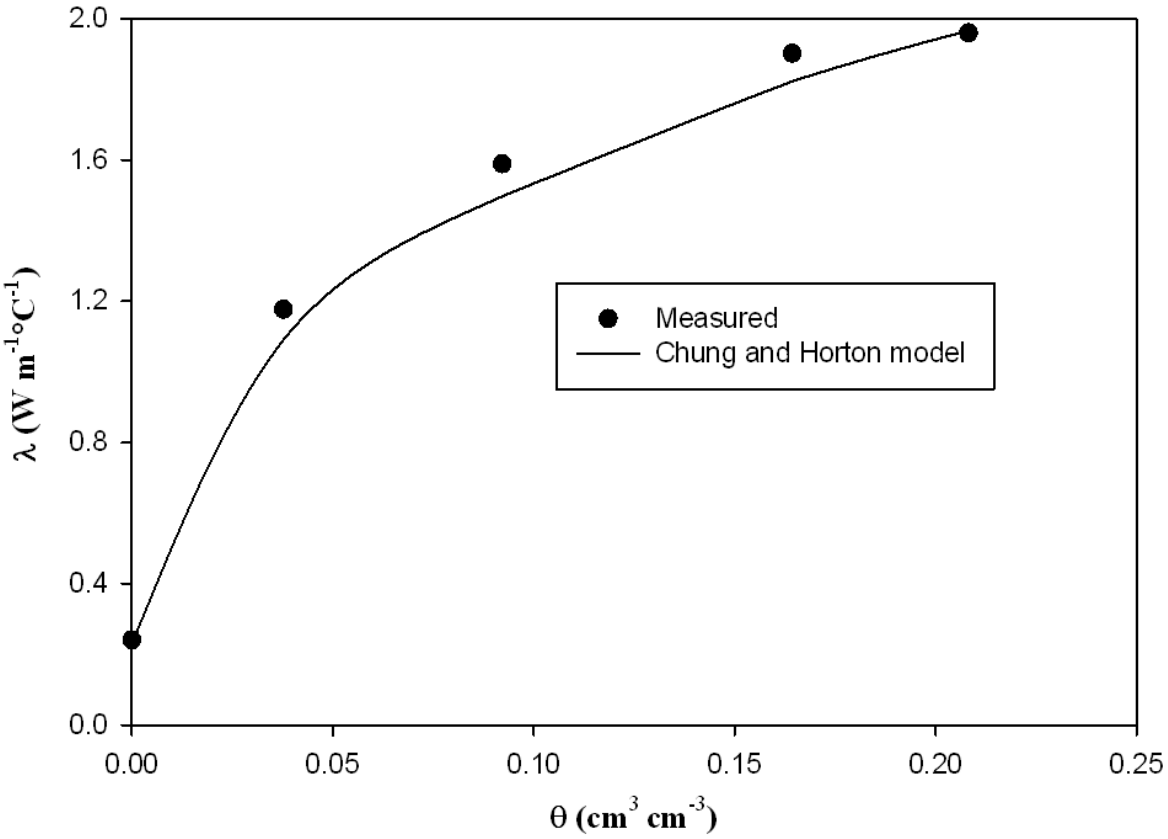

Figure 2.3 Soil thermal conductivity (λ) as it varies with water content (θ) for the soil used in the experiments. Measurements were collected at bulk density = 1.65 g cm^{-3}. The Chung and Horton (1987) model for sandy soil is shown for comparison.

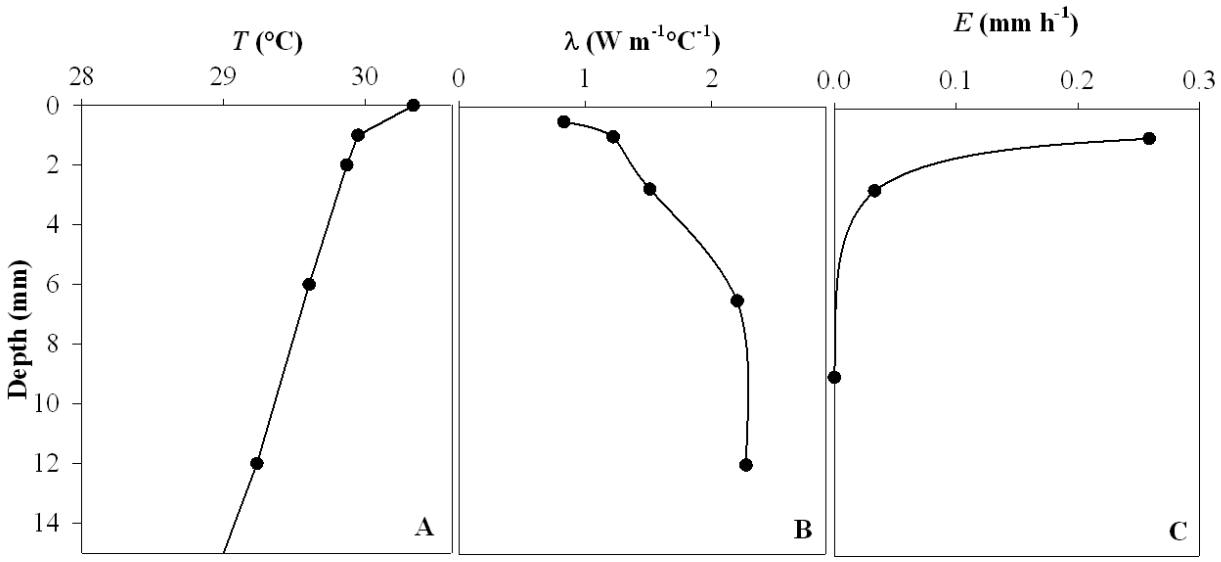

Figure 2.4 (A) Temperature (T) profile during steady-state evaporation. Note that temperature at the lower boundary (34 cm depth, not shown) was maintained at 20°C for the entire duration of the study. (B) Thermal conductivity (λ) profile during steady-state evaporation measured with the heat-pulse method. Values for the 0-1 and 1-2 mm depth increments were estimated as described in the text. (C) Steady-state subsurface evaporation (E) from different depth layers determined by the sensible heat balance approach during the constant rate evaporation.

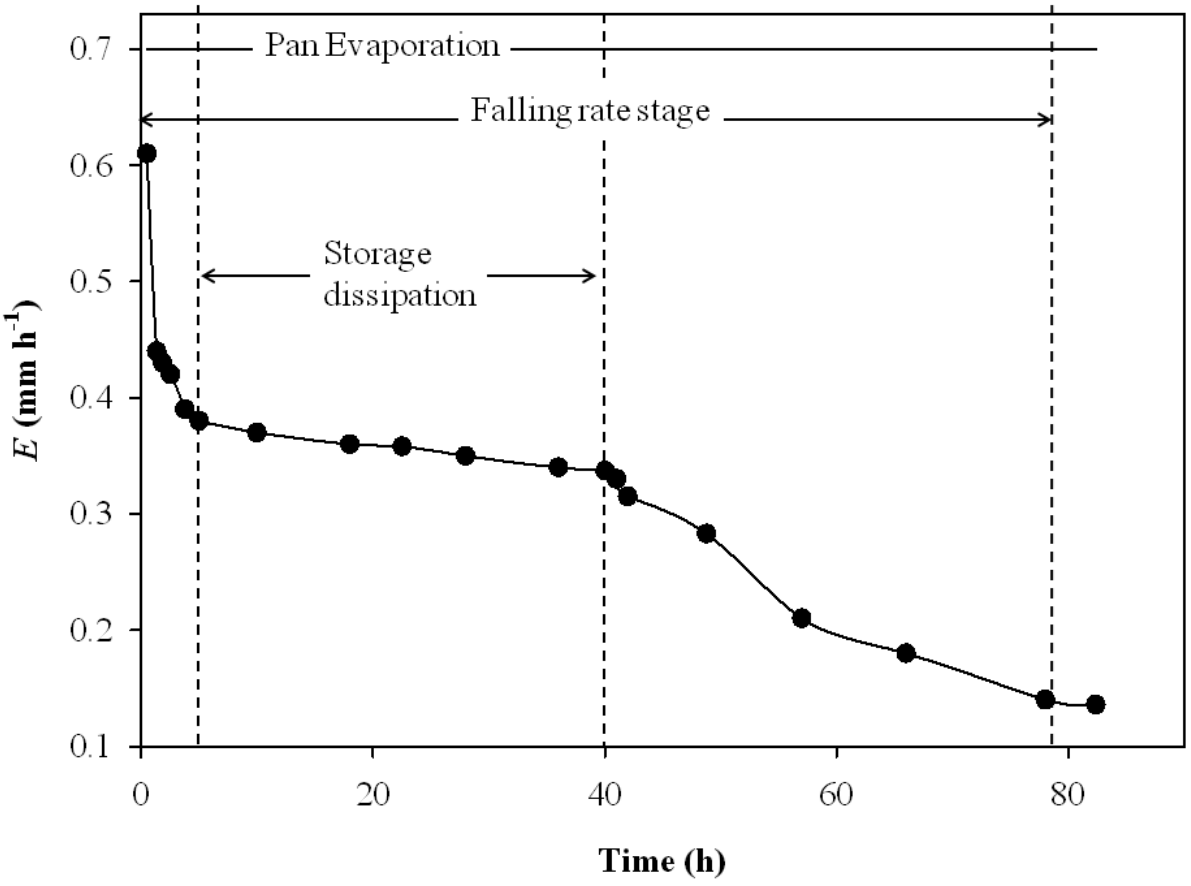

Figure 2.5 Evaporation (E) from the soil column determined by mass balance during transient evaporation.

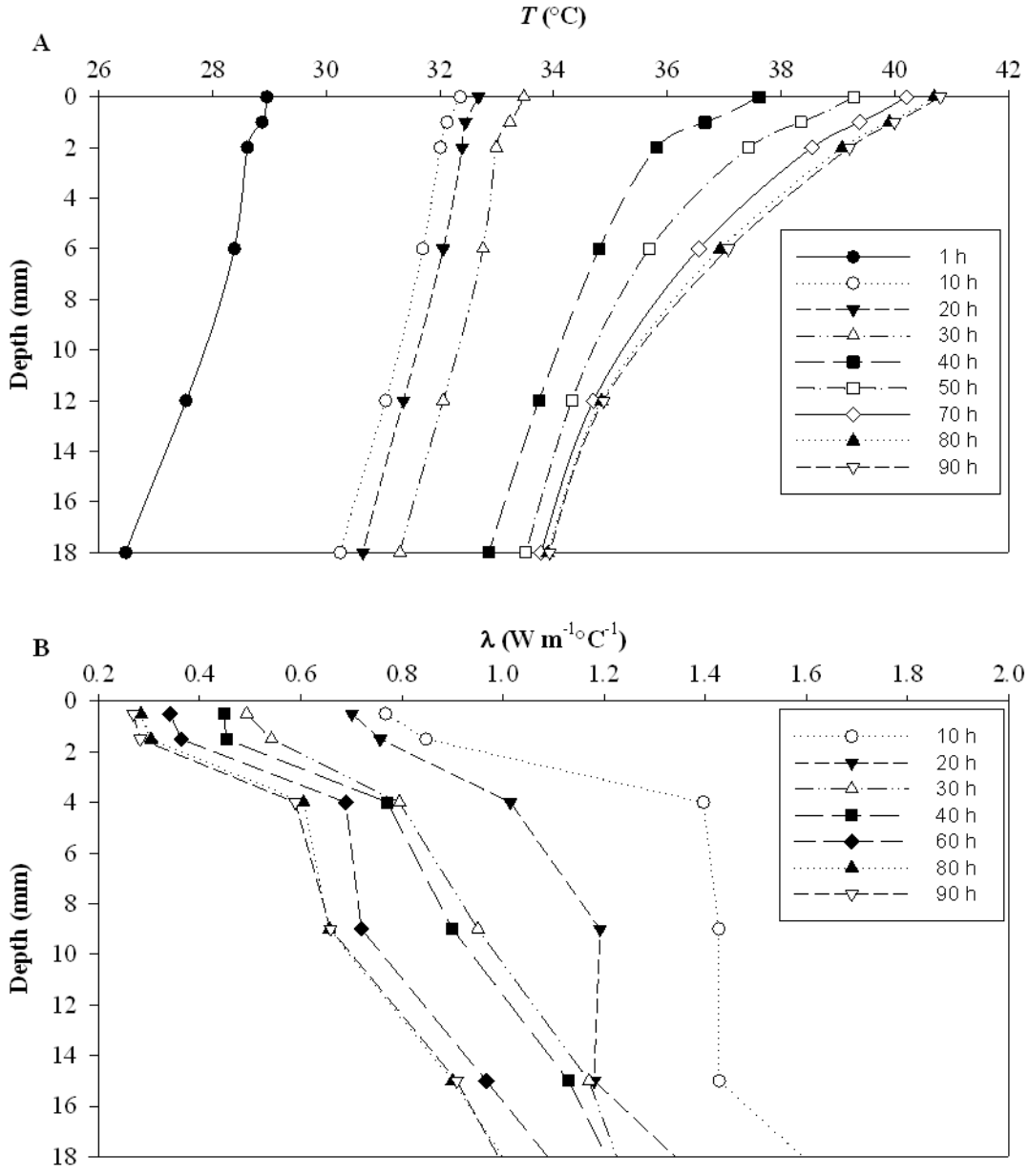

Figure 2.6 (A) Near-surface soil temperature (T) profiles during transient evaporation. Note that T at the lower boundary (34 cm depth, not shown) was maintained at approximately 20°C for the duration of the study. (B) Measured thermal conductivity (λ) during transient evaporation.

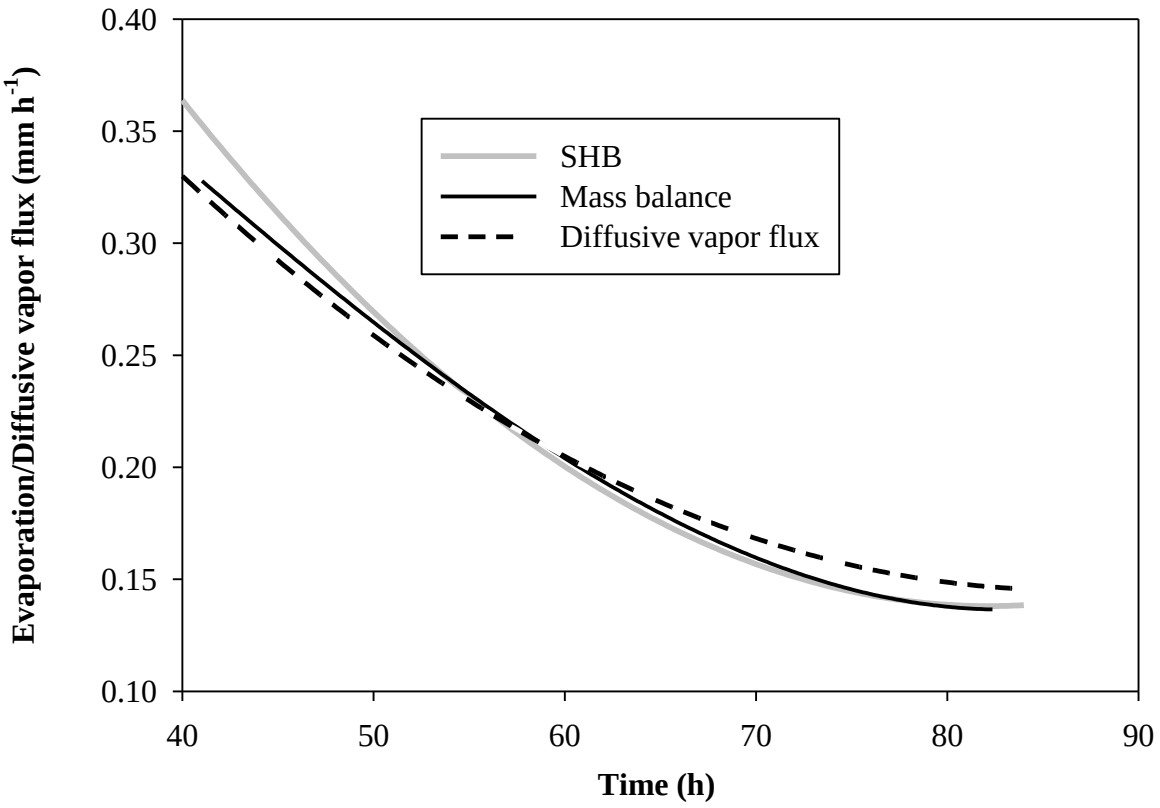

Figure 2.7 Evaporation rate determined by the sensible heat balance (SHB) and mass balance approaches and diffusive vapor flux during the transient stage-2 evaporation.

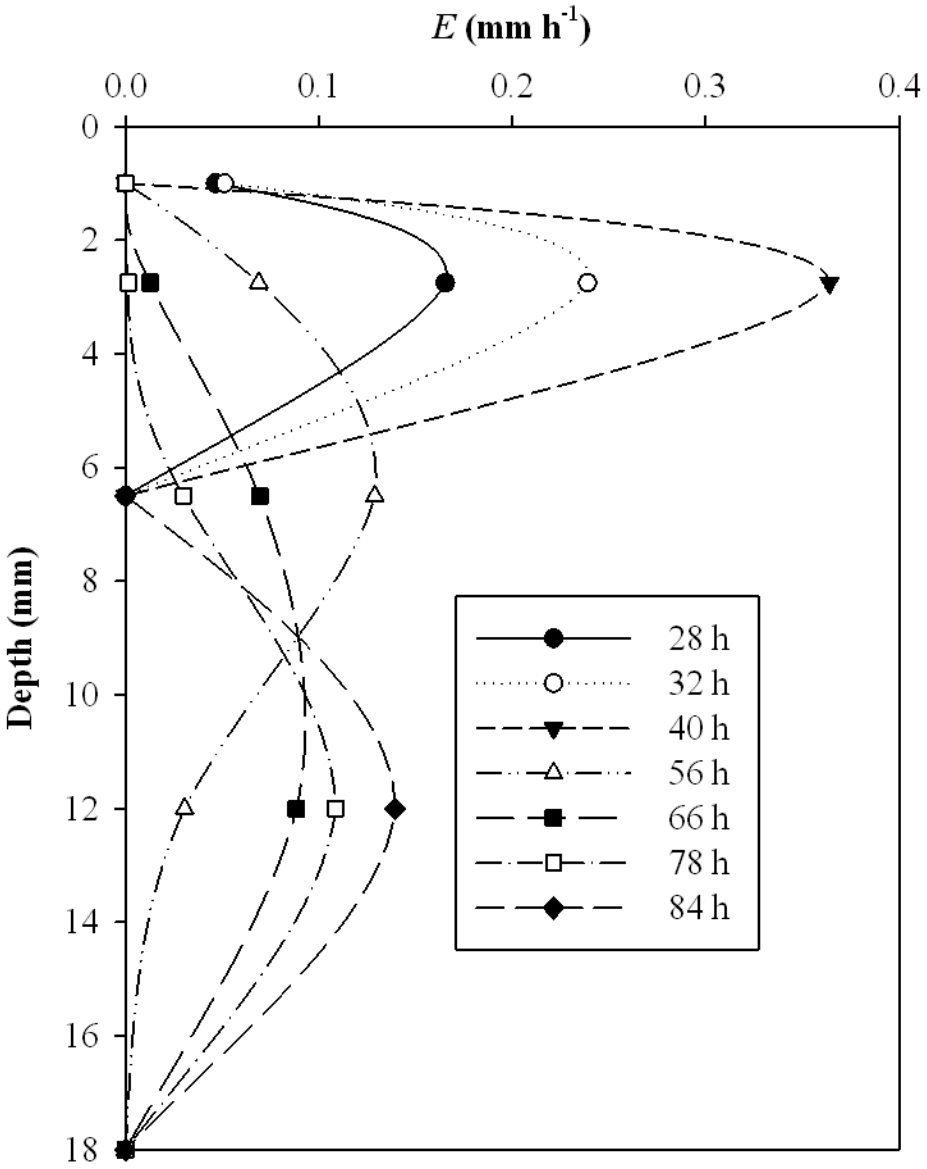

Figure 2.8 Sensible heat balance estimated sub-surface, evaporation (E) profiles at different times during transient evaporation.

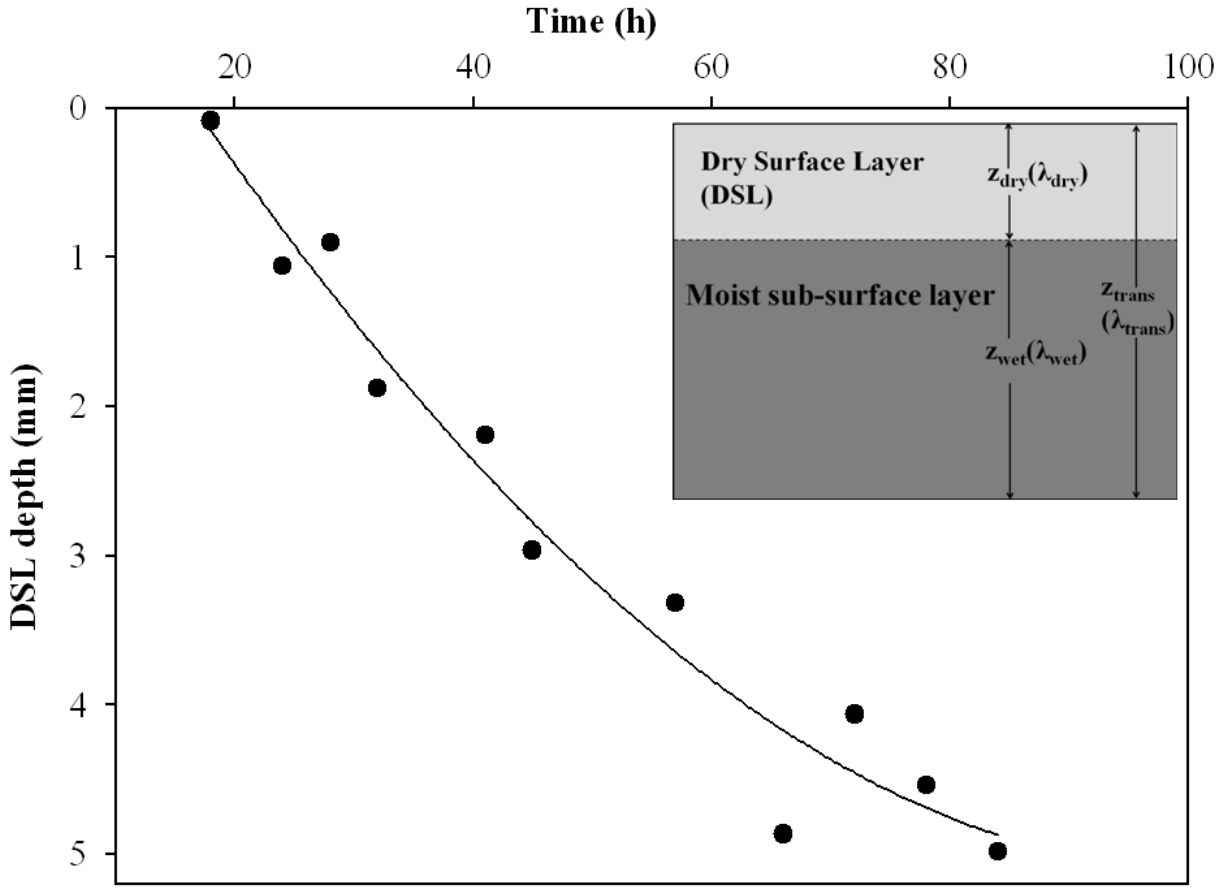

Figure 2.9 Estimated thickness of the dry surface layer (DSL) during transient evaporation. The line indicates the approximate trend. Inset: Conceptual structure of near-surface transition layer used for estimating thickness of the dry surface layer (DSL) with thickness (z) and thermal conductivity (λ).

3. Inception and Magnitude of Subsurface Evaporation in a Bare Field

Abstract

Net radiation at the soil surface is partitioned between sensible and latent heat. Evaporation from a wet soil occurs at the soil surface. The soil surface dries when a wet soil is exposed to the sun and a dry surface layer (DSL) forms. The evaporation front then moves to the subsurface and vaporization of water then takes place at the bottom boundary of the DSL. For computing an accurate surface energy balance it is very important to account for the subsurface latent heat sink which can be measured using a sensible heat balance (SHB) approach. However, there is no clear evidence of timing of the shift from surface to subsurface with respect to the evaporation stages. Previous studies under non-isothermal laboratory conditions have found that the shift from surface to subsurface evaporation occurred early in the falling rate evaporation stage (stage 2). To address the need to investigate the onset of subsurface evaporation and corresponding effects on evaporation rates and the surface energy budget under more complex field conditions, we conducted bare field experiments. Our objective was to determine the onset of the subsurface evaporation stage with respect to the three stages of evaporative drying. We estimated total and subsurface evaporation rates using micro-lysimeter (ML) and SHB approaches, respectively, and also measured soil surface albedo (α) for bare surface conditions under natural wetting-drying cycles. Results from the field study showed that the onset of the subsurface evaporation stage coincided with the onset of falling rate (stage-2) evaporation. The

evaporation front moves into the subsurface when evaporation rates (E) fall below the potential rate (E_0), which corresponds to the onset of falling rate evaporation. For the loamy sand bare field under study, a low soil moisture dependent α of approximately 0.26 was observed when evaporation was taking place at the surface and α of 0.32-0.40 was observed when evaporation was occurring in the subsurface (deeper than 1mm). Based on the daily E/E_0 vs. α relationship, we estimated a threshold α value of 0.29 indicating the onset of the subsurface evaporation stage. For a given soil, α measurements can be used to distinguish days subject to potential (i.e., surface) and falling rate (i.e., subsurface evaporation) stages. The results also show that once the DSL forms (indicated by threshold α) then DSL thickness estimates can be used to study the dynamics of the evaporation front at finer time scales.

3.1 Introduction

Net radiation at the soil surface is partitioned between sensible and latent heat. As soil dries, the location of this partitioning encompasses both soil surface and subsurface zones. After surface soil dries, evaporation occurs in the subsurface. This can be observed in the field when a wet soil is exposed to the sun. Drying of the soil surface results in the formation of a dry surface layer (DSL), also referred to as "soil mulch" [Kimball, 1973]. The DSL acts as a barrier to liquid water flow from the moist sub-surface to the dry soil surface [Jalota and Parihar, 1998], forcing vaporization of water to take place at the bottom boundary of the DSL [Yamanaka et al., 1998; Novak, 2010]. There remains debate in the literature as to when this shift from surface to subsurface evaporation occurs, relative to the timing of the shift between potential and falling rate evaporation [Shokri and Or, 2011; Deol et al., 2012].

Evaporative drying of a soil has historically been considered as a three stage process [Lemon, 1956; Feddes, 1971; Idso et al., 1974]. Stage-1 evaporation occurs in the beginning of a drying event when, after rainfall or irrigation, evaporation is mainly controlled by atmospheric evaporative demand and occurs at the potential rate. As the soil moisture at the surface is depleted, stage-2 evaporation begins, during which time evaporation drops below the potential rate and decreases with time. This shift in the evaporation regime has also been referred to as the falling rate or transition stage [Shokri and Or, 2011]. Eventually, a very low and relatively constant evaporation rate is observed during stage-3 evaporation, when evaporation corresponds solely to diffusion of water vapor from the wet subsurface across a DSL.

Idso et al. [1974] were among the first to report clear observations of the three classical stages of evaporation in the field. They related the transition in evaporation stages to changes in soil surface albedo. Various studies indicate a strong negative correlation between soil moisture content and soil surface albedo. Idso et al. [1975] reported a linear relation between soil albedo and surface soil moisture content. Liu et al. [2008] on the other hand reported that the surface albedo decreases exponentially with increase in soil moisture. Guan et al. [2009] also found an exponential relationship between soil moisture and albedo. Idso et al. [1974] connected changes in surface albedo (indicating surface drying) with the onset of falling-rate evaporation, which may suggest a loss of liquid water connectivity to the surface at the beginning of falling-rate evaporation. Idso et al. [1975] further suggested a connection between the surface energy budget and changes in atmospherically controlled (stage-1) to

soil controlled evaporation stage (stage-2), and used increasing soil surface temperatures to mark the transition to falling-rate evaporation. Recent laboratory studies demonstrated "jumps" in the evaporation front from the surface to the subsurface at the end of stage 1, and reported that loss in hydraulic connectivity to the surface marks the onset of late stage low-rate evaporation in an initially saturated porous media under isothermal conditions [Shokri and Or, 2011]. The "jump" length was reported to be affected primarily by porous media properties and less so by boundary conditions. These findings may be limited in terms of applicability to natural drying of soil in the field where drying is significantly affected by radiation boundary conditions resulting in steep temperature gradients in the near-surface soil [de Vries and Philip, 1986; Mayocchi and Bristow, 1995; Novak, 2010, Heitman et al., 2010]. The effect of radiation boundary conditions and soil temperature on the evaporation front dynamics under field conditions has also been previously demonstrated by Yamanaka et al. [1999]. They observed that in addition to the daytime vaporization of water at the bottom boundary of DSL, transient vaporization (in morning) and condensation (evening and night) also occur within the DSL.

Although research has continued to model and predict evaporation stages, the location of the evaporation zone has not been explicitly confirmed during the shift to falling rate evaporation. The main reason for this is the difficulty in studying the evaporation front dynamics in the highly dynamic near-surface zone. For example, the shallowest measurement by Yamanaka et al. [1999] were taken for 0-1 cm depth layer which might have limited their ability to study the subsurface evaporation process from its inception. Numerical simulation

studies by Novak [2010] have shown the diurnal and inter-diurnal dynamics of the subsurface evaporation profile in the near-surface zone and have emphasized the need for measurement based studies to evaluate the existing theories based on modeling exercises.

Heitman et al., [2008a,b] have demonstrated that subsurface evaporation can be measured in the field using a sensible heat balance (SHB) approach by accounting for the latent heat flux originating below soil surface which is not taken into account in the traditional surface energy balance equation. The SHB approach uses temperature and thermal property measurements taken at mm-scale using the heat-pulse technique. Previous studies [Deol et al., 2012] have tested the SHB approach against mass balance for quantifying non-isothermal subsurface evaporation under controlled laboratory conditions. These laboratory studies demonstrated the dynamics of the sub-surface evaporation profile at mm-scale during a continuous drying event and suggested that the loss in liquid water connectivity to the surface occurs early in the falling-rate stage. There remains a need to take this improved measurement-based estimation of subsurface evaporation to more complex field and surface boundary conditions to further study the sub-surface evaporation stage from its inception.

In order to further examine the shift in surface to subsurface evaporation with respect to classical evaporation stages, we conducted bare field experiments. Our objective was to determine the timing of the onset of subsurface evaporation with respect to the three stages of evaporative drying. We used micro-lysimeter and SHB approaches to estimate total and subsurface evaporation over several natural drying events under field conditions in a bare

loamy-sand soil. Based on previous research findings discussed above, we hypothesized that formation of a DSL and switch from surface to sub-surface evaporation will be accompanied by dramatic changes in soil moisture dependent albedo.

3.2 Materials and Methods

3.2.1 Field Site and Semi-Continuous Measurements

A bare field evaporation study was conducted at the Central Crops Research Station in Clayton, NC from June 2011 to July 2012. The field site is located on a relatively flat terrain (2-6 % slope) at approximately 107 m elevation. The soil at the study site has been classified as Varina series (fine, kaolinitic, thermic Plinthic Paleudult) with a loamy sand surface texture (USDA-NRCS Web Soil Survey). A bulk density of 1.57 g/cm^3 and sand, silt and clay content of 85.5, 10.6 and 3.9 %, respectively, were recorded for 0-10 cm surface layer. Water retention data for -1x 10^4 to -1.3x 10^8 Pascal pressure head are presented in Figure 3.1. A 6 m x 5 m plot within a 0.2-ha bare field was maintained undisturbed for the drying study. Water retention data were collected using pressure plate apparatus [Richards and Ogata, 1961] and dew point potentiometer following Tuller and Or [2005]. The area surrounding the plot was maintained bare via frequent tillage. A suite of instruments were installed in the bare plot (Figure 3.2) on June 10, 2011 to collect measurements described below. These measurements were recorded for several drying periods following rainfall events.

Incident and reflected short wave radiation were recorded at 1-min interval, using two LI-200X pyranometers (Campbell Scientific, Logan, UT). The pyranometers were installed at

approximately 30 cm height above the soil surface with one pyranometer facing upward and another downward to record incident and reflected short wave radiation, respectively. Soil surface albedo (α) was calculated from measurements of the short wave radiation components as:

$$\alpha = S_u / S_d \quad [1]$$

where S_u is the total upward solar radiation (reflected solar radiation) and S_d is the total downward (incident) solar radiation reaching the surface.

Soil surface albedo is generally influenced by soil color, surface roughness, soil moisture, solar elevation angle, and snow cover, among others [Roxy et al., 2010]. Solar elevation angle and soil moisture, however, are considered the two main factors which influence the α for bare soil conditions [Li and Hu, 2009]. Therefore, α data were screened to select only soil moisture-dependent data by correlating α with solar zenith angle and discarding data which showed dependency of solar zenith angle.

Net radiation was measured at 1-minute interval using a NR-LITE2-L net radiometer (Campbell Scientific) installed at 30-cm height above the soil surface. Subsurface soil thermal properties and temperature were recorded with an 11-needle heat-pulse probe [Zhang et al., 2012; Figure 3.3] to calculate sub-surface energy balance. All of the above data were recorded using two data loggers: CR 3000 and CR 1000 (Campbell Scientific).

A weather station, maintained by the State Climate Office of NC, was located at approximately 10-m distance from the experimental bare field. Air temperature (2 m), relative humidity (2 m) and wind speed (10 m) data from this weather station were used for potential evaporation (E_0) calculations following the FAO56 Penman Monteith method [Allen et al., 1998]. Precipitation data were also collected from the weather station via a tipping bucket rain gage.

Our approach for quantifying subsurface evaporation was based on an approximate sensible heat balance (SHB) for a soil layer [Gardner and Hanks, 1966]:

$$LE = (H_1 - H_2) - \Delta S \qquad [2]$$

where LE is latent heat flux (W m^{-2}), H_1 and H_2 are soil heat flux at two depths (W m^{-2}), and ΔS is change in sensible heat storage (W m^{-2}) of the soil layer between these depths. All terms in this relationship were computed from continuous soil temperature and thermal property measurements taken via the heat-pulse probe (HPP).

The HPP was installed with its needles parallel to the soil surface and the top needle barely covered with soil. The probe has 11 needles, the shorter needles contain thermocouples, while the longer needles contain both a thermocouple and a resistance heater (Figure 3.3). The upper three needles are vertically spaced at 1 mm and are at radial distance of 6 mm from the fourth needle. The remaining needles are spaced at 6 mm vertical distance. The HPP passively measures temperature, and actively measures thermal properties by periodically

sending a small heat pulse through the resistance heaters. Thermal properties are estimated by the temperature response to the applied heat pulse. More details about the multi-needle heat pulse probe and SHB calculations are given by Zhang et al. [2012] and Heitman et al. [2008 a,b]. The HPP measurements were assumed to provide an indication of evaporation occurring in the subsurface (1-9 mm soil depths) only [Zhang et al., 2012; Deol et al., 2012].

3.2.2 Periodic Measurements

In addition to SHB measurements, independent daytime (10:00-18:00 h) evaporation measurements were taken using micro-lysimeters (MLs), similar in design to those used by Heitman et al. [2010]. The 10 cm long MLs were constructed using 3-in SDR 21 polyvinyl chloride (PVC) pipe with an inside diameter of 8 cm. One end of the MLs was beveled for easy penetration into the soil during installation. The MLs were installed into the soil by placing a wooden block on top of the PVC column and hammering it until its top was flush with the soil surface. Evaporation measurements were made by extracting MLs, sealing the bottom using a plastic sheet and tape, cleaning the soil off of the outside walls, weighing the MLs and reinstalling them in the same position. Mass of the MLs was recorded at 0.01 g precision at 4 h intervals, three times at 10:00, 14:00 and 18:00 h each day of measurement. A set of four MLs were extracted each day of measurement. The ML evaporation data were collected for 13 d spread over three drying events during March and July 2012. The ML data were assumed to provide an indication of total evaporation occurring at the surface and in the subsurface.

Destructive measurements of the thickness of the visible DSL were also taken daily at 14:00 h during all days when ML evaporation was recorded. For measuring DSL thickness, a vertical soil face was exposed and thickness of the visible DSL was measured using a ruler (Figure 3.4). Each day the DSL measurements were taken at three locations within the experimental plot.

3.3 Results and discussion

3.3.1 Evaporation Rates and Transition from the Surface to Subsurface

Evaporation data were collected using SHB and ML approaches for a 5-day drying event in March 2012 (DOY 86-90). Rainfall depths of 2.9 and 0.03 cm were observed on DOY 84 and 85, respectively. Figure 3.5A shows air temperature, humidity and wind speed during the 5-day drying event. Net radiation data for the same drying event are shown in Figure 3.5B. The net radiation data are not continuous because of power loss at night due to low charge from the solar panel.

Micro-lysimeter evaporation rates for the daytime (10:00-14:00 h) were 0.73, 0.33, 0.30, 0.27 and 0.10 mm/h on DOY 86, 87, 88, 89 and 90, respectively. Figure 3.6 shows daytime (10:00-14:00 h) evaporation (E) estimated by ML and SHB approaches, expressed as a proportion of E_0. An actual to potential evaporation ratio (E/E_0) of 0.96 was observed on the first day (DOY 86) of the drying event, then E/E_0 decreased to 0.53 on DOY 87 and reached 0.12 by DOY 90 (the fifth day of the drying event). The E/E_0 value (0.96) on DOY 86

indicates stage-1 evaporation, whereas the drop below E_0 on subsequent days indicates falling rate evaporation.

Depth integrated subsurface evaporation for the 1-9 mm soil layer from the SHB approach closely matched ML evaporation for DOY 87, 88, 89 and 90. However, a very low subsurface evaporation rate of 0.12 mm/h, in comparison to 0.73 mm/h ML evaporation, was observed in the 1-9 mm depth zone on DOY 86 (first day of drying event). The disparity between the ML and SHB measurements suggests that transition to subsurface evaporation started on DOY 86, but with most of evaporation still occurring at the surface (< 1mm depth). Because of the rainfall distribution preceding the drying event (2.9 cm on DOY 84 and 0.03 cm on DOY 85), there was likely adequate time for downward soil water redistribution (i.e., drainage) prior to observations on DOY 86. The loamy sand soil texture permits rapid drainage of gravitational water from the surface layer. Therefore, on DOY 86, the evaporation front was already spreading into the near surface soil layer (1-9 mm) due to slightly limited water supply, though with most evaporation still occurring at the soil surface (< 1 mm depth). Strong agreement between SHB and ML estimates on subsequent days indicates that subsurface evaporation was predominant after DOY 86.

Subsurface evaporation in the 1-9 mm depth layer was estimated using the SHB approach with an 11-needle HPP. Using the field data and SHB approach, it was not possible to measure evaporation within the 0-1 mm depth layer near the surface. This differs from results using the same probe under controlled laboratory conditions [Deol et al., 2012], but is similar

to prior results using the 11-needle HPP in the field [Zhang et al., 2012]. Due to sensor geometry constraints imposed by the heat-pulse method [Zhang et al., 2012], the top three HPP needles located at 0 mm (barely covered), 1 mm and 2 mm depth are not vertically aligned in our study. This resulted in inconsistent temperature profiles in the 0-2 mm depth zone, especially in the morning and evening hours. This might be because variations in micro-topography. For example, the near-surface temperature profile on DOY 86 at 9:00 h shows that temperature at 1 mm was higher than that at 0 mm (Figure 3.7), whereas, the temperature profile at 12:00 h on same day shows a continuous decreasing trend with depth. Therefore, for daytime (10:00-14:00 h) SHB evaporation estimates, we didn't use the temperature measurement at 1mm. The calculated shallowest temperature gradient was thus centered at 1 mm depth, using temperature measurements at 0 and 2 mm, unlike laboratory studies of Deol et al. [2012].

In this field study, we used the HPP data for calculating evaporation occurring at the surface (i.e., shallower than 1 mm) by considering an alternate approach. We computed an energy balance for the 0-1 mm depth layer by taking the difference between measured net radiation (Rn) and soil heat flux (G) at 1 mm depth, estimated from HPP measurements [Heitman et al., 2010]. For the first day of drying (DOY 86) with water still readily available at the visibly wet soil surface, we assumed that sensible heat flux was negligible. Therefore, the available energy (Rn-G) was partitioned only into latent heat flux and change in sensible heat storage for 0-1 mm depth layer. This gave a surface evaporation rate of 0.60 mm/h, which was about 79% of potential evaporation (Figure 3.6). By summing evaporation estimates for

the subsurface (1-9 mm) from SHB and for the surface (< 1 mm) from available energy, the total evaporation rate was 0.72 mm/h, which compares favorably against ML evaporation of 0.73 mm/h measured at the same time.

3.3.2 Subsurface Evaporation Depth-Distributions

In addition to depth-integrated evaporation rates, the SHB approach also provides an estimate of the distribution of the evaporation zone [Deol et al., 2012]. Evaporation profiles estimated by SHB show that the evaporation front started spreading into the subsurface on DOY 86 with an evaporation rate of 0.16 mm/h in the 1-4 mm soil layer (Figure 3.8). Based on results described in the previous section, this represented only about 10% of the total evaporation with most of the evaporation (~90%) still occurring at the surface. From DOY 87 onwards, the evaporation front moved completely into the subsurface and all evaporation occurred in the subsurface zone of 1-9 mm. Within 1-9 mm evaporation zone, most evaporation occurred in the 1-4 mm depth layer on DOY 87. However, on DOY 88, evaporation spread equally into the 1-4 and 4-9 mm depth layers. With further drying, evaporation occurred in the 4-9 mm soil layer on DOY 89 and 90 with subsurface evaporation rates of 0.27 and 0.1 mm/h, respectively. The results from this study show that starting from the onset of falling rate evaporation, all of the evaporation occurred in the subsurface (deeper than 1mm). These results are consistent with previous results from Deol et al. [2012] for a sandy soil under non-isothermal laboratory conditions.

3.3.3 DSL Thickness

The soil surface remained visibly wet on DOY 86, following rainfall on the preceding days. Dry surface layer formation started on DOY 87 with an approximately 1 mm thick DSL (Figure 3.9). Further drying of the soil surface resulted in increase in DSL thickness to approximately 3, 5 and 6 mm on DOY 88, 89 and 90. The SHB estimated evaporation profiles (Figure 3.8) are consistent with independently measured DSL thickness with subsurface evaporation occurring at the bottom of the DSL. This agrees with previous reports by Yamanaka et al. [1998].

Previous lab studies [Deol et al., 2012] used heat-pulse estimated thermal conductivity and independently measured dry soil thermal conductivity to estimate DSL thickness by assuming an approximate structure of the DSL and underlying soil. We used this field experiment as an opportunity to test the estimated DSL thickness following Deol et al. [2012] against the destructively measured thickness of DSL in the field under natural drying conditions. Figure 3.9 shows data for both estimated and measured DSL thickness during the 5-d drying event (DOY 86-90). Heat-pulse measurements for DSL estimation were scheduled for 9:00, 12:00, 15:00 and 18:00 h. However, loss of power due to low solar panel charge in mornings and evenings and the need to replace a broken sensor towards the end of drying event resulted in some missing data points. Even after missing some data points, more data were recorded per day for estimating DSL as compared to destructive measurements of DSL thickness which was done once daily at 14:00 h (Figure 3.9). The estimated DSL thickness

trend closely matched measurements early in the drying event but underestimated the DSL thickness (by ~1 mm) towards the end of drying period on DOY 89 and 90. Estimated DSL also showed diurnal variation with an increasing trend during the day (e.g., increase from 0.93 mm to 2.3 mm on DOY 87). However, a lower estimated DSL thickness of 1.87 mm was observed on the following morning (DOY 99 at 9:00 h), indicating a decrease in DSL thickness during the preceding night. The diurnal fluctuation was more pronounced from DOY 87 to 88 compared to a lower variation between DOY 88 and 89. The subsurface evaporation profiles (Figure 3.8) show that evaporation was occurring below the estimated DSL thickness throughout the drying event. Therefore, the DSL thickness estimates following Deol et al. [2012] gave a good estimation of location of the subsurface evaporation front. Although there were some missing data points as explained above, this is the first study to give measurement based estimation of variations in DSL thickness indicating diurnal and inter-diurnal changes in location of evaporation front at mm-scale. These variations in DSL thickness, which were relatively more pronounced during early subsurface evaporation stage, agree with the numerical simulation results of Novak [2010].

3.3.4 Albedo and Evaporation Rates

Soil moisture-dependent α was also measured for the same 5-day drying event (DOY 86-90) (Figure 3.6). Soil moisture-dependent α was 0.26 on DOY 86 when most evaporation was occurring at the surface. On DOY 87 and 88, the albedo increased to 0.32 and 0.36; this corresponded with the days when all evaporation occurred in the subsurface with top of the

evaporation zone still very close to the soil surface, in the 1-4 mm depth layer (Figure 3.8). With further drying, a relatively high and constant albedo of 0.39 was observed on DOY 89 and 90 (Figure 3.6) when the evaporation zone completely moved into the 4-9 mm depth zone (Figure 3.8). The albedo data show a low value in the beginning of the drying event which increased and eventually became almost constant.

To further investigate the relationship between α and the onset of subsurface evaporation, another data campaign was completed in July 2012. Figure 3.10 shows daily (10:00-18:00 h) ML E/E_0 in relation to α observed on the same days. The data shown in Figure 3.10 are from 13 days of observations spread over three drying events, including the 5-d drying event (DOY 86-90) discussed in the previous section.

An inverse relation was observed between α and E/E_0 (Figure 3.10). The data can be clearly divided into two groups. One group of three days has high E/E_0 (ranging 0.90-0.96) and low α (ranging 0.25-0.27). Relatively lower E/E_0 values (ranging 0.53-0.12) and an $\alpha > 0.32$ (ranging 0.32-0.40) were observed in the second group consisting of 10 days out of a total 13 days of observations. The first group of data consists of the days following a wetting event when the soil surface was visibly wet and the evaporation was occurring mainly at the soil surface at depths shallower than 1 mm (as shown for DOY 86 in Figure 3.6). The second group consists of days at different stages of drying with a visible DSL and all of the evaporation occurring in subsurface at more than 1 mm depth (as shown for DOY 87, 88, 89 and 90 in Figure 3.6 and Figure 3.8). These data suggest that α measurements for a given soil

can be used to indicate whether the evaporation is occurring at the surface or in the subsurface. We fit a linear regression line to the second group of points, which were for days with a visibly dry surface. We used this linear regression equation to estimate a threshold α (above which the surface becomes visibly dry and evaporation occurs in the subsurface) by determining the value of albedo corresponding to average E/E_0 observed for days when surface was visibly wet (where the dotted lines intersect Figure 3.10). The estimated threshold α was 0.29. The data collected for our experimental field show that $\alpha < 0.29$ indicated surface evaporation, with $E/E_0 \approx 1$ indicating stage-1 evaporation. An albedo > 0.29 indicates subsurface evaporation, which coincided with the onset of falling rate or stage-2 evaporation as discussed in the previous section (Figure 3.6). Observations also show that after only 1 to 2 d of drying, α reached 0.39-0.4 and became almost constant, which corresponded with subsurface evaporation front moving to >3 mm depth as shown for DOY 89 and 90 in Figure 3.8.

Similar field studies for a given soil can be used to determine a threshold α, above which evaporation occurs in the subsurface. Simple albedo measurements can then be used to distinguish between days when evaporation mainly occurred at the surface at rates approaching E_0 from the days when evaporation was occurring in the subsurface (i.e., deeper than 1mm).

3.4 Conclusions

The results from these field measurements showed that at the onset of stage-2 or falling rate evaporation, evaporation occurred in the subsurface. Microlysimeter and SHB evaporation data suggest that the evaporation zone starts spreading into the subsurface immediately after the drainage of water from the surface, even when the soil surface is visibly wet and evaporation rates are close to E_0. This is followed by a complete transition to subsurface evaporation, which occurred on the second day of drying in the field under study, for a 5-d drying period (DOY 86-89) following a rainfall of ~3 cm. This coincided with the onset of stage-2 evaporation, indicated by E/E_0 ratio of 0.53. Therefore, the main finding from this loamy sand bare field study is that evaporation occurs in the subsurface at the onset of falling-rate stage evaporation. This is supported by SHB, DSL, and α measurements. The timing of this change from surface to subsurface evaporation can be indicated by α measurements. A threshold α value of 0.29 was estimated for the field soil using the observed E/E_0 versus α relationship. Similar studies for a given soil may help in estimating a threshold α value above which the evaporation occurs in the subsurface. These findings are based on daytime evaporation and soil moisture dependent α measurements, so are applicable only to daily changes in evaporation rates and the location of the evaporation front. Our data also show that DSL thickness estimates following Deol et al. [2012] gave reasonable indication of the top of the subsurface evaporation profile. These estimates are however based on the assumption that there is a DSL present at the surface. Therefore, α measurement can first be used to indicate the presence of DSL and then DSL estimates by

using continuous heat-pulse measurements may provide information on dynamics of evaporation front in the field at a finer time scale.

The change in surface to subsurface evaporation also indicates a change in surface energy balance because of the shift in the location of the latent heat sink from surface to subsurface [Heitman et al., 2010]. Therefore, our findings highlight the important role of α in accurate estimation of surface energy balance. Large scale modeling studies by Donohue et al. [2010] also demonstrated the importance of understanding the role that even subtle changes in α can play in dynamics in the surface energy balance. However, α is rarely treated as a variable in potential evaporation formulations which are used to predict large scale hydrologic and climatic patterns. The findings from this study will help in more precise estimate of surface energy balance by not double counting the LE term in energy balance equation for the days when LE originates in the subsurface which can be indicated by α measurements. Broader applications of the findings from this study, therefore, include a better characterization of near-surface energy balance and improved understanding of large scale hydrologic and climatic patterns.

3.5 References

Allen, R.G., Pereira, L.S., Raes, D., Smith, M., 1998. Crop Evapotranspiration: Guidelines for Computing Crop Water Requirements. *United Nations Food and Agriculture Organization, Irrigation and Drainage Paper 56*. Rome, Italy, 300 pp.

Bristow, K. L., G. J. Kluitenberg and R. Horton (1994), Measurement of soil thermal properties with a dual-probe heat-pulse technique, *Soil Sci. Soc. Am. J*., 58, 1288-1294.

Campbell, G.S. (1985), *Soil Physics with Basic Transport Models for Soil-Plant System*. Elsevier, New York.

Deol, P., J.L. Heitman, A. Amoozegar, T. Ren, and R. Horton (2012), Quantifying Non-isothermal Sub-surface Soil Water Evaporation. *Water Resour. Res.* 48, W11503, doi:10.1029/2012WR012516.

Feddes, R.A. (1971), Water, heat and crop growth, PhD thesis, Comm. Agric. Univ., Institute of Land and Water Management Research, Wageningen, 184pp.

Gardner, H. R. and R. J. Hanks (1966), Evaluation of the evaporation zone in soil by measurement of heat flux, *Soil Sci. Soc. Am. J*., 30, 425-428.

Guan X. D., J. P. Huang, N. Guo, J. R. Bi and G. Wang (2009), Variability of soil moisture and its relationship with surface albedo and soil thermal parameters over the Loess Plateau. *Adv. Atmos. Sci.*, 26(4), 692–700.

Heitman, J.L., R. Horton, T.J. Sauer, and T.M. DeSutter (2008a), Sensible heat observations reveal soil-water evaporation dynamics, *J. Hydromet*., 9, 165-171.

Heitman, J.L., R. Horton, T.J. Sauer, T.S. Ren, and X. Xiao (2010), Latent heat in soil heat flux measurements, *Ag. Forest. Met.*, 150, 1147-1153.

Heitman, J.L., X. Xiao, R. Horton, and T.J. Sauer (2008b), Sensible heat measurements indicating depth and magnitude of subsurface soil water evaporation, *Water Resour. Res.*, 44, W00D05. doi:10.1029/2008WR006961.

Hillel, D. (1971), *Soil and Water: Physical Principles and Processes*. Academic Press, New York.

Idso, S.B., R.D. Jackson, and R.J. Reginato (1975), Estimating evaporation: A technique adaptable to remote sensing, *Science*, 189, 991-992.

Idso, S.B., R.J. Reginato, R.D. Jackson, B.A. Kimball, and F.S. Nakayama (1974), The three stages of drying of a field soil, *Soil Sci. Soc. Am. Proc.*, 38, 831-837.

Jalota, S.K. and S.S. Prihar (1998), *Reducing soil-water evaporation with tillage and straw mulching*. Iowa State University Press, Ames (ISBN 0-8138-2857-0), p. 142.

Kimball, B.A. (1973), Water vapor movement through mulches under field conditions, *Soil Sci. Soc. Am. Proc.*, 37, 813−818.

Lemon, E. R. (1956), The potentialities for decreasing soil moisture evaporation loss, *Soil Sci. Soc. Am. Proc*., 20, 120-125.

Li Y. and Z. Hu (2009), A study on parameterization of surface albedo over grassland surface in the northern Tibetan Plateau. *Adv. Atmos. Sci*., 26(1), 161–168.

Liu H. Z., B. M. Wang and C. B. Fu (2008), Relationships between surface albedo, soil thermal parameters and soil moisture in the semi-arid area of Tongyu, Northeastern China, *Adv. Atmos. Sci.*, 25(5), 757–764.

Liu, B.C., W. Liu, S.W. Peng. (2005), Study of heat and moisture transfer in soil with a dry surface layer, *International Journal of Heat and Mass Transfer*, 48 (21–22), 4579-4589.

Mayocchi, C.L., and K.L. Bristow (1995), Soil surface heat flux: some general questions and comments on measurements, *Ag. Forest Meteor*. 75, 43-50.

Novak, M.D. (2010), Dynamics of the near-surface evaporation zone and corresponding effects on the surface energy balance of a drying bare soil, *Ag. Forest Meteor*., 150, 1358-1365.

Philip, J.R., and D.A. de Vries (1957), Moisture movement in porous materials under temperature gradients. Transactions, American Geophysical Union, 38(2), 222-232.

Richards, L.A., and G. Ogata, 1961. Psychrometric measurements of soil samples equilibrated on pressure membranes. *Proc. Soil Sci. Soc. Am*. 25:456–459.

Roxy M. S., V. B. Sumithranand, G. Renuka (2010), Variability of soil moisture and its relationship with surface albedo and thermal diffusivity at astronomical observatory, Thiruvananthapuram, South Kerala. *J. Earth Sys. Sci*., 2010, 119(4): 507-513.

Sakai, M., S.B. Jones, and M. Tuller (2011), Numerical evaluation of subsurface soil water evaporation derived from sensible heat balance. *Water Resour. Res*., 47, W02547.

Shokri, N., and D. Or. (2011), What determines drying rates at the onset of diffusion controlled stage-2 evaporation from porous media? *Water Resour. Res*., 47, W09513.

Soil Survey Staff, Natural Resources Conservation Service, United States Department of Agriculture. Web Soil Survey. Available online at http://websoilsurvey.nrcs.usda.gov/ . Accessed [11/14/2011].

Tuller, M. and D. Or. 2005. Water films and scaling of soil characteristic curve at low water contents. Water Resour. Res. 41:W09403.

Xiao, X., R. Horton, T. Sauer, J.L. Heitman, and T. Ren (2011), Cumulative soil water evaporation as a function of depth and time, *Vadose Zone J*., 10, 1016-1022.

Yamanaka, T. and, T. Yonetani (1999), Dynamics of the evaporation zone in dry sandy soils, *J. of Hydrol.*, 217(1–2), 135-148.

Yamanaka, T., A. Takeda, and J. Shimada (1998), Evaporation beneath the soil surface: Some observational evidence and numerical experiments. , *Hydrol. Process.*, 12, 2193-2203.

Zhang X., J.L. Heitman, R. Horton, and T. Ren (2012), Measuring subsurface soil-water evaporation with an improved heat-pulse probe. *Soil Sci. Soc. Am. J.*, 76, 876-879.

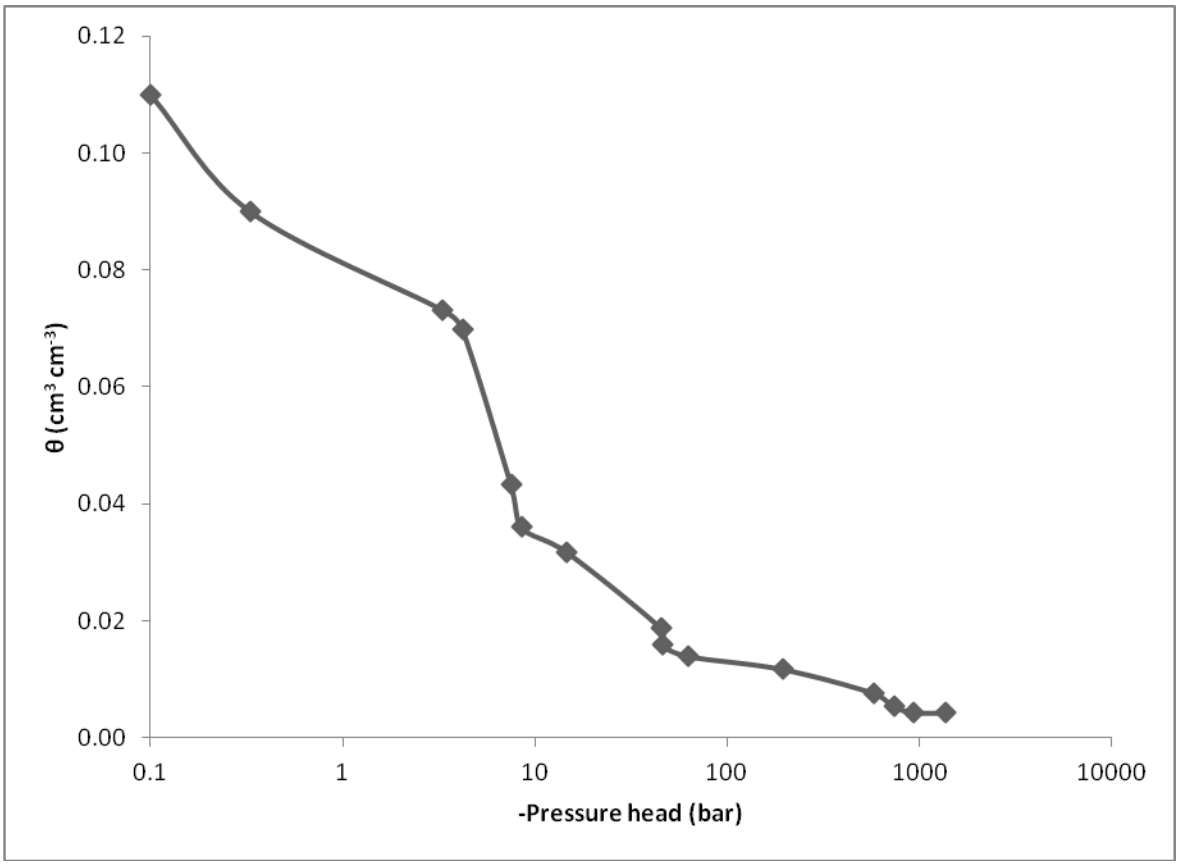

Figure 3.1 Water retention for the surface soil (0-10 cm) at study site

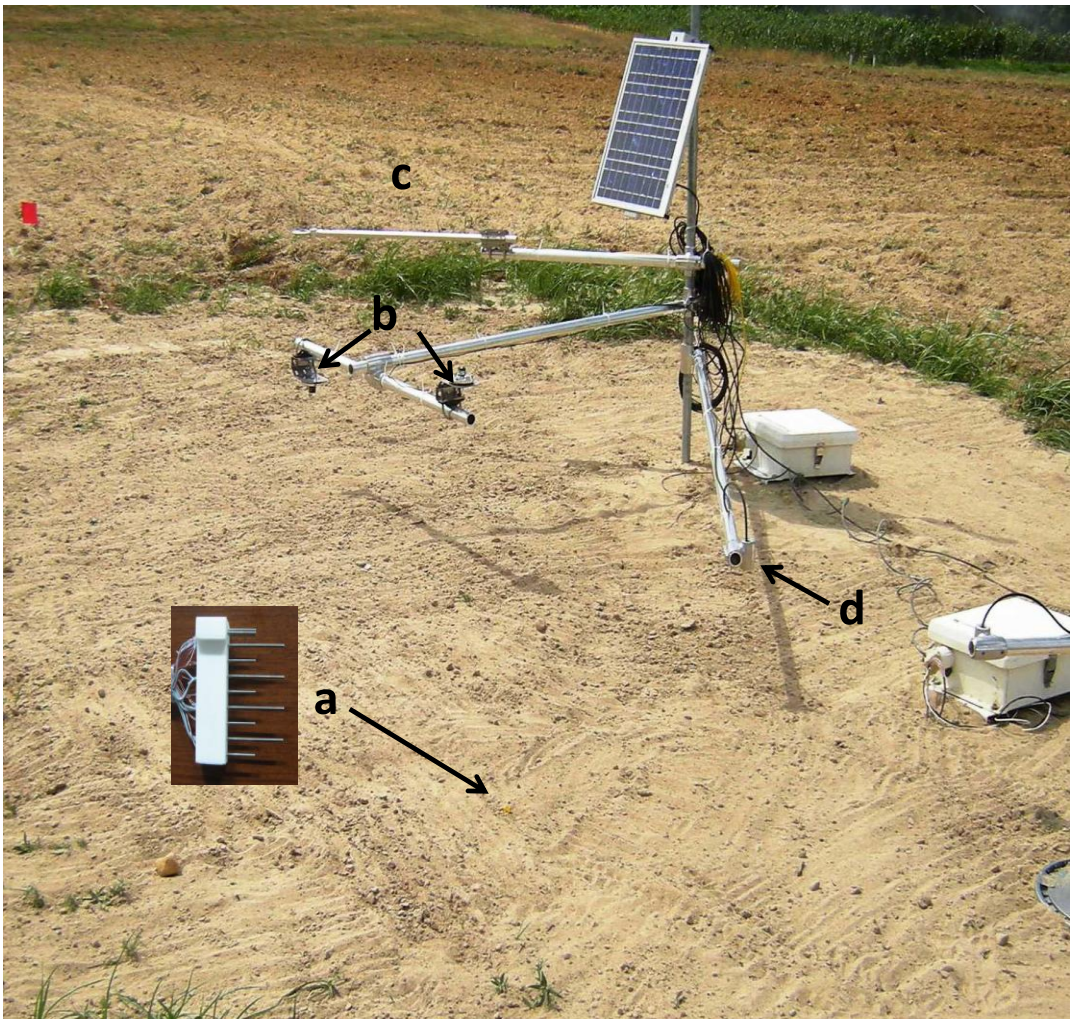

Figure 3.2 Field instrumentation: (a) heat-pulse probe installed below ground (see details in Fig. 3) (b) pyranometers, upward and downward facing, and (c) net radiometer (d) infrared thermometer

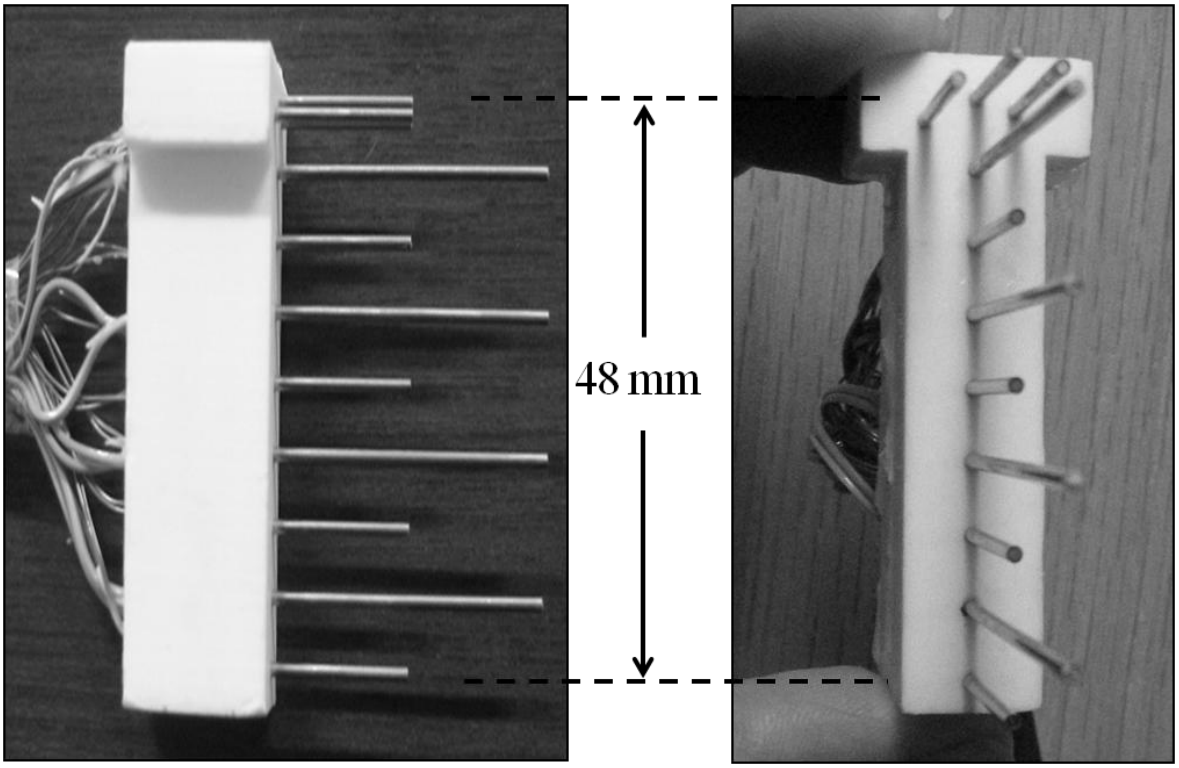

Figure 3.3 Multi-needle Heat Pulse Probe (after Zhang et al., 2012)

Figure 3.4 Visible dry surface layer (DSL) thickness in the field

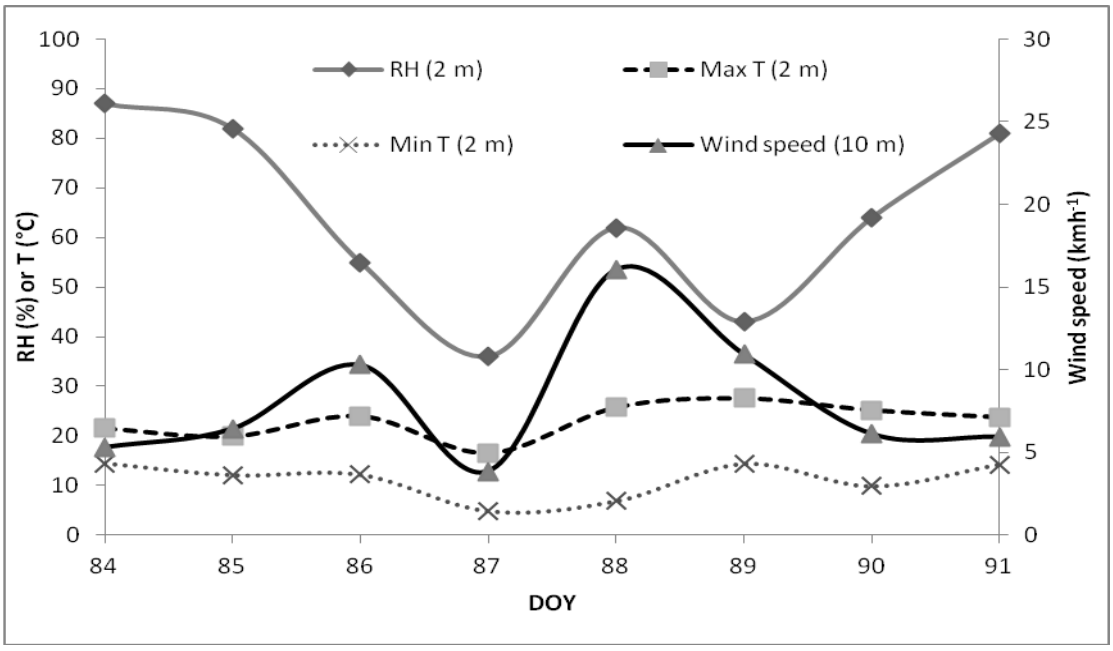

A

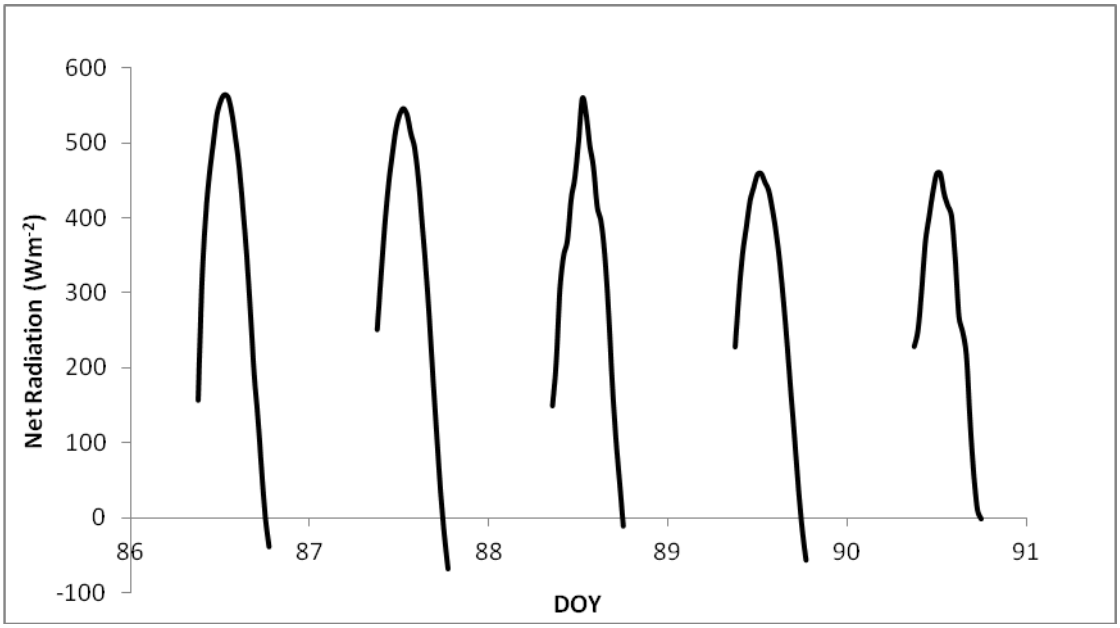

B

Figure 3.5 (A) Average hourly air temperature, relative humidity and wind speed during the 5-day drying event (DOY 86-90). (B) Net radiation during the 5-day drying event (DOY 86-90). Note: The curves are broken because of loss of power due to low night time charge from solar panel.

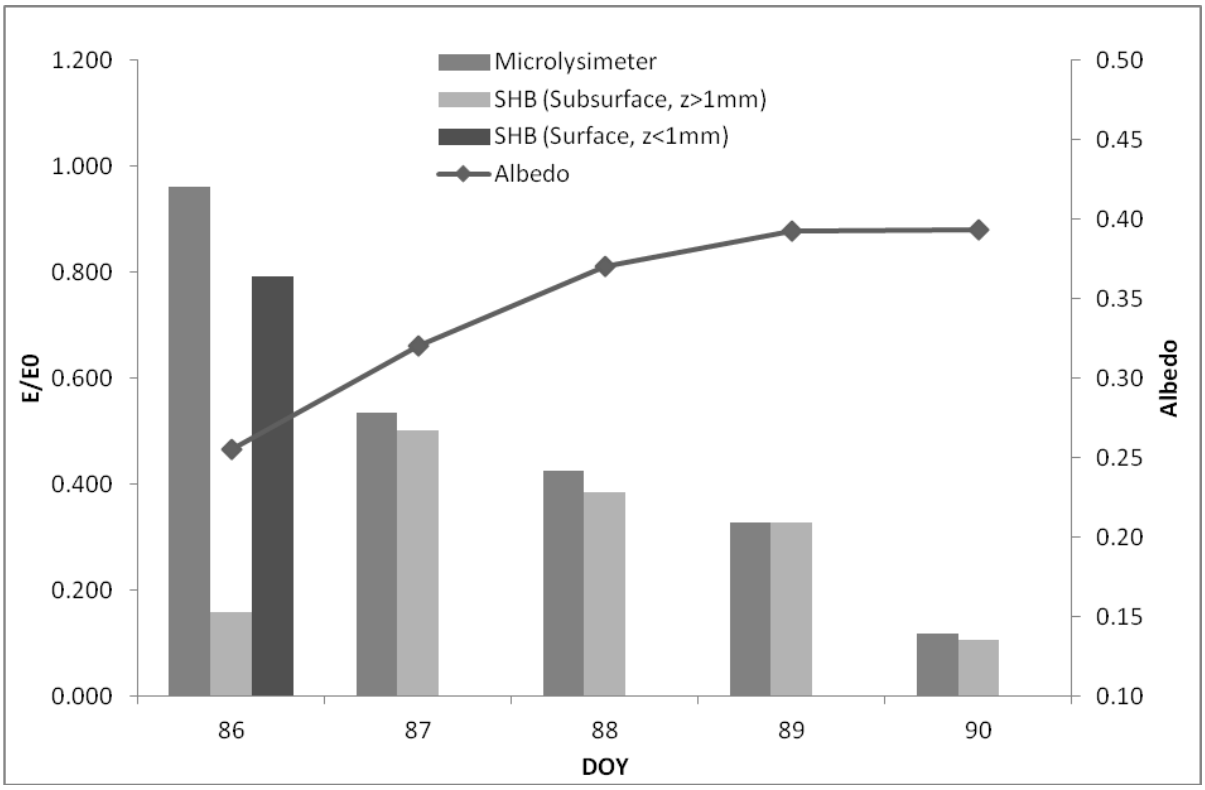

Figure 3.6 Soil moisture dependent albedo and daytime (10 am-2pm) evaporation (E) measured by using micro-lysimeter and Sensible Heat Balance (SHB) approaches expressed as proportion of Penman Monteith evaporation (E_0).

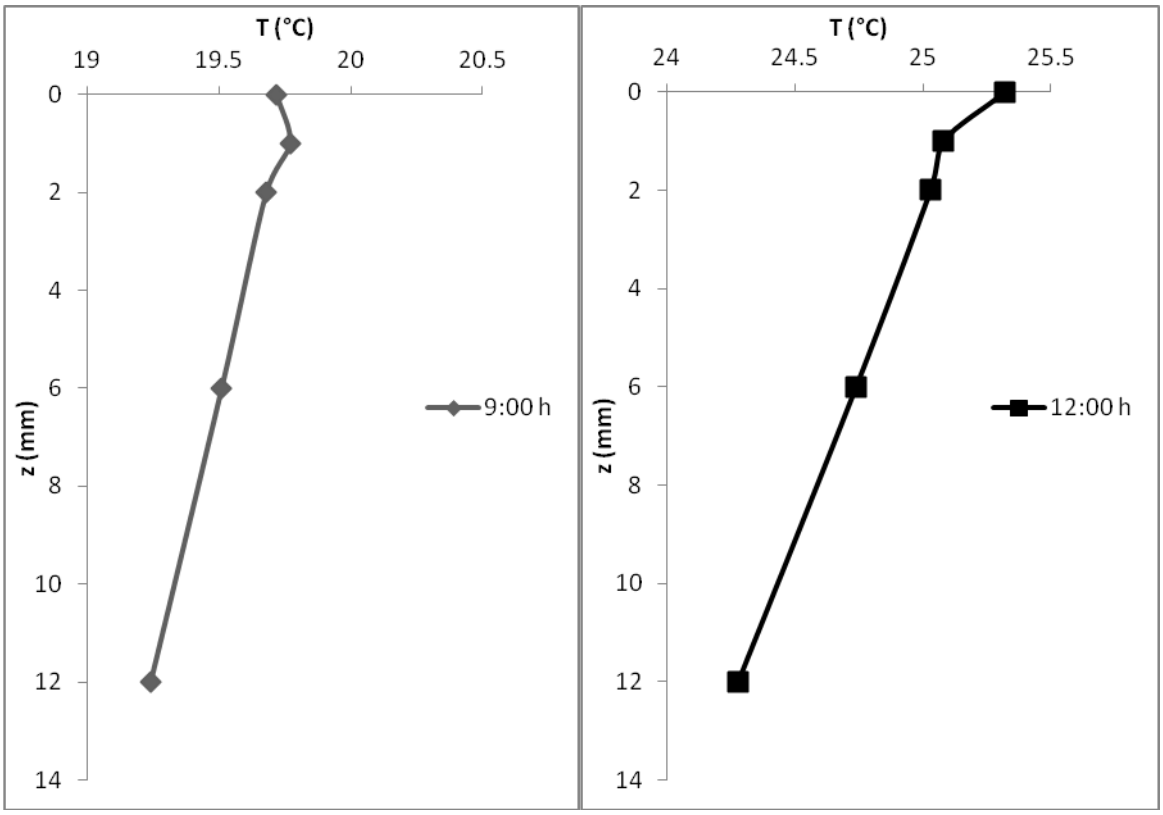

Figure 3.7 Near-surface temperature profiles at 9:00 and 12:00 on DOY 86. (Note the inconsistency in temperature profile at 9:00 h, at z=1mm, when solar radiation was heating the surface at an angle as compared to the temperature profile at noon showing a continuous decreasing trend with depth).

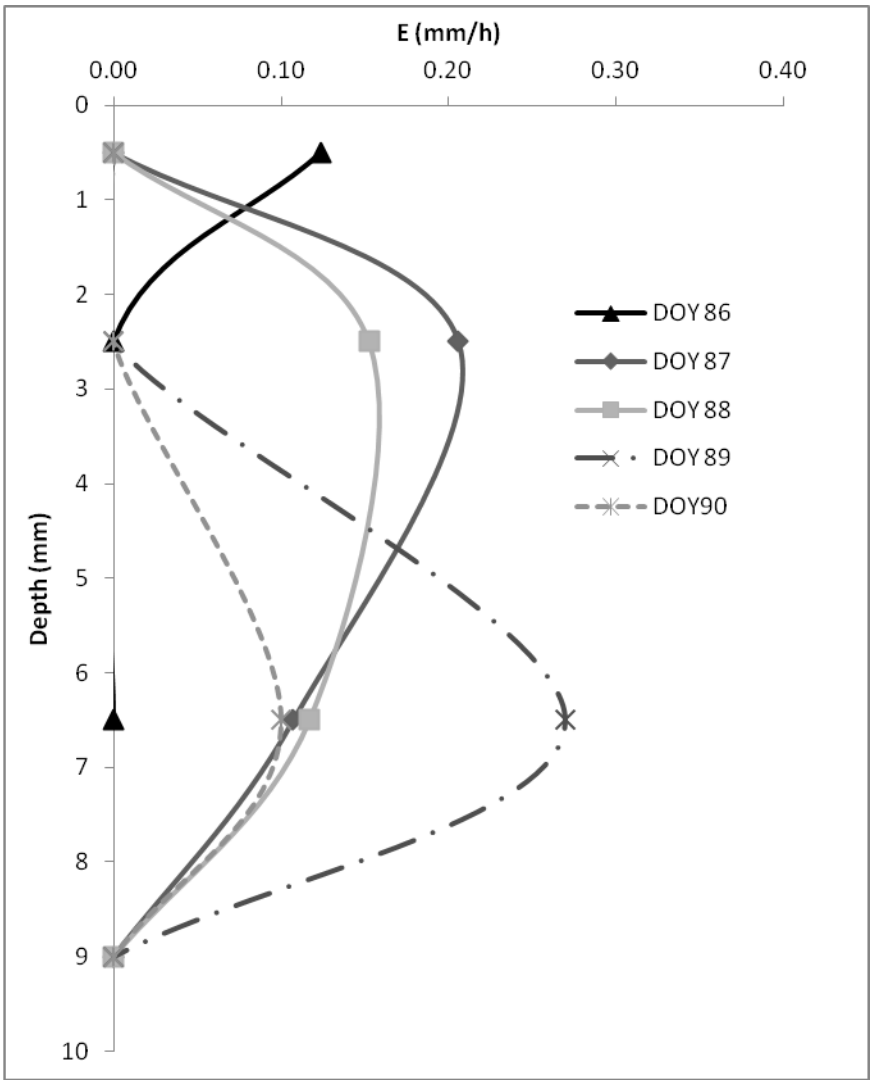

Figure 3.8 Sub-surface evaporation profiles estimated using sensible heat balance (SHB) approach during a 5-day drying period (DOY86-90)

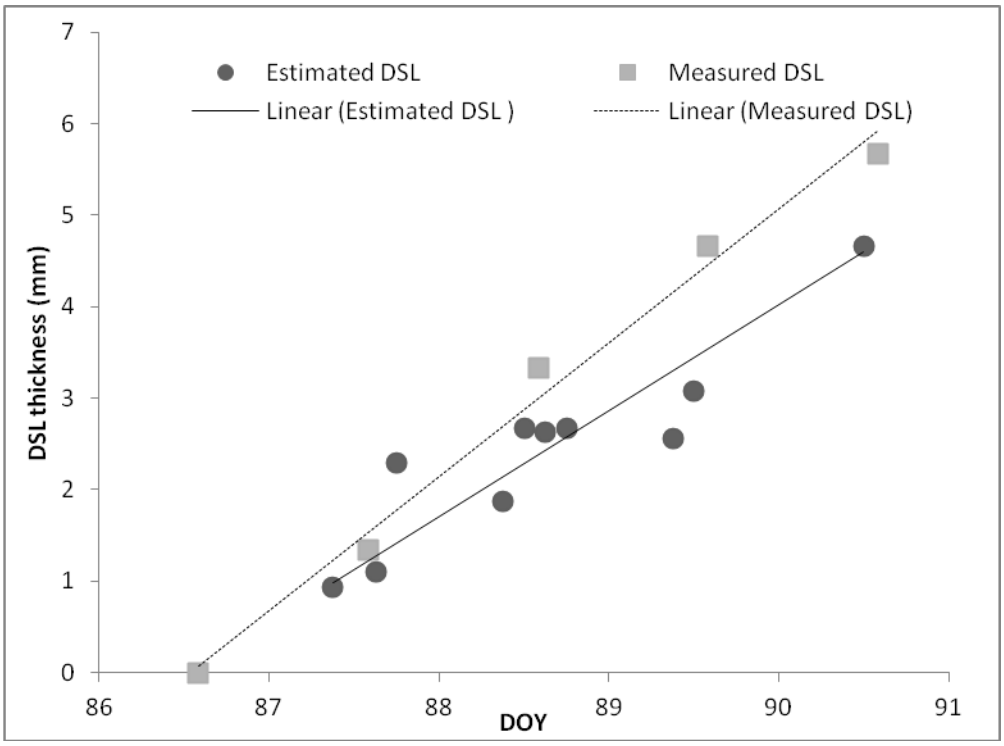

Figure 3.9 Dry Surface Layer (DSL) thickness during 5-d drying period (DOY 86-90).

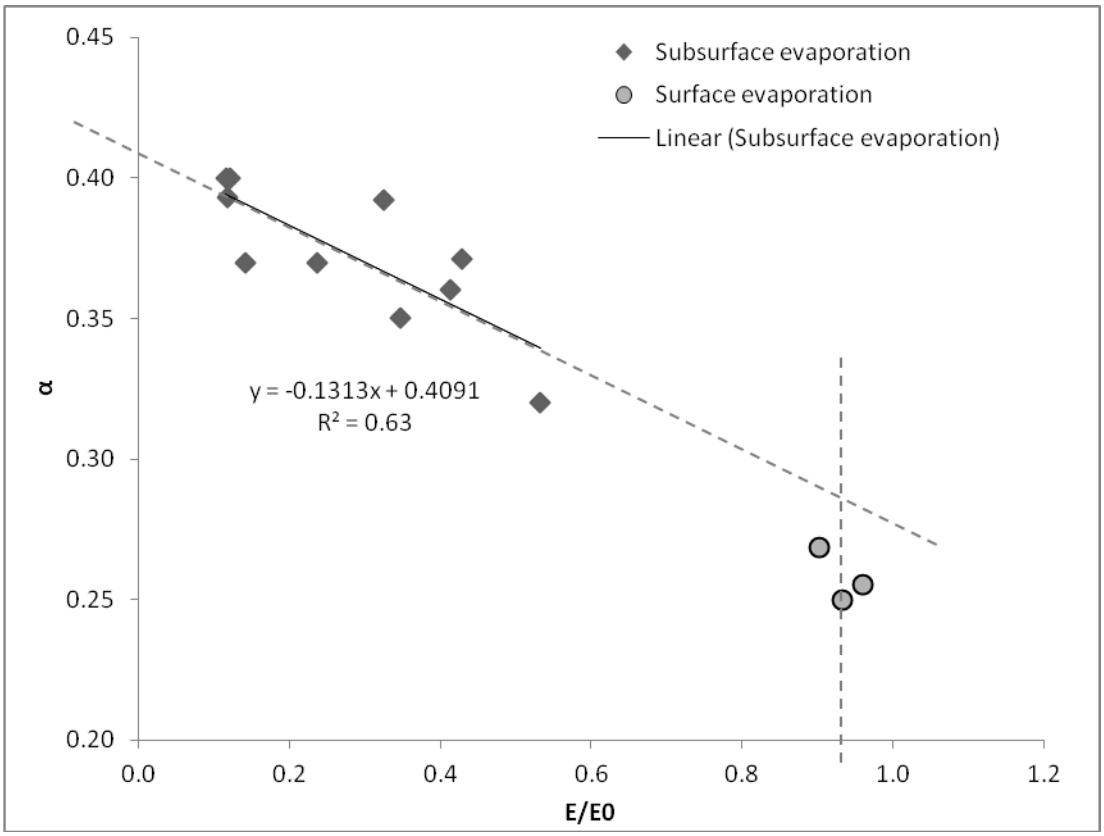

Figure 3.10 Daytime (10:00-18:00 h) micro-lysimeter evaporation (E) as a fraction of potential evaporation (E_0) for 13 days spread over three drying events in April and July 2012 and soil moisture dependent albedo (α) for respective days. Point of intersection of dotted lines corresponds to threshold α value of 0.29.

4. Soil-limited evaporation under radiative vs. non-radiative surface boundary conditions

Abstract

Formation of a of a dry surface layer (DSL), due to rapid depletion of surface water content, results in soil-limited evaporation, which is difficult to measure and is often estimated from pan evaporation or other potential evaporation estimates. We conducted controlled laboratory studies with objectives to investigate the effects of non-radiative and radiative boundary conditions on 1) evaporation front dynamics under transient conditions, and 2) actual to potential evaporation ratios under steady-state soil-limited evaporation conditions. A transient evaporation study was conducted using open top columns (34-cm long, 15.25 cm inside diameter) packed uniformly with a sand soil at a bulk density of 1.65 g/cm^3. The initial condition for water content was a drained column with water table depth of 29 cm. The soil surface was exposed to a radiation emitter which was turned off after 94 h of drying to change surface boundary conditions. Heat-pulse measurement based estimates of DSL thickness decreased in response to change from radiative to non-radiative surface boundary conditions. These results suggest diurnal changes in the location of evaporation front in the near-surface zone, which agrees with previous reports from numerical simulation studies. We also conducted steady-state evaporation studies using the same soil column to investigate the effect of non-radiative vs. radiative boundary conditions on steady-state soil-limited evaporation under conditions with the same potential evaporative demand (0.7 mm/h) and

constant water table depth of 29 cm. A greater steady-state evaporation rate of 0.28 mm/h was observed under surface radiation despite the formation of a DSL as compared to convection-driven (0.15 mm/h) conditions under which the soil surface remained moist at steady-state. Overall, results indicate that under the same evaporative demand, the soil-limited evaporation rate and the dynamics of the evaporation front are different under non-radiative vs. radiative conditions. These findings have implications for use of potential evaporation to estimate actual evaporation without specifically considering the role of different climate forcings, and for applying isothermal modeling schemes to predict soil water evaporation.

4.1 Introduction

Evaporation from bare soil is an important component of water and energy budgets not only in arid regions, but also in semi-arid and humid regions, as large agricultural areas remain bare during field preparation, planting, crop establishment and other field operations. Evaporation in the field commonly occurs during day time under radiation boundary conditions. When the soil surface is wet after an irrigation or rainfall event, most of the available energy at the soil surface is used for soil water evaporation. At this stage, because water is readily available at the surface, vaporization generally takes place at the soil surface. Under these conditions, evaporation initially occurs at a high rate, mainly limited by atmospheric evaporative demand (stage-1 evaporation). Rapid depletion of surface soil moisture, due to drying of soil under radiation boundary conditions, results in onset of a soil-limited evaporation stage. This stage, referred to as the falling-rate stage because evaporation

falls below the potential rate and decreases with time. At this stage, the soil surface becomes visibly dry due to formation of a dry surface layer (DSL), and the evaporation front moves from the surface to the subsurface (Chapter 3). After formation of a dry surface, vaporization of water takes place at the bottom boundary of the DSL [Yamanaka et al., 1999].

There remains debate as to the main factors affecting the onset and rate of soil-limited evaporation [Shokri and Or, 2011; Deol et al., 2012]. Recently, Shokri and Or [2011] demonstrated "jumps" in the evaporation front from the surface to the subsurface at the end of stage 1 under isothermal laboratory conditions. They reported that the "jump" length is affected primarily by porous media properties and less so by boundary conditions. However, under field conditions, drying has been reported to be significantly affected by radiation boundary conditions, which result in steep temperature gradients in the near-surface soil [de Vries and Philip, 1986; Mayocchi and Bristow, 1995; Novak, 2010; Heitman et al., 2010]. The role of steep near-surface temperature gradients on the soil water evaporation process is often ignored in many hydrologic and land surface models.

Evaporation is often predicted based on evaporative demand, which is often measured in terms of pan evaporation or other estimates of potential evaporation. Pioneering work by Penman [1948] to use standard meteorological data for estimating potential evaporation did not include near surface temperature measurements, possibly because of the challenging nature of these measurements, and also because of interest in developing a universal model for both vegetation and soil. Although many attempts have been made to understand soil

water evaporation, challenges still exist in its accurate determination. Decreasing trends in pan evaporation are widely observed across the world and have been attributed to changes in temperature, precipitation, incoming radiation and wind speed. Nevertheless, we only partially understand how these trends are linked to actual evaporation [Brutsaert and Parlange, 1998].

Implementation of the seemingly simple concept of potential evaporation for soil water evaporation is problematic and ambiguous due to many ways that potential evaporation can be, and has been, formulated [Donohue et al., 2010]. Recent studies [for example see Donohue et al., 2010; van Heerwaarden et al., 2010] show that in order to estimate possible effects of climate change on evaporative demand, and eventually on actual evaporation, it is very important to consider spatially and temporally dynamic data describing all drivers of evaporative demand. Due to lack of mechanistic understanding, as well as difficulty in measuring near-surface temperature, many land surface models employ an isothermal scheme, which results in their poor performance under arid and semi-arid regions [Li and Sun, 2008]. Recent studies have emphasized the need for physics-based models and consideration of thermal boundary effects and DSL formation to accurately estimate energy balance components for better understanding of large scale hydrologic and climatic patterns [Heitman et al., 2010; Novak, 2010; Zeng et al., 2011].

Yamanaka et al. [1998 and 1999] studied changes in DSL thickness and the dynamics of the evaporation front. They reported diurnal and inter-diurnal changes in DSL thickness.

However, their studies were conducted at cm-scale with the shallowest observation taken from 0-1 cm soil depths. Recently, Novak [2010] demonstrated the mm-scale dynamics of the evaporation front in the near-surface soil using numerical modeling and reported that transition between surface and subsurface evaporation occurs daily during early stages of drying. The Novak (2010) simulation also showed corresponding changes in the surface energy balance, near-surface temperature and water content profiles, and emphasized the need for measurement-based studies to evaluate the existing theories based on modeling exercises.

Heat-pulse measurements have been used to study fine-scale near-surface temperature and thermal property profiles, which are otherwise very difficult to measure. These measurements can be used to estimate sub-surface evaporation with a sensible heat balance (SHB) approach [Heitman et al., 2008ab; Xiao et al., 2012; Deol et. al., 2012]. In a controlled laboratory study, Deol et al. [2012] used near-surface thermal conductivity measurements to estimate DSL thickness during a drying event in a sandy soil. In a field study (Chapter 3), we found that heat-pulse measurement-based estimate of DSL thickness closely matched with actual measurements of visual DSL thickness in a bare loamy sand soil and gave a reasonable estimate of the location of the evaporation front.

Understanding of the physics of soil water evaporation, especially the role of thermal boundary conditions in soil-limited evaporation process and the dynamics of the evaporation front, is currently lacking. Recent improvements to measurement techniques, however, make

it possible to collect detailed data on these processes. Using these measurement techniques (i.e., heat-pulse sensor measurements), we conducted controlled laboratory studies to investigate the effect of non-radiative and radiative boundary conditions on 1) evaporation front dynamics under transient conditions, and 2) actual to potential evaporation ratios under steady-state, soil-limited conditions.

To achieve the objectives, we first used heat-pulse measurements to study the effect of changes in thermal boundary conditions on DSL thickness during a continuous drying period. This study is a continuation of the transient evaporation study discussed in Deol et al. [2012] where a radiation heat emitter was used to create radiative surface boundary conditions for 90 h. In the experiments discussed here, the heat emitter was turned off after the 90-h radiative drying event, changing the boundary conditions to non-radiative and allowing redistribution of the evaporation zone. Removing radiation (by turning off the heat emitter above the soil) also involved a change in evaporative demand. To specifically compare the effect of radiative vs. non-radiative boundary conditions on soil-limited evaporation and DSL thickness, we also conducted two separate steady-state evaporation experiments. For these experiments the potential evaporative demand was the same, but one case involved non-radiative boundary conditions generated using a fan to adjust wind speed, while the other employed a radiation heat emitter to generate radiative surface boundary conditions.

4.2 Materials and Methods

4.2.1 General Experimental Set-up and Soil Properties

A 34-cm long open top column, constructed of 6-inch (15.25 cm inside diameter) polyvinyl chloride (PVC) pipe, was packed with sand material, similar to that used by Arya et al. [2008 and 2010], at a uniform bulk density of 1.65 g/cm^3. The bottom of the column was connected to a Marriott bottle to wet the soil from the bottom and also to control the saturated zone within the column (Figure 4.1A). The soil column and Marriott bottle were placed on separate digital weighing scales for measuring the mass losses of water. Mass losses of water from soil column and Marriott bottle were manually recorded at 0.1 g resolution. A multi-needle heat-pulse probe (Figure 4.1B) was installed in a vertical orientation on top of the column with its needles parallel to the soil surface and the top needle, barely covered with soil (described further below). The particle size distribution and saturated hydraulic conductivity of the sand material are given in (Table 4.2) [adapted from Arya et al., 2008]. Wet-end water retention at zero (saturation) to 100 cm tension (equivalent to -100 cm soil water pressure head) was determined destructively following Howard et al. [2010] (Figure 4.2; data shown for 0 to -30 cm range).

4.2.2 Transient Evaporation Experiment

For the transient evaporation study and radiative steady-state evaporation studies (next section), a ceramic heat emitter (150 W) was installed at 20 cm distance above the column to uniformly heat the soil surface. The column was first saturated and drained such that the

initial water content condition mimicked the drained profile shown in Figure 4.2 with a water table at 29 cm depth. The upper boundary conditions were constant radiation maintained via the ceramic heat emitter, zero wind speed and constant relative humidity (30%) at constant air temperature (20^{o}C). An open pan evaporation rate of 0.7 mm/h was observed under these boundary conditions. The lower boundary condition was a constant temperature (20^{o}C). For the transient experiment, water supply to the column was disconnected at 0 h. At the same time, the heat emitter was turned on to maintain a constant radiation load at the soil surface. For the 0 to 90-h period, mass losses of water from soil column and Marriott bottle were manually recorded at 0.1 g resolution using separate digital scales. In order to simulate change from day time radiation boundary conditions to nighttime conditions, the heat emitter was turned off to change surface boundary conditions from radiative to non-radiative after 90 h. Soil temperature and heat-pulse data were collected for a total of 120 h, including the period of approximately 30 h without surface radiation.

4.2.3 Steady-state Evaporation Experiments

Two separate steady-state evaporation experiments were conducted to study soil-limited evaporation under non-radiative and radiative boundary conditions. In both experiments the soil was initially saturated and then drained to reach equilibrium with a constantly maintained water table at 29 cm below the soil surface. For the radiative experiment, the upper boundary conditions were constant radiation maintained via the ceramic heat emitter (150 W), zero wind speed and constant relative humidity (30%) at constant air temperature

(20^{o}C). An open pan evaporation rate of 0.7 mm/h was observed under these boundary conditions. The same relative humidity (30%) and temperature (20^{o}C) were maintained for the non-radiative study, however, a fan was used to create the same evaporative demand as that maintained for radiative conditions, i.e., 0.7 mm/h. The lower boundary condition for both non-radiative and radiative experiments, was a constant temperature (20 ^{o}C) at equilibrium with the simulated water table, positioned and maintained 29 cm below the soil surface using the Marriott bottle. The initial condition for water content was a drained profile at equilibrium with the water table (Figure 4.2). The column was left under these boundary conditions until the soil column mass became constant and a steady change in mass with time was observed for the Marriott bottle, indicating steady-state evaporation conditions. In both experiments steady-state evaporation (i.e., constant rate) was observed (via mass measurements) after approximately 72 h. Thereafter, temperature, heat-pulse and mass balance measurements were recorded from 72 to 120 h for each surface boundary condition.

4.2.4 Soil temperature and thermal conductivity measurements

An 11-needle heat-pulse probe [Zhang et. al, 2012] was used for measurement of soil temperature and thermal properties. All 11 needles of the HPP contained 40-gauge type E (chromel-constantan) thermocouples for temperature measurement (Figure 4.1B). The four longer needles also contained a resistance heater made of 38-gauge Nichrome 80 wire for producing a heat-pulse. Further details on the HPP design are given in Zhang et al. [2012]. The HPP was installed in vertical orientation with its needles parallel to the soil surface and

the top needle barely covered with soil. The HPP was used for two functions: (i) collecting soil temperature data each hour to assess temperature gradients imposed between the surface and subsurface boundaries of the soil column; and (ii) making heat-pulse measurements from each heater needle every 2 h to determine soil thermal properties. Temperature responses of needles adjacent to heater needles were used to compute soil thermal diffusivity and volumetric heat capacity following Bristow et al. [1994] and Knight and Kluitenberg [2004], respectively, and thermal conductivity (λ) was determined as the product of thermal diffusivity and volumetric heat capacity.

In addition to heat-pulse data that were collected as described below, the λ-volumetric water content (θ) relationship for the sand was determined independently by packing the soil in a separate column at a bulk density of 1.65 g/cm^3 and measuring λ at various θ using the KD2 Pro Thermal Property Sensor (Decagon Devices Inc., Pullman, WA). The observed λ-θ relationship for this soil closely matched the Chung and Horton [1987] model for λ for sandy soils (Figure 4.3).

4.2.5 DSL thickness estimates

The DSL thickness was estimated using heat-pulse measurements following Deol et al., [2012]. The near-surface soil layer (transition layer with thickness z_{trans}) was considered to consist of two zones, a DSL of thickness z_{dry} and a wet subsurface layer of thickness z_{wet}, so that $z_{trans} - z_{wet} = z_{dry}$. Thermal conductivity of the near-surface transition layer (λ_{trans}) can be

expressed as the depth weighted harmonic mean of λ of the constituent layers [Deol et. al, 2012]:

$$\frac{z_{trans}}{\lambda_{trans}} = \frac{z_{dry}}{\lambda_{dry}} + \frac{z_{wet}}{\lambda_{wet}} \qquad [1]$$

where, subscripts dry and wet indicate properties for dry and wet layers, respectively.

We estimated λ_{trans} from the bulk heat-pulse measurements in the 0-6 mm depth (near-surface layer). Thermal conductivity for the wet subsurface layer was estimated from heat-pulse measurements at the bottom boundary of the transition layer, i.e., 6-12 mm depth. Thermal conductivity of the DSL (λ_{dry}) was estimated from independent measurements of dry soil at the same bulk density. The thickness of the DSL (z_{dry}) was then calculated by substituting these measured values in Eq. [1].

4.3 Results and Discussion

4.3.1 Evaporation front dynamics under changing thermal boundary conditions

This study is a continuation of the transient evaporation study discussed in Deol et al. [2012]. The detailed data for the first 84 h of the drying event, discussed in Deol et al., [2012], showed that mass balance evaporation decreased from 0.61 mm/h at 1h to 0.14 mm/h at 84 h under radiative boundary conditions maintained using a heat emitter. For this study, we

turned off the heat emitter at 94 h to simulate a change in surface boundary conditions from radiative daytime conditions to non-radiative nighttime conditions. Temperature and heat-pulse measurements were taken throughout the drying period (0-120 h). Detailed temperature and thermal property data for the first 85 h have been discussed in Deol et al., [2012]. The temperature profile at 94 h showed temperature decreasing from 40.28 °C at the surface to 30.85°C at 4.8 mm depth (Figure 4.4). The soil temperature reached equilibrium with room temperature (20°C) at 105 h, indicating a complete transition to approximately isothermal conditions. The temperature profile at 105 h shows a relatively uniform temperature ranging from 19.60 °C at the surface to 20.04 °C at 4 mm depth (Figure 4.4).

Figure 4.5 shows estimated DSL depth/thickness during the initial radiative (0-94 h) and then non-radiative (94-120h) surface drying conditions. The data show that DSL thickness increased from nearly 0 at 18 h to 6 mm at 92 h. However, the trend reversed with the transition into non-radiative conditions. The DSL thicknesses of 4.5, 2.7 and 2.6 mm were observed at 94, 96 and 104 h, respectively. Thereafter, DSL thickness became almost constant with values ranging between 2.1 to 2.6 mm.

Data presented in Deol et al. [2012] showed that from 40 h onward, evaporation occurred in the subsurface and mass balance evaporation during this period matched with Fickian diffusive vapor flux. Figure 4.6 shows the diffusive vapor flux (J) for both radiative and non-radiative boundary conditions, calculated according to Fick's Law using estimated z_{dry} and the diffusion coefficient model for dry porous media given by Millington [1959]:

$$J = \varepsilon^{4/3} D \frac{e_{soil} - e_{air}}{z_{\mathrm{dry}}} \qquad [2]$$

where, ε is the soil air-filled porosity, D is the diffusion coefficient of water vapor in free air, e_{soil} is water vapor density at the drying front, and e_{air} is water vapor density in the air above the column at ambient air temperature (20°C) and humidity (30%).

Calculated flux, J, decreased from 0.33 mm/h at 40 h to 0.14 mm/h at 84 h (Figure 4.6). Equation 2 shows that diffusive flux is inversely proportional to DSL thickness (z_{dry}), so J should increase with decreasing DSL thickness after 94 h, when all other terms are held constant. However, a decrease in soil temperature also lowered e_{soil} after the transition to non-radiative boundary conditions, resulting in lower J (0.13 and 0.12 mm/h at 100 and 120 h, respectively) for non-radiative boundary conditions, which is as would be expected. The data indicate that the evaporation front moved from the near-surface to approximately 6 mm depth under radiative conditions while the evaporation rate showed a decline. When the surface boundary conditions changed to non-radiative, however, the evaporation front receded back towards the surface, eventually stabilizing at approximately 2.5 mm depth yet with a lower evaporation rate than that observed when the evaporation zone was at similar depths during surface irradiation. These laboratory observations suggest a decrease in DSL thickness in the field when soil cools down after the sunset and consequently diurnal cycling in the evaporation front depth. These results are consistent with previous findings from numerical simulation studies by Novak [2010].

4.3.2 Steady-state soil-limited evaporation under radiative vs. non-radiative conditions

In the laboratory study discussed in the previous section, a decrease in DSL thickness was observed with change in surface boundary conditions from radiative to non-radiative by turning off the heat emitter. However, turning off the heat emitter also changed the atmospheric evaporative demand. As such, it is unclear whether the changes in DSL thickness observed in our study from radiative conditions to non-radiative conditions are simply due to change in evaporative demand, or are instead due to the effect of temperature on the soil-limited evaporation process. In an attempt to answer this question, we conducted another experiment to investigate the effect of non-radiative vs. radiative conditions on soil-limited evaporation by keeping the evaporative demand constant under both sets of conditions. Non-radiative and radiative steady-state evaporation studies were conducted under controlled laboratory conditions. A fan and a heat emitter were used for non-radiative and radiative studies, respectively. The fan distance and speed were adjusted to obtain a pan evaporation rate of 0.7 mm/h (to create the same evaporative demand under both conditions).

Near-surface temperature profiles under steady-state radiative and non-radiative conditions are shown in Figure 4.7. Data for radiative conditions show relatively higher temperatures than for non-radiative conditions as well as a decreasing trend in temperature with increasing depth. For radiative conditions, the steepest temperature gradient was observed for the 0-1 mm soil layer. The inflection point in the observed temperature profile was at approximately

1 mm, suggesting a heat sink and/or a sharp contrast in soil thermal properties in this depth [Heitman et al., 2008a]. The temperature profile under non-radiative conditions showed a slight decreasing trend in temperature with increasing depth (Figure 4.7). Very similar near-surface thermal property distributions were observed during both non-radiative and radiative conditions, though with slightly higher λat depths below 1 mm under radiative conditions, suggesting slightly higher soil water content (Figure 4.8). For both cases, λdecreased with depth in the upper 6 mm of the profile and then became nearly constant with depth.

The soil surface color was observed for both sets of conditions and compared with the color of dry soil. During steady-state evaporation for radiative boundary conditions, the soil surface was dry. For similar conditions, Deol et al. (2012) observed a DSL thickness of approximately 0.5 mm. Whereas, under non-radiative conditions, the soil surface became lighter in color than the initial condition but remained moist at steady-state.

A steady-state mass evaporation rate (E) of 0.28 mm/h (ranging from 0.26 to 0.32 mm/h) was observed under radiative conditions, as compared to a lower E of 0.15 mm/h (ranging from 0.14to 0.17 mm/h) under non-radiative conditions. Both sets of surface boundary conditions were chosen to allow the same evaporative demand measured as pan evaporation (0.7 mm/h). However, a higher E to pan evaporation (Ep) ratio, E/Ep = 0.39, was observed under radiative conditions, as compared to E/Ep = 0.21 under non-radiative conditions. The same evaporative demand producing very different E/Ep, depending on thermal boundary conditions, suggests the important role of temperature and heat transfer in the soil-limited

evaporation process. Radiative boundary conditions resulted in greater, externally-driven available energy for the vaporization of water as compared to non-radiative conditions. This allowed quick depletion of the soil water available at the surface which was not matched by the supply of water to the surface from the subsurface soil, resulting in formation of a DSL, indicated by drying of the soil surface. A higher evaporation rate was sustained under radiative conditions even in the presence of a DSL, which acts as a barrier (i.e. mulch) to water transport from the subsurface to the surface [Jalota and Parihar, 1998] and forces the evaporation to occur in the subsurface at the bottom boundary of the DSL. In contrast, under non-radiative conditions, the system was energy limited (i.e., no external radiation heat to dissipate) and evaporation occurred at a lower rate, even when the soil surface remained moist.

As discussed above, the near-surface thermal conductivity profiles are similar in both cases with slightly higher thermal conductivities under radiative conditions (Figure 4.8). The main difference was the presence of a ~0.5 mm thick DSL and steep temperature gradients in the near-surface under radiative conditions (Figure 4.7). Soil conduction heat flux (H) was computed as a product of temperature gradient and λ for each set of conditions using a sign convention such that a negative H indicates downward heat conduction. Under radiative boundary conditions, estimated H values at 0.5, 1.5 and 4 mm layers were -292, -100 and -96 W/m^2, respectively. These are compared to a much smaller magnitude and opposite direction H (4, 13 and 26 W/m^2 for corresponding depths, respectively) in the case of non-radiative boundary conditions (Figure 4.9). The trend of decreasing magnitude in H with depth for

radiative boundary conditions indicates a significant heat sink, either from soil warming or latent heat flux, between the 0.5 and 4 mm soil depths. Because conditions were steady-state with no change in temperature (i.e., no warming), differences in H with depth were attributed to the latent heat flux, LE [Gardner and Hanks, 1966]:

$$LE = (H_1 - H_2) \qquad [3]$$

where H_1 and H_2 are the conduction heat fluxes at the upper and lower boundaries of the soil layer, respectively.

Calculations using Eq. [3] indicate a depth-integrated (0.5 to 4 mm) E of 0.29 mm/h for radiative boundary conditions, which closely matches the mass balance E of 0.28 mm/h. This shows that steep temperature gradients in the near-surface under radiative conditions resulted in large magnitude H near the surface (Figure 4.9). Because irradiation is externally controlled, energy must be dissipated even as the soil surface dries and evaporation drops below the potential rate. This energy in the dry near-surface was used for vaporization of water, resulting in quick depletion of moisture. A constant supply of water was maintained for steady-state conditions, so the depleted water was quickly replenished resulting in relatively large sustained E.

Using Eq. [3], a depth-integrated (0.5 to 4 mm) E of 0.03 mm/h was computed for non-radiative boundary conditions. This was only 20% of the observed mass balance E (0.15 mm/h). This shows that evaporation under non-radiative conditions was energy limited, or

essentially self-regulated in terms of external energy draw. The system has to draw energy from the external environment (constant temperature of 20 °C and 30% RH) via surface sensible heat flux or from within the soil system as upward soil heat flux, i.e., from the lower boundary maintained at 20°C, towards the cooler evaporating surface (Figure 4.7). As the liquid water supply towards the surface declines, owing to the reduced soil hydraulic conductivity with drying, the demand for energy (i.e., energy draw) diminishes. About 20% of the evaporation was supported by sensible energy from the subsurface (0.5-4 mm depth zone) and the remaining 80% occurred at the surface (<0.5 mm depth), drawing the energy from the environment. Even though the evaporative demand remained the same under both boundary conditions, the energy-limited system could not maintain the same rate of evaporation and was likely limited by upward liquid water flux. Without the need to dissipate externally supplied radiation energy, the soil surface drying wasn't as fast as under radiative boundary conditions, and the soil surface stayed moist.

Based on evaporation studies under isothermal (non-radiative) conditions, Shokri and Or [2011] reported that evaporation rate during soil-limited evaporation stage is controlled by capillary flow from secondary drying front in the subsurface towards the primary drying front where vaporization of water takes place. Our findings, however, show that this rate of water flow towards the vaporization plane is, in turn, limited by energy available for evaporation at the vaporization plane. The location of the evaporation plane itself is also affected by energy availability for the evaporation process. In these experiments, the water table was maintained at the same depth (29 cm) for both cases and potential evaporative

demand was kept constant. The main difference was that under radiative conditions the evaporation was driven by the requirement that externally imposed energy be dissipated, whereas under non-radiative conditions the energy consumed for evaporation was dictated by the rate at which the soil could provide water to the surface. Overall, results show that under similar evaporative demand, soil-limited evaporation rate as well as the location of the evaporation front is different under non-radiative vs. radiative conditions. One example of the implications of our findings is that progression of soil-limited evaporation during a hot day with clear sky and low wind speed may not be the same as on a windy and cooler day, even when the potential evaporative demand is the same under both sets of conditions.

4.4 Summary and conclusions

The transient evaporation study, using heat-pulse measurement-based estimates of DSL thickness, demonstrated a decrease in DSL thickness in response to change in radiative to non-radiative surface boundary conditions, simulating the changes occurring in field during after sunset. These results suggest diurnal changes in the location of the evaporation front in the near-surface zone. With a constant water table depth and the same evaporative demand, high steady-state evaporation rates were sustained under radiative, energy driven evaporation, even when the soil surface was visibly dry. In contrast, relatively low evaporation rates were observed under non-radiative, convection driven, energy limited conditions with the same potential evaporative demand and water table depth, even though the soil surface remained moist. These results demonstrate that the progression of evaporation is different under non-radiative and radiative conditions. Formation of a DSL

and change from surface to subsurface evaporation may occur much earlier in drying under radiative, energy driven evaporative drying as compared to non-radiative, convection-driven drying, yet with a higher sustained evaporation rate for radiation-driven conditions.

Results also indicate that relationship between *E* and *Ep* will be different under radiation-driven vs. convection-driven drying. These findings have important implications for generalizations about actual evaporation and pan evaporation relationships, and for using isothermal models to study the process of soil drying in the field. The role of temperature and steep temperature gradients in the near-surface needs to be carefully considered for understanding evaporative drying of soil as most soil water evaporation occurs during the day time and under radiative conditions. Further investigation is needed to study the difference in progression of evaporation for the entire drying curve under non-radiative versus radiative conditions for a wide range of textures and boundary conditions.

4.5 References

Arya, L.M., D.C. Bowman, B.B. Thapa, and D.K. Cassel (2008), Scaling soil water characteristics of golf course and athletic field sands from particle size distribution, *Soil Sci. Soc. Am. J.*, 72, 25-32, doi: 10.2136/sssaj2006.0232.

Arya, L.M., J.L. Heitman, B.B. Thapa, and D.C. Bowman (2010), Predicting saturated hydraulic conductivity of golf course sands from particle-size distribution, *Soil Sci. Soc. Am. J.*, 74, 33-37, doi: 10.2136/sssaj2009.0022.

Bristow, K. L., G. J. Kluitenberg and R. Horton (1994), Measurement of soil thermal properties with a dual-probe heat-pulse technique, *Soil Sci. Soc. Am. J.*, 58, 1288-1294.

Brutsaert, W., and M. B. Parlange (1998), Hydrologic cycle explains the evaporation paradox, *Nature*, 396, 30.

Chung, S. O., and R. Horton (1987), Soil heat and water flow with a partial surface mulch, *Water Resour. Res.*, 23, 2175-2186.

Deol, P., J.L. Heitman, A. Amoozegar, T. Ren, and R. Horton (2012), Quantifying Non-isothermal Sub-surface Soil Water Evaporation. *Water Resour. Res.* 48, W11503, doi:10.1029/2012WR012516.

Donohue, R. J., T. R. McVicar, and M. L. Roderick (2010) Assessing the ability of potential evaporation formulations to capture the dynamics of evaporative demand with a changing climate. J. Hydrol., 386, 186-197.

Gardner, H. R. and R. J. Hanks (1966), Evaluation of the evaporation zone in soil by measurement of heat flux, *Soil Sci. Soc. Am. J*., 30, 425-428.

Heitman, J.L., R. Horton, T.J. Sauer, and T.M. DeSutter (2008a), Sensible heat observations reveal soil-water evaporation dynamics, *J. Hydromet*., 9, 165-171.

Heitman, J.L., R. Horton, T.J. Sauer, T.S. Ren, and X. Xiao (2010), Latent heat in soil heat flux measurements, *Ag. Forest. Met.*, 150, 1147-1153.

Heitman, J.L., X. Xiao, R. Horton, and T.J. Sauer (2008b), Sensible heat measurements indicating depth and magnitude of subsurface soil water evaporation, *Water Resour. Res.*, 44, W00D05. doi:10.1029/2008WR006961.

Howard, A., J.L. Heitman, D. Bowman (2010), A Simple Approach for Demonstrating Water Retention and Field Capacity, *J. Nat. Res. Life Sci. Ed.*, 39, 120-124.

Idso, S.B., R.D. Jackson, and R.J. Reginato (1975), Estimating evaporation: A technique adaptable to remote sensing, *Science*, 189, 991-992.

Idso, S.B., R.J. Reginato, R.D. Jackson, B.A. Kimball, and F.S. Nakayama (1974), The three stages of drying of a field soil, *Soil Sci. Soc. Am. Proc.*, 38, 831-837.

Jalota, S.K. and S.S. Prihar (1998), *Reducing soil-water evaporation with tillage and straw mulching*. Iowa State University Press, Ames (ISBN 0-8138-2857-0), p. 142.

Kimball, B.A. (1973), Water vapor movement through mulches under field conditions, *Soil Sci. Soc. Am. Proc.*, 37, 813–818.

Knight, J.H. and G.J. Kluitenberg (2004), Simplified computational approach for the dual-probe heat-pulse method, *Soil Sci. Soc. Am. J*., 68, 447-449.

Li, Q., and S. F. Sun (2008), Development of universal and simplified soil model coupling heat and water transport. *Science in China Seriers (D)*, 51, 88–102.

Mayocchi, C.L., and K.L. Bristow (1995), Soil surface heat flux: some general questions and comments on measurements, *Ag. Forest Meteor*. 75, 43-50.

Novak, M.D. (2010), Dynamics of the near-surface evaporation zone and corresponding effects on the surface energy balance of a drying bare soil, *Ag. Forest Meteor*., 150, 1358-1365.

Penman HL (1948) Natural evaporation from open water, bare soil and grass. *Proc R Soc LondA Math Phys Sci* 193:120–146. doi:10.1098/rspa.1948.0037

Philip, J.R., and D.A. de Vries (1957), Moisture movement in porous materials under temperature gradients. Transactions, American Geophysical Union, 38(2), 222-232.

Shokri, N., and D. Or. (2011), What determines drying rates at the onset of diffusion controlled stage-2 evaporation from porous media? *Water Resour. Res*., 47, W09513.

van Heerwaarden, C. C., J. Vilà- Guerau de Arellano, and A. J. Teuling (2010), Land- atmosphere coupling explains the link between pan evaporation and actual evapotranspiration trends in a changing climate, *Geophys. Res. Lett.*, 37, L21401, doi:10.1029/2010GL045374.

Xiao, X., R. Horton, T. Sauer, J.L. Heitman, and T. Ren (2011), Cumulative soil water evaporation as a function of depth and time, *Vadose Zone J*., 10, 1016-1022.

Yamanaka, T. and, T. Yonetani (1999), Dynamics of the evaporation zone in dry sandy soils, *J. of Hydrol.*, 217(1–2), 135-148.

Yamanaka, T., A. Takeda, and J. Shimada (1998), Evaporation beneath the soil surface: Some observational evidence and numerical experiments. , *Hydrol. Process.*, 12, 2193-2203.

Zeng, Y., Z. Su, L. Wan, and J. Wen (2011), Numerical analysis of air-water-heat flow in unsaturated soil: Is it necessary to consider airflow in land surface models?, *J. Geophys. Res.*, 116, D20107, doi:10.1029/2011JD015835.

Zhang X., J.L. Heitman, R. Horton, and T. Ren (2012), Measuring subsurface soil-water evaporation with an improved heat-pulse probe. *Soil Sci. Soc. Am. J.*, 76, 876-879.

Table 4.1 Particle size distribution, bulk density and saturated hydraulic conductivity of the soil used in the study. Size separate classifications are according to USDA-NRCS system. (After Arya et. al. [2008])

Particle diameter, mm									
0.002	0.002-0.053	0.053-0.106	0.106-0.180	0.180-0.250	0.250-0.355	0.355-0.500	0.500-0.710	0.710-1.000	1.000-2.000
Clay	Silt	Very Fine Sand	Fine Sand		Medium Sand		Coarse Sand		Very Coarse Sand
----------% particles by weight----------									
0	0	2.1	6.9	11.6	29.7	27.2	14.3	6.1	2.2

Bulk Density, g/cm	1.65
Saturated Hydraulic Conductivity , m/h	2.8

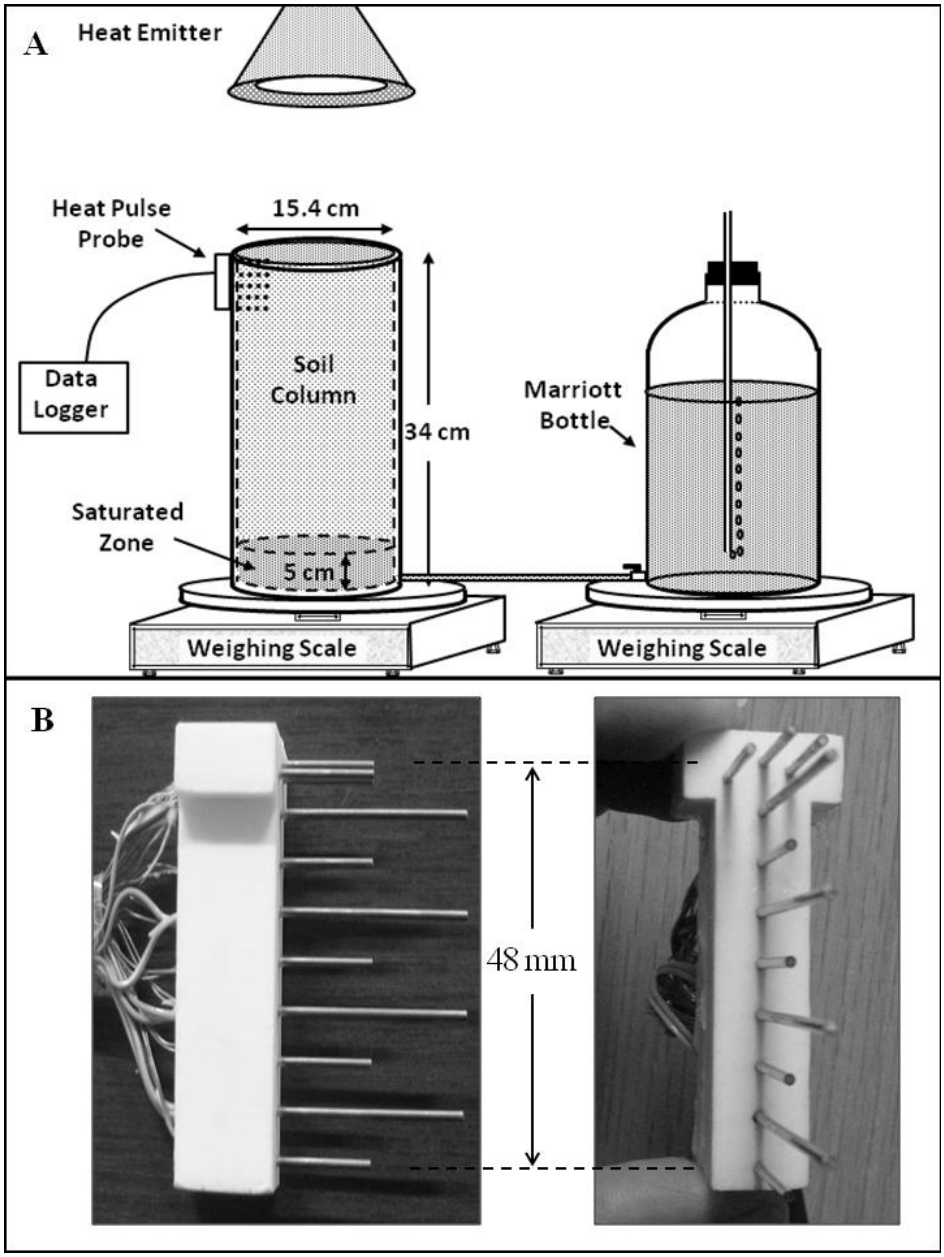

(Deol et al., 2012)

Figure 4.1 (A) Set-up for soil column experiments. The Marriott bottle was disconnected for transient experiment. For steady-state non-radiative study a fan was used instead of the heat emitter (B) Multi-needle heat-pulse probe used in the experiments. All 11 needles contain thermocouples. The four long needles also contain a resistance heater. Spacing between adjacent needles is 6-mm for needles positioned along the vertical midline of the probe. The upper three needles are spaced at 1-mm increments vertically; each of the three uppermost needles is at 6 mm radial spacing from the uppermost heater needle.

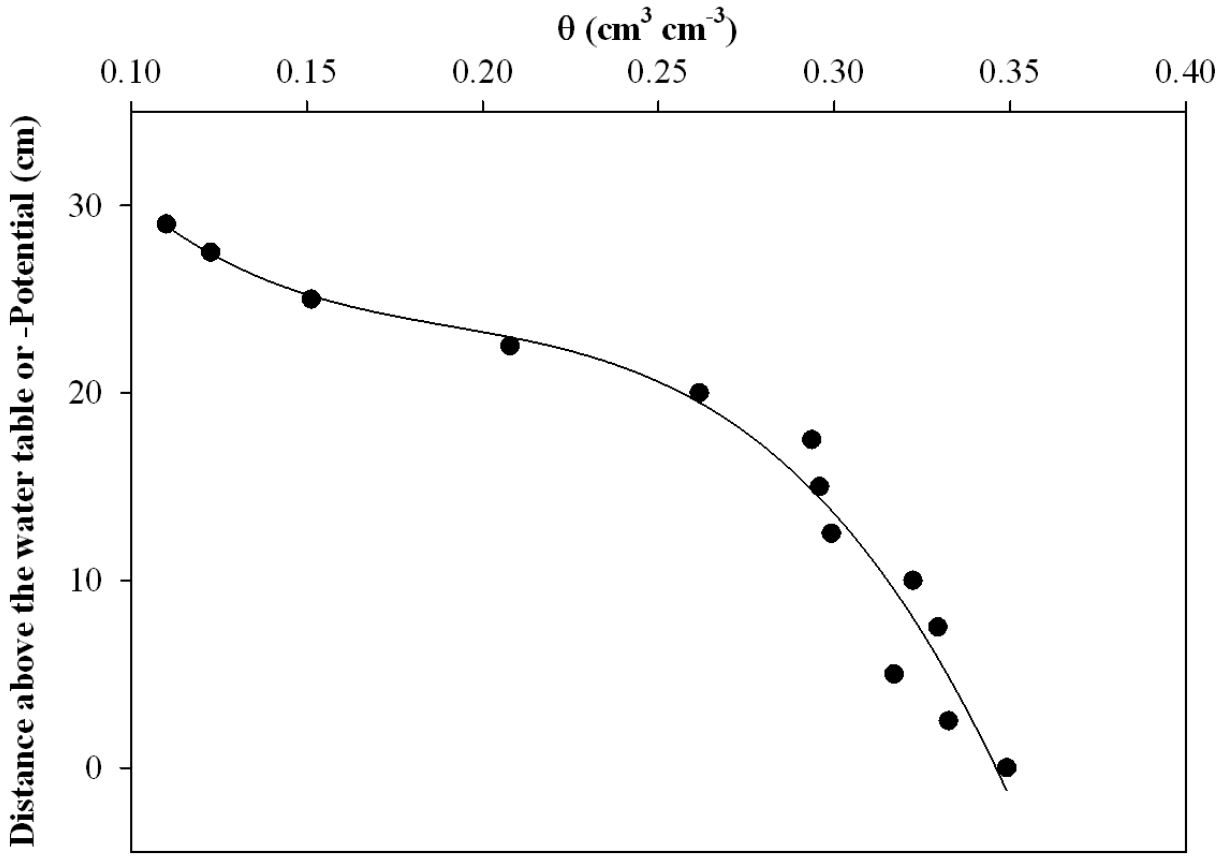

Figure 4.2 Initial volumetric water content (θ) at different depths in the drained column with water table at 29 cm depth. These data also correspond to water retention for the 0 to -30 cm potential range.

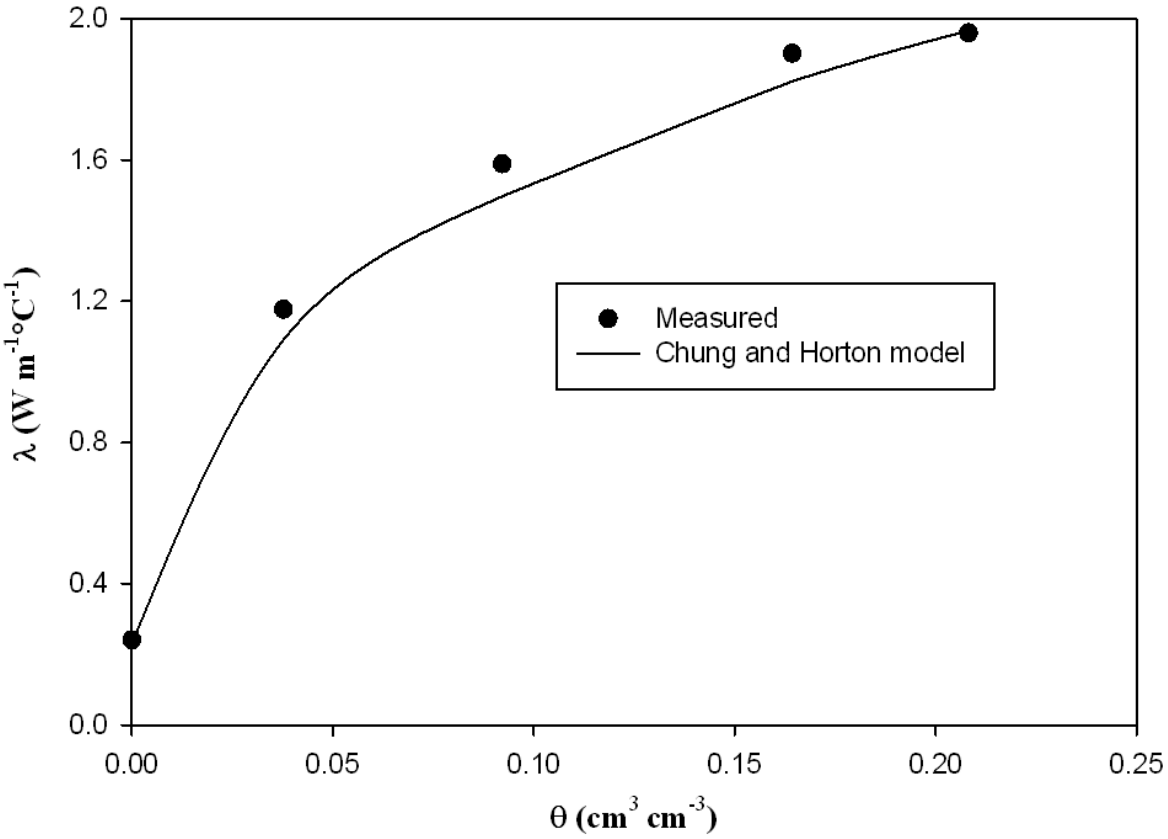

Figure 4.3 Soil thermal conductivity (λ) as it varies with water content (θ) for the soil used in the experiments. Measurements were collected at bulk density = 1.65 g cm^{-3}. The Chung and Horton (1987) model for sandy soil is shown for comparison.

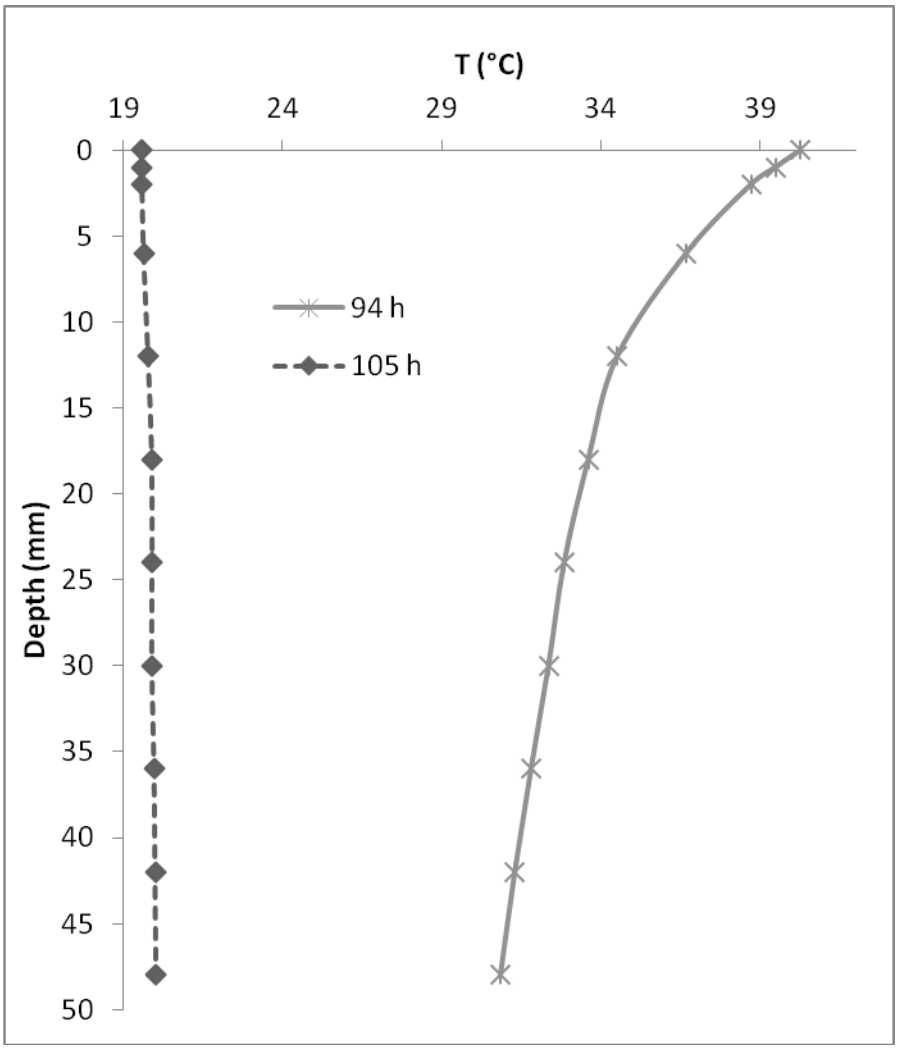

Figure 4.4 Near-surface temperature profiles at 94 and 105 h during the transient evaporation study.

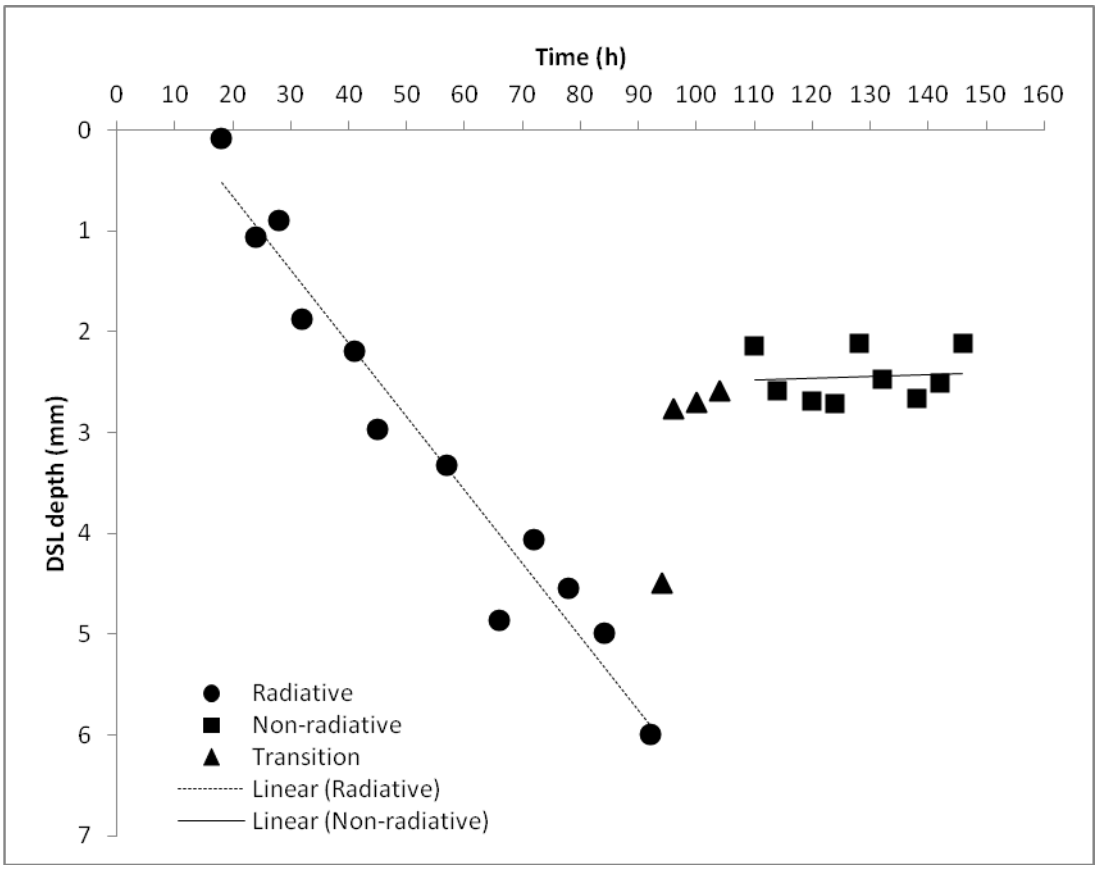

Figure 4.5 Dry surface layer (DSL) depth during a drying event under radiative and non-radiative surface boundary conditions. Boundary conditions were maintained by using a heat emitter which was turned on at 0 h and then turned off at 94 h.

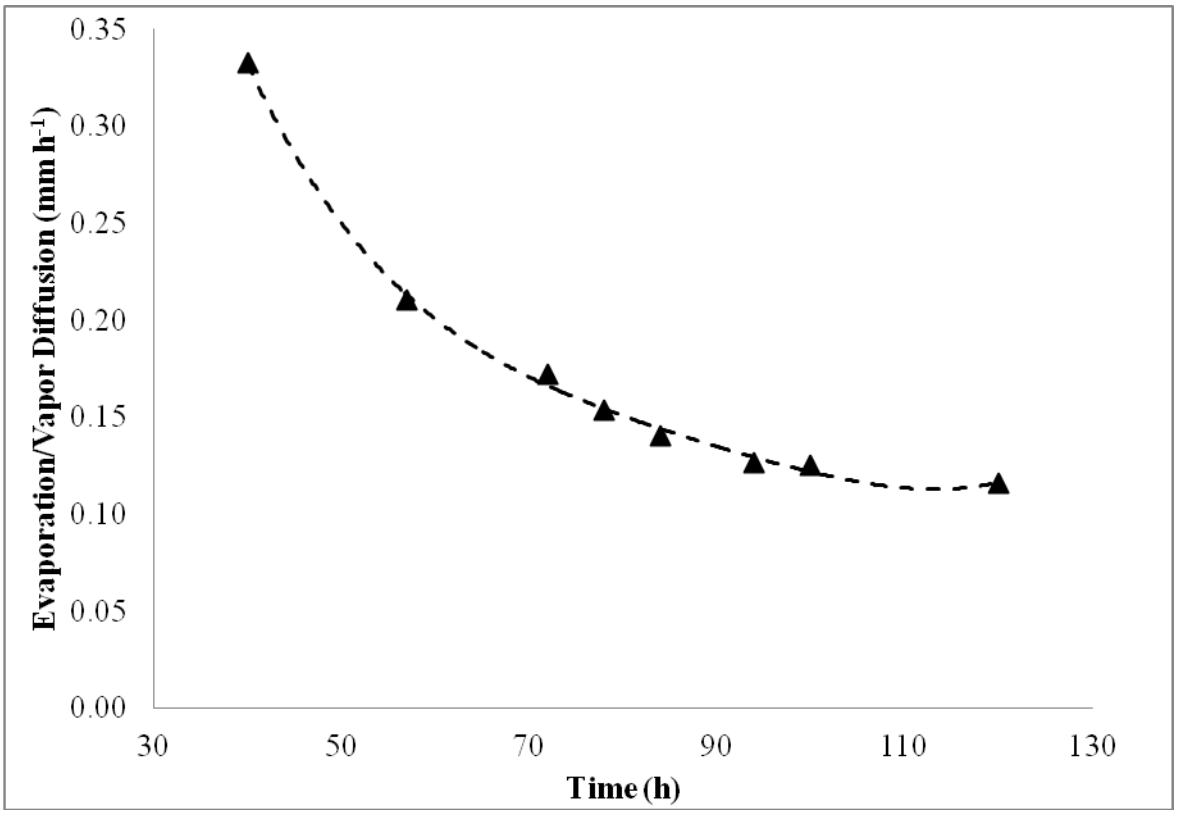

Figure 4.6 Diffusive vapor flux for falling-rate evaporative drying during the transient evaporation study.

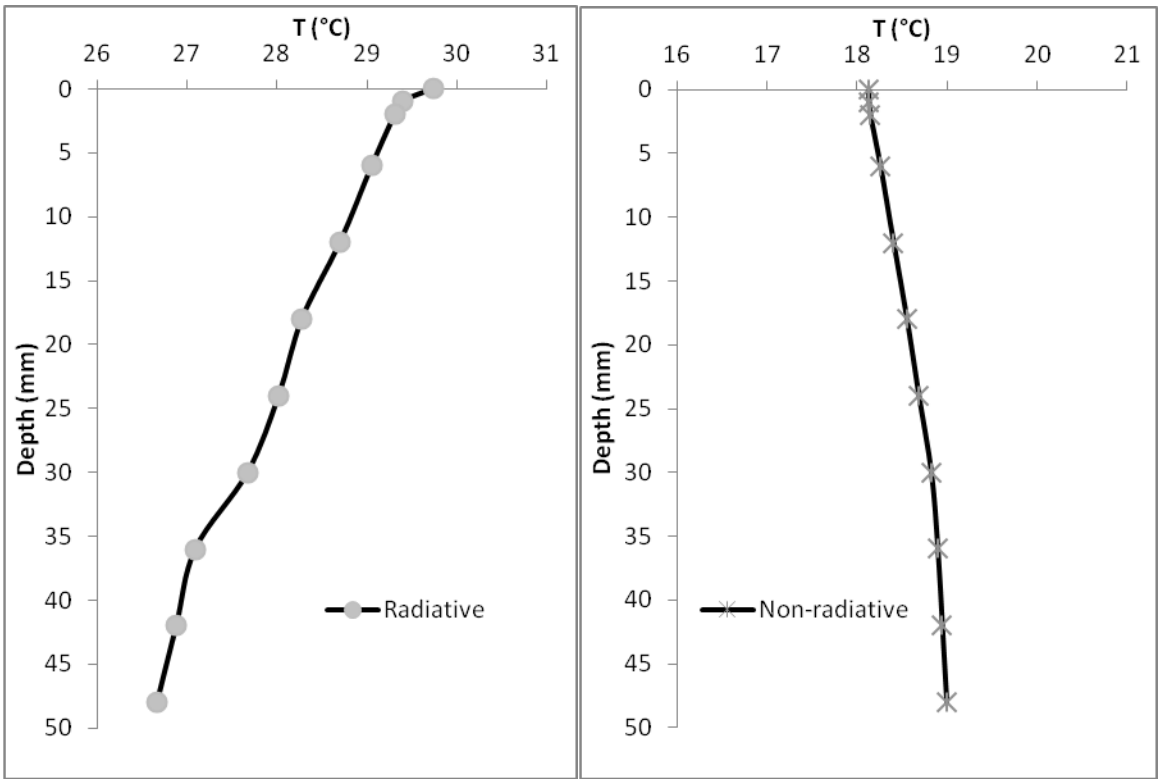

Figure 4.7 Near surface soil temperature profiles under radiative (left) and non-radiative (right) steady state evaporation conditions. Note differences in the temperature scale in each panel.

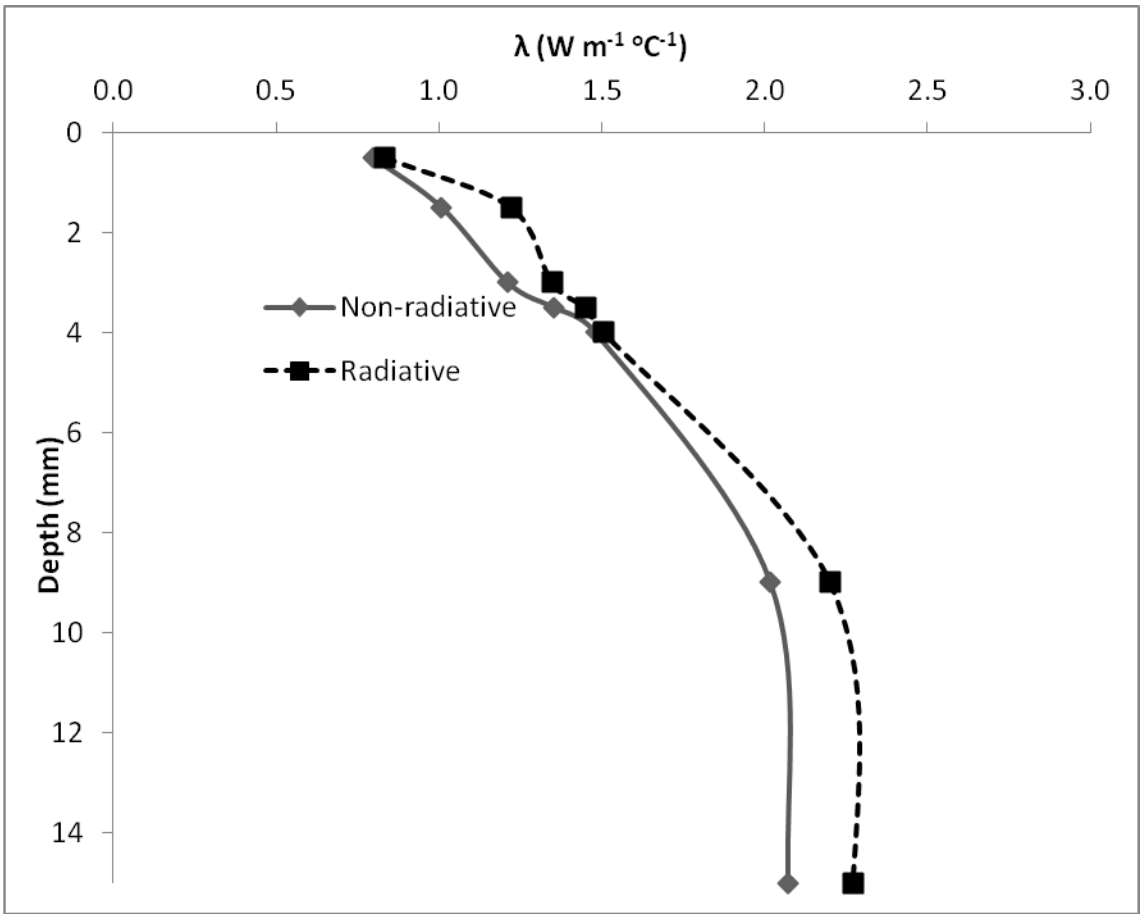

Figure 4.8 Near-surface thermal conductivity profiles under radiative and non-radiative steady-state evaporation conditions

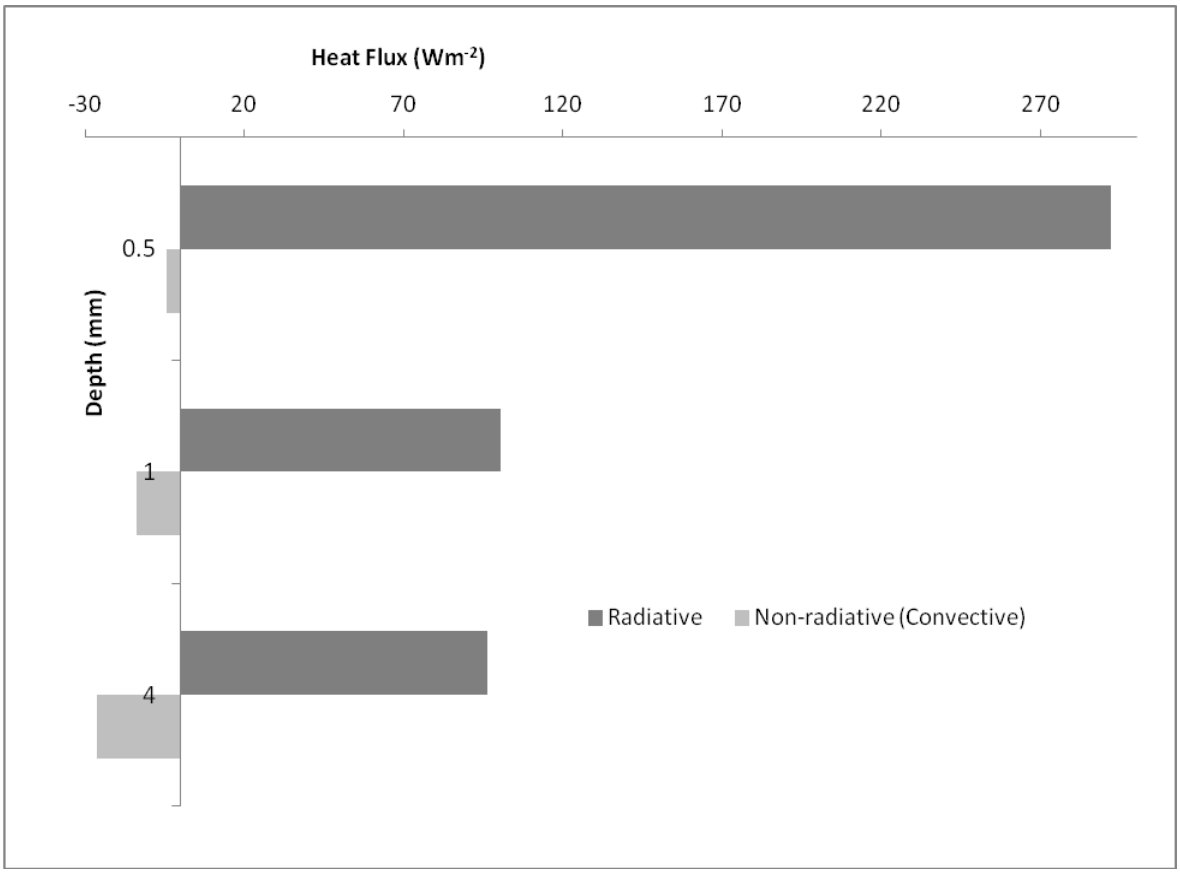

Figure 4.9 Near-surface heat flux magnitude (logarithmic scale) for 0-1, 1-2 and 2-6 mm depth layers under thermal and convective boundary conditions. Note that heat fluxes were directed downward in the case of radiative boundary conditions and upward for non-radiative boundary conditions.

5. Summary and Conclusions

Most efforts to quantify energy and mass exchange at the land surface during the evaporation process are limited to modeling; few detailed measurements are available for validation of these models. Thermal effects on the evaporation process are often ignored in large scale modeling because of the challenging nature of temperature and thermal property measurements in the highly dynamic near surface zone. We conducted a series of laboratory and bare field experiments to study the dynamics of the evaporation front in the near-surface and to quantify subsurface evaporation profiles based on near-surface temperature and thermal property measurements. The overall goal of our research was to determine when the evaporation front moves from the surface to subsurface with respect to the three classic stages of evaporative drying and to study the effect of radiative boundary conditions on the timing of the onset and rate of soil-limited evaporation.

In our controlled laboratory study using a sandy soil, a sensible heat balance (SHB) approach provided measurement-based quantification of subsurface, non-isothermal evaporation profiles (i.e., the distribution of the evaporation zone) at mm-scale over a drying event. Subsurface evaporation matched mass balance in the early falling rate stage, indicating a loss in liquid water connectivity to the surface. We used heat-pulse measurements along with independent measurements of soil thermal conductivity (λ) for dry soil to continuously estimate the thickness of the dry surface layer (DSL) over a drying period. The estimated thickness of the DSL was used to compute diffusive vapor flux with Fick's Law, which

closely matched the mass balance evaporation and subsurface evaporation estimated by the SHB approach confirming the loss in liquid water connectivity to the surface.

Our field studies using microlysimeter and SHB evaporation estimates further confirmed that the evaporation front moved into the subsurface at the onset of the falling rate evaporation stage, which occurred on the second day of a 5-d natural drying event in a bare field with loamy sand soil after ~3cm rainfall. The timing of this change from surface to subsurface evaporation was also indicated by soil surface albedo (α) measurements. A threshold α value of 0.29 was estimated for the field soil using the observed actual/potential evaporation versus α relationship. An α value higher than threshold α indicated subsurface evaporation. Similar studies for a given soil may help in distinguishing days subject to surface evaporation at the potential rate from the days with subsurface evaporation at rates below potential evaporation.

Effects of radiative and non-radiative boundary conditions on evaporation front dynamics were studied during a drying event under controlled laboratory conditions. This study demonstrated a decrease in DSL thickness in response to change in radiative to non-radiative surface boundary conditions suggesting diurnal changes in the location of evaporation front in the near-surface zone, which agrees with previous reports from numerical simulation studies. We also investigated the effect of radiative vs. non-radiative boundary conditions on steady-state soil-limited evaporation under the same potential (pan-measured) evaporative demand and constant water table depth. Higher steady-state evaporation rates were observed under surface radiation compared to convection-driven conditions, despite the formation of a

DSL only under surface radiation conditions. The results show that under radiative boundary conditions, temperature gradients, in addition to hydraulic properties of porous media play an important role in evaporation dynamics, resulting in relatively quick drying of the soil surface and formation of a DSL. These results indicate that under the same evaporative demand, the soil-limited evaporation rate and the dynamics of the evaporation front are different under radiative vs. non-radiative conditions.

Heat-pulse measurement-based mm-scale estimates of DSL thickness, and subsurface evaporation profiles provide an opportunity to test existing theories and help in developing new models capable of precise estimates of near-surface energy and mass transfer occurring at the land surface. Simple measured α values, which can be collected remotely, can be used to identify days subject to subsurface evaporation and to distinguish between days when evaporation is occurring at or below the potential rate. Our studies also emphasize the need to consider radiative boundary conditions and resulting temperature gradients in the near surface soil while modeling soil water evaporation. In addition, our findings have implications for use of pan evaporation or other potential evaporation formulations to estimate actual evaporation without considering the relative role of different climate forcings.

The improved knowledge about the soil water evaporation process and near-surface energy and mass transfer will influence research and understanding of various natural processes occurring at a wide range of scales (e.g., microclimate for seeds and microbes in the near-surface to large scale hydrologic and climatic patterns), and has a wide range of applications,

such as agricultural and forestry water management and conservation, evaporation from pastures and other exposed surfaces, industrial drying processes and vapor fluxes of various substances from the land surface.

5.1 Suggestions for future work

The formation of the DSL and onset of subsurface evaporation front was found to coincide with the onset of falling rate evaporation under controlled laboratory as well as bare field conditions. The laboratory studies and bare field studies were conducted on sandy and loamy-sand soils, respectively. Further studies with a wider range of soils are required to understand the effect of soil texture on the progression of evaporation and the timing of the onset of subsurface evaporation with respect to the three stages of evaporation.

Bare field evaporation studies also showed the important role that α plays in detecting the formation of the DSL, which affects the mass and energy transfer at the land surface. However, α is not considered to be a variable in most large scale modeling studies. Field studies similar to ours on different soil types (i.e. with different textures and colors) can be conducted to determine threshold α for subsurface evaporation. This information on soil type dependent threshold α can be used to indicate the formation of a DSL and help to determine whether the evaporation on a particular day occurred on the surface or in the subsurface. Field studies under a wider range of textures and with more frequent heat-pulse measurements are needed. These will help in confirming the previous numerical modeling based findings showing inter-diurnal and diurnal dynamics of evaporation front and switch between surface and subsurface evaporation at early stages of drying. Based on our research

findings, we suggest that that in future modeling studies, role of steep temperature gradients, formation of DSL and shift in position of latent heat sink be considered for accurate estimation of surface energy balance

We studied actual and pan evaporation relationship under radiative and non-radiative conditions under steady-state soil-limited evaporation conditions. Our studies showed that it is possible to collect precise near-surface temperature and thermal property measurements under steady-state controlled laboratory conditions. Steady-state conditions allow repeated measurements of temperature, thermal property and evaporation profiles which are not changing with time. Similar studies using heat-pulse measurements, with different combinations of boundary conditions can allow studying the evaporation profiles at different stages of drying, which can then be pieced together to understand the entire drying curve. Finally, further investigation is needed to study the difference in progression of evaporation for the entire drying curve under radiative vs. non-radiative conditions for a wide range of textures and boundary conditions.